Electrochemical lithium migration to mitigate alkali-silica reaction in existing concrete structures

Silva De Souza, Lourdes

DOI
10.4233/uuid:443835f4-d172-4267-8412-dd3cfe24330a

Publication date
2016

Document Version
Final published version

Citation (APA)
Silva De Souza, L. (2016). *Electrochemical lithium migration to mitigate alkali-silica reaction in existing concrete structures*. [Dissertation (TU Delft), Delft University of Technology]. https://doi.org/10.4233/uuid:443835f4-d172-4267-8412-dd3cfe24330a

ELECTROCHEMICAL LITHIUM MIGRATION TO MITIGATE ALKALI-SILICA REACTION IN EXISTING CONCRETE STRUCTURES

ELECTROCHEMICAL LITHIUM MIGRATION TO MITIGATE ALKALI-SILICA REACTION IN EXISTING CONCRETE STRUCTURES

Proefschrift

ter verkrijging van de graad van doctor
aan de Technische Universiteit Delft,
op gezag van de Rector Magnificus prof. ir. K.C.A.M. Luyben,
voorzitter van het College voor Promoties,
in het openbaar te verdedigen op dinsdag 6 september 2016 om 12:30 uur

door

Lourdes Maria SILVA DE SOUZA

Mestre em Engenharia Civil, Universidade Federal do Rio de Janeiro, Brazilië.
geboren te Rio de Janeiro, Brazilië.

Dit proefschrift is goedgekeurd door de

promotor: Prof. dr. R. B. Polder
copromotor: Dr. O. Çopuroğlu

Samenstelling promotiecommissie:

Rector Magnificus,	voorzitter
Prof. dr. R. B. Polder,	Technische Universiteit Delft
Dr. O. Çopuroğlu	Technische Universiteit Delft
Onafhankelijke leden:	
Prof. dr. ing. E. Fairbairn	Universidade Federal do Rio de Janeiro, Brazilië
Prof. dr. B. Elsener	Eidgenössische Technische Hochschule Zürich, Zwitserland
Prof. dr. M.R. Geiker	Norges Teknisk-Naturvitenskapelige Universitet, Noorwegen
Dr. T.G. Nijland	TNO, Nederland
Prof. dr. ir. E. Schlangen	Technische Universiteit Delft
Prof. dr. ir. L.J. Sluys	Technische Universiteit Delft, reservelid

The work reported in this thesis is part of the STW project "Modelling, non-destructive testing and Li-based remediation of deleterious Alkali-Silica Reaction in concrete structures" (code No.10971), which is a part of an STW Perspectief Program "Integral Solutions for Sustainable Construction (IS2C)"

Keywords: Alkali-silica reaction; Electrochemical lithium migration; Electrochemical treatment; Durability; Multi-ion transport model

Cover design: Cissa Monteiro.

ISBN 978-94-6186-705-6

An electronic version of this dissertation is available at
http://repository.tudelft.nl/.

Aos meus pais

Don't panic.
D. Adams

CONTENTS

1 Introduction **1**
- 1.1 Background of the thesis . . . 2
- 1.2 Objective of the thesis. . . . 3
- 1.3 Modeling, non-destructive testing and Li-based remediation of deleterious ASR in concrete structures . . . 3
- 1.4 Outline of the thesis. . . . 4
- References . . . 6

2 Literature review **9**
- 2.1 Alkali silica reaction - overview . . . 10
  - 2.1.1 Chemistry of alkali silica reaction . . . 10
  - 2.1.2 Expansion mechanism of ASR . . . 12
- 2.2 Measures to prevent ASR . . . 13
  - 2.2.1 Effects of lithium admixtures against ASR . . . 14
- 2.3 Suggested interventions against ASR . . . 15
- 2.4 Electrochemical treatment against ASR . . . 19
- 2.5 Concluding remarks . . . 30
- References . . . 31

3 Lithium migration in mortar specimens **37**
- 3.1 Introduction . . . 38
- 3.2 Effect of anolyte solution on migration . . . 38
  - 3.2.1 Experimental procedure . . . 38
  - 3.2.2 Results and discussion . . . 41
  - 3.2.3 Conclusions . . . 51
- 3.3 Effect of time on migration . . . 52
  - 3.3.1 Experimental procedure . . . 52
  - 3.3.2 Results and discussion . . . 53
  - 3.3.3 Conclusions . . . 64
- 3.4 Effect of embedded cathode on migration . . . 65
  - 3.4.1 Experimental procedure . . . 65
  - 3.4.2 Results and discussion . . . 66
  - 3.4.3 Conclusions . . . 74
- References . . . 75

4 Modeling of lithium migration in mortar **77**
- 4.1 Introduction . . . 78
- 4.2 Mathematical model . . . 78
  - 4.2.1 Transport in solution. . . . 78
  - 4.2.2 Transport in concrete . . . 80

4.3 Numerical implementation . . . 82
4.4 Results and discussion . . . 85
4.5 Conclusions . . . 95
References . . . 97

5 Effect of lithium migration on ASR induced expansion 99
5.1 Introduction . . . 100
5.2 Experimental procedure . . . 100
5.2.1 Materials and specimen preparation . . . 100
5.2.2 Methods . . . 101
5.3 Results and discussions . . . 105
5.3.1 Expansive behavior of concrete without any treatment . . . 105
5.3.2 Influence of ASR expansion on migration . . . 105
5.3.3 Influence of lithium migration on ASR expansion . . . 115
5.4 Main findings . . . 129
5.5 Conclusions . . . 131
References . . . 132

6 Concluding remarks 135
6.1 General conclusions . . . 136
6.2 Recommendations for further research . . . 137

A Appendix A 139

B Appendix B 145

Acknowledgements 149

Summary 151

Samenvatting 153

Curriculum Vitæ 157

List of Publications 159

1

INTRODUCTION

Parts of this chapter have been published in Souza and Polder, Fifth International PhD Student Workshop on Durability of Reinforced Concrete, 2012) [1].

1

1.1. BACKGROUND OF THE THESIS

ALKALI-silica reaction (ASR) is a deterioration mechanism that affects the durability of concrete structures worldwide. In the Netherlands, it has been diagnosed in tunnels, bridges and locks. The most noticeable case being the bridges on motorway A59 [2]. During the reaction, hydroxyl and alkali ions present in the pore solution react with certain reactive siliceous compounds present in the aggregate producing a hygroscopic ASR gel. Alternatively, the silica structure is dissolved by hydroxyl ions and the degraded structure acts as a hygroscopic silica gel. The gel (or gel-like structure) swells - which may lead to the expansion and cracking of the concrete element [3], [4].

While the expansion of concrete elements may affect the functionality of the structure, cracking may also facilitate the ingress of moisture and aggressive agents (e.g. chloride) which contributes for the development of other deterioration mechanisms [3], [5],[4]. The reaction is slow – it takes 5 to 15 years (and even longer in some cases) to be noted. This means that, even though precautionary measures to avoid ASR have been acknowledged for decades, it is still possible to encounter newly diagnosed cases [3].

Once a concrete structure is diagnosed as affected by ASR, the intervention options currently available are limited [4]. If the symptoms are treated (e.g. crack filling, cutting new joints), the reaction will continue and repair will have to take place repeatedly, increasing the total life-cycle cost of the structure. Amongst the procedures that address the causes of ASR, limiting the ingress of external water by the application of sealers or improving drainage seems to be the most viable [4]. Nevertheless, such methods have limitations (e.g. application on massive concrete structures) and their effectiveness has shown to be variable [6]. There is still need for an effective intervention method. In this framework, the application of lithium compounds has been investigated as a possible alternative mitigation method.

The beneficial effects of the addition of lithium based admixtures in the reduction or prevention of deleterious ASR expansion have been acknowledged since the 1950's (e.g. [7], [8],[9]). Several studies have investigated the influence of varied lithium salts ($LiNO_3$, LiOH, Li_2CO_3, amongst others) in concretes and mortars composed with different reactive aggregates. At certain addition levels (depending on the type of lithium salt and reactive aggregate) ASR expansion is suppressed. Figure 1.1 shows the effects of the addition of LiOH on the development of the reaction on the surface of opal particles. It is generally agreed that the presence of lithium salts alters the reaction mechanism either by hindering the formation of the ASR gel or modifying the gel into a less expansive product [10], [11], [12], [4].

On one hand, the use of lithium based admixtures is a valuable preventive method to be taken into account during the design of new concretes structure. On the other, when treating already existing structures, the incorporation into the fresh mixture is, obviously, no longer possible. In this case, lithium needs to be transported into the material.

Potential treatment methods of existing structures such as spraying and vacuum impregnation [14],[15] have been investigated. However, in those studies, penetration depth is limited - most lithium ions do not penetrate more than about 25 mm. Some investigations compared different methods, such as submitting samples to immersion, vacuum impregnation, wet-dry cycles or electrochemical migration and the latter showed to be the most suitable, providing better penetration and higher concentration [15], [16].

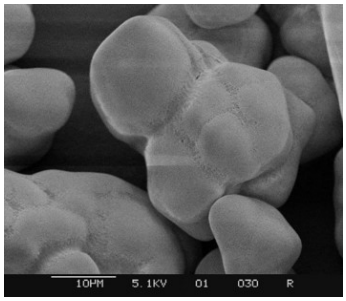

(a)

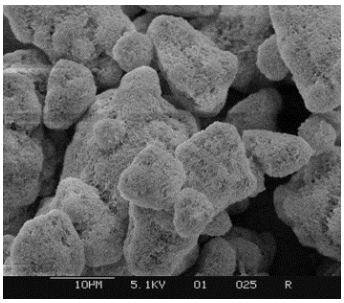

(b)

Figure 1.1: Scanning electron microscope images of opal particles after 28 days in $Ca(OH)_2$ and KOH solution. LiOH was added to the solution of the grains shown in (b). Figure (a) shows the formation of a gel-like product and the loss of angularity of the grains, indicating that dissolution or erosion took place. On the other hand, Figure (b) shows more angular particles, with rougher surface, indicating that lower levels of dissolution occurred and less product was deposited [13].

Electrochemical lithium migration has been investigated by numerous authors (e.g. [17], [15], [18], [19]). Nevertheless, there is still no consensus on the effectiveness of lithium migration as a treatment against deleterious ASR expansion. Indeed, deeper understanding of the basics behind lithium migration and its effects on ASR affected concrete is still necessary.

1.2. OBJECTIVE OF THE THESIS

THIS thesis aims to give further insights in the feasibility of electrochemical lithium injection as a treatment against deleterious ASR expansion. In order to do so, this project aims to elucidate qualitative and quantitative basics of lithium migration, oriented towards application, and possible effects on ASR affected concrete. A better understanding of lithium migration basics was obtained by studying the influence of different parameters on ionic transport, both experimentally and by means of a numerical model. Two-chamber set-ups, with external cathodes, were used in most experiments as this configuration allows both lithium ingress and alkali (sodium and potassium) removal. The influence of embedded cathodes on migration was also studied. The potential impact of ASR development (and possible cracking) on lithium migration was experimentally investigated. The effects of the electrochemical treatment on ASR development were evaluated by monitoring the post-treatment expansive behavior.

1.3. MODELING, NON-DESTRUCTIVE TESTING AND LI-BASED REMEDIATION OF DELETERIOUS ASR IN CONCRETE STRUCTURES

THE research developed in this thesis is part of a larger research project entitled "Modeling, non-destructive testing and Li-based remediation of deleterious Alkali-Silica

Reaction in concrete structures". The project was divided into three different topics, as shown in Figure 1.2. The first two subjects are being investigated at TU Eindhoven while the third, present in this thesis, was studied at TU Delft. The topic "Non-destructive measurement of sodium, lithium and water transport in cementitious matrix and ASR gel" is currently under investigation by the PhD candidate Sofiia Venglovska. The topic "The fundamentals of ASR and influence of lithium ions on the development of ASR", will be the subject of research in the near future. Finally, the project entitled "Lithium migration for remediation of ASR at macro level in existing (hardened) concrete" is present in this thesis.

The research project was funded by STW (Dutch Technology Foundation) and was part of a program entitled "Integral Solutions for Sustainable Construction" (IS2C).

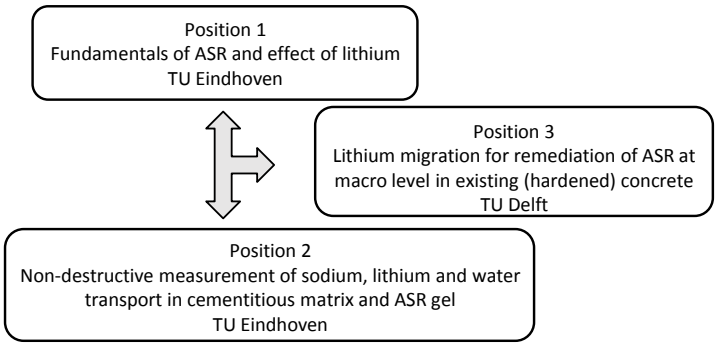

Figure 1.2: An overview of the IS2C project - Modeling, non-destructive testing and Li-based remediation of deleterious ASR in concrete structures.

1.4. OUTLINE OF THE THESIS

THIS thesis is composed by six chapters and it is organized as shown in Figure 1.3. Chapter 1 presents the introduction of the thesis with a brief overview on alkali-silica reaction, the limited available possibilities of repair and the use of lithium on as mitigation method.

Chapter 2 presents a literature review on ASR, the chemistry involved and proposed expansion mechanisms. A survey on preventive measures against ASR is then presented, with emphasis on the use of lithium-based admixtures. Currently available interventions against ASR are then reviewed and the limitations of their applications are discussed. Finally, a review of electrochemical lithium-based treatment against ASR is presented.

Chapter 3 evaluates the influence of various parameters on lithium migration in mortar specimens. The effect of use of different lithium solutions, at different concentrations and from different lithium salts, on migration is analyzed. This chapter also presents the investigation of the influence of treatment time on lithium transport and the possible effects of longer treatment periods on the specimens. Finally, a study on the influence of the use of embedded cathodes on migration is presented. As the reinforcement of structures affected by ASR may be used as cathode, like in treatments such as electrochem-

ical chloride extraction, this possibility needs to be investigated. The test parameters that provided best lithium migration, in terms of higher lithium content and best penetration depth, and least undesirable side effects were determined and used in following experiments.

Chapter 4 presents a mathematical model for ionic transport in porous media due to migration, diffusion and convection. In addition, it shows the numerical implementation of such a model for experiments presented in Chapter 3. Experimental results for electrolyte concentrations, ionic profiles in the specimens and passing current densities are compared with values obtained from the model, in order to validate it.

Chapter 5 investigates lithium migration in ASR affected concrete. Test parameters, such as anolyte solution and treatment time, were determined based on the findings of previous chapters. The influence of different expansion levels at the beginning of the treatment was studied as well as the effect of lithium migration on ASR expansion. This chapter also shows the effects of other treatments, such as lithium diffusion and alkali removal (under current), on ASR expansion.

Finally, Chapter 6 presents the concluding remarks and recommendations for future research.

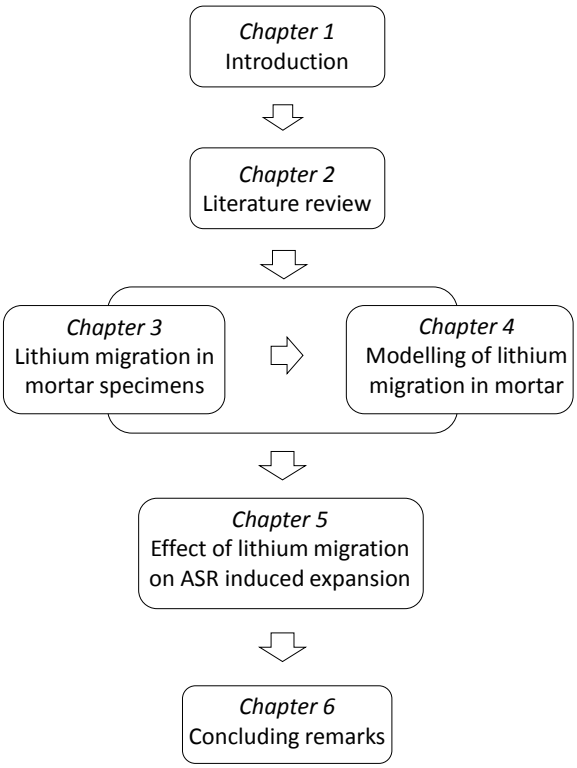

Figure 1.3: Thesis outline

1

REFERENCES

[1] L. M. S. Souza and R. B. Polder, *Studies on electrochemical lithium migration for remediation of alkali-silica reaction at macro level in concrete structures,* in *Proceedings of the Fifth International PhD Student Workshop on Durability of Reinforced Concrete. From Composition to Service Life Design* (VTT Technical Research Centre of Finland, 2012) pp. 50–62.

[2] T. G. Nijland and A. J. M. Siemes, *Alkali-silica reaction in the Netherlands: Experiences and current research,* Heron **47**, 81 (2002).

[3] A. Poole, *Introduction to alkali-aggregate reaction in concrete,* (Blackie, London, 1992) pp. 1–29.

[4] F. Rajabipour, E. Giannini, C. Dunant, J. H. Ideker, and M. D. Thomas, *Alkali-silica reaction: Current understanding of the reaction mechanisms and the knowledge gaps,* Cement and Concrete Research **76**, 130 (2015).

[5] M. D. Thomas, B. Fournier, K. J. Folliard, J. H. Ideker, and Y. Resendez, *The Use of Lithium to Prevent or Mitigate Alkali-Silica Reactions in Concrete Pavements and Structures*, Tech. Rep. FHWA-HRT-06-133 (Federal Highway Administration, 2007).

[6] P. J. Nixon and I. Sims, *RILEM Recommendations for the Prevention of Damage by Alkali-Aggregate Reactions in New Concrete Structures: State-of-the-Art Report of the RILEM Technical Committee 219-ACS*, Vol. 17 (Springer, 2015).

[7] W. McCoy and A. Caldwell, *New approach to inhibiting alkali-aggregate expansion,* in *ACI Journal Proceedings*, Vol. 47 (ACI, 1951).

[8] D. Stark, B. Morgan, and P. Okamoto, *Eliminating or minimizing alkali-silica reactivity*, Tech. Rep. SHRP-C-343 (Strategic Highway Research Program, 1993).

[9] R. L. Hooper, P. J. Nixon, and M. D. Thomas, *Considerations when specifying lithium admixtures to mitigate the risk of ASR,* in *Proc. 12 th Int. Conf. on Alkali-Aggregate Reaction in Concrete* (2004) pp. 554–563.

[10] X. Feng, M. Thomas, T. Bremner, B. Balcom, and K. Folliard, *Studies on lithium salts to mitigate ASR-induced expansion in new concrete: a critical review,* Cement and Concrete Research **35**, 1789 (2005).

[11] X. Feng, *Effects and Mechanisms of Lithium Nitrate on Controlling Alkali-silica Reaction*, Ph.D. thesis, University of New Brunswick (2008).

[12] K. J. Folliard, M. D. Thomas, B. Fournier, K. E. Kurtis, and J. H. Ideker, *Interim recommendations for the use of lithium to mitigate or prevent alkali-silica reaction (ASR)*, Tech. Rep. FHWA-HRT-06-073 (Federal Highway Administration, 2006).

[13] L. D. Mitchell, J. J. Beaudoin, and P. Grattan-Bellew, *The effects of lithium hydroxide solution on alkali silica reaction gels created with opal,* Cement and Concrete Research **34**, 641 (2004).

[14] D. Stokes, J. Pappas, M. Thomas, and K. Folliard, *Field cases involving treatment or repair of ASR-affected concrete using lithium,* in *Proceedings of the 6th CANMET/ACI International Conference on Durability of Concrete* (2002) pp. 631–642.

[15] M. Thomas and D. Stokes, *Lithium impregnation of ASR-affected concrete: preliminary studies,* in *Proceedings of the 12th International Conference on Alkali-Aggregate Reaction in Concrete* (2004) pp. 659–667.

[16] A. Santos Silva, M. Salta, M. Melo Jorge, M. Rodrigues, and A. Cristino, *Research on the suppression expansion due to ASR. Effect of coatings and lithium nitrate,* in *Proceedings of the 13th International Conference on Alkali-Aggregate Reaction in Concrete* (2008).

[17] D. Whitmore and S. Abbott, *Use of an applied electric field to drive lithium ions into alkali-silica reactive structures,* in *Proceedings, 11th International Conference on Alkali-Aggregate Reaction* (2000) pp. 1089–1098.

[18] T. Ueda, Y. Yoshida, K. Yamaguchi, and M. Ashida, *Electrochemical migration of lithium ions into hardened concrete and ASR expansion after treatment,* Proceedings of structural faults & repair-2006 (2006).

[19] J. Pacheco and R. B. Polder, *Preliminary study of electrochemical lithium migration into cementitious mortar,* in *2nd International Symposium on Service Life Design for Infrastructures* (RILEM Publications SARL, 2010) pp. 1093–1100.

2

LITERATURE REVIEW

Parts of this chapter have been published in Souza and Polder, Fifth International PhD Student Workshop on Durability of Reinforced Concrete, 2012) [1].

2.1. ALKALI SILICA REACTION - OVERVIEW

ALKALI-silica reaction (ASR) is a deleterious process in which alkali and hydroxyl ions from the pore solution in concrete react with reactive siliceous compounds from the aggregate. Hydroxyl ions dissolve the silica structure, which then acts like a hygroscopic silica gel. Alternatively, a hygroscopic ASR gel is formed from the dissolved silica. Either way, the gel (or gel-like structure) swells, leading to the development of internal stresses and expansion and cracking of the concrete element [2], [3].

ASR symptoms include cracking, misalignment of structural elements, closing of joints, spalling of concrete over reactive aggregate particles and gel exudation from cracks [2],[4]. Figure 2.2 shows examples of ASR effects.

Concrete structures worldwide are affected by alkali-silica reaction. Stanton [5] first reported it in 1940, in his investigation on cracked concrete structures in California. Since then, numerous cases have been reported all over the world. In fact, in 1992, Poole [2] reported that only a few countries had not identified structures damaged by ASR and that there were affected constructions in all continents. It is a slow degradation mechanism - although it typically takes from 5 to 15 years for its effects to be noted, there are reported cases in which damage was observed only after 25-40 years post construction [2].

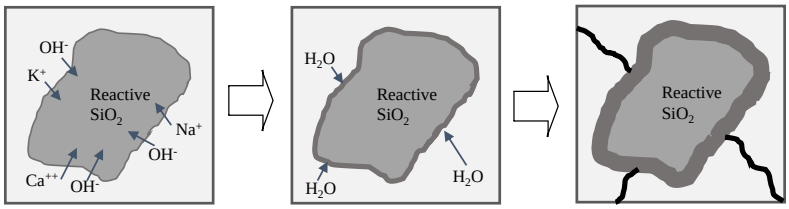

Figure 2.1: Scheme showing ASR evolution. Hydroxyl and alkali ions react with reactive silica in aggregate particle, producing a hygroscopic gel. As the gel absorbs water, it expands, leading to expansion and cracking of the concrete element(adapted from [4] and [6]).

2.1.1. CHEMISTRY OF ALKALI SILICA REACTION

SILICATES are primarily composed of a 3D framework of silica (SiO_2) tetrahedrons, with four oxygen atoms surrounding a central Si atom [3],[10],[11]. The reactivity of the silica in the aggregate depends on its crystal structure. In order to be ASR reactive, the siliceous aggregate should have a poorly crystalline form of silica or contain many lattice defects or be amorphous (or glassy). Opaline silica, chalcedony, volcanic glass and cryptocrystalline (or microcrystalline) quartz are some of the materials that have been identified as ASR reactive in concrete [2].

Dent-Glasser and Kataoka [12], [13] described the dissolution of the reactive silica as a two-stage process. First, the high pH pore solution attacks the reactive silica, breaking the siloxane bonds (Si-O-Si) into silanol (Si-OH) bonds. Then, hydroxyl ions react with the silanol bonds previously formed, converting them into $Si\text{-}O^-$ groups. Siloxane bonds may also be attacked by hydroxyl ions and form $Si\text{-}O^-$ groups. The reactions of silica dissolution are shown below:

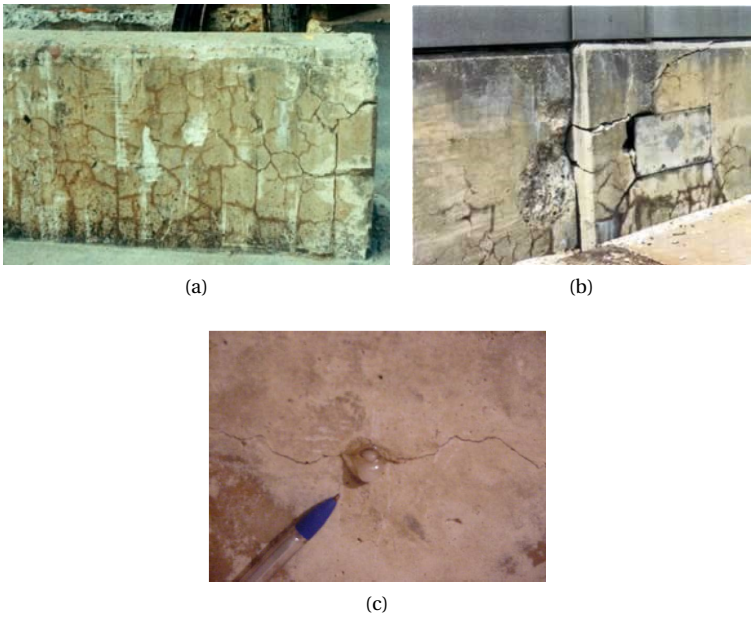

(a) (b)

(c)

Figure 2.2: (a) ASR-induced map-cracking [7]; (b) Misalignment of adjacent concrete elements due to ASR expansion [8]; (c) Gel exuding from a crack [9].

$$Si-O-Si+H_2O \longrightarrow Si-OH...HO-Si \tag{2.1}$$

$$Si-OH+OH^- \longrightarrow Si-O^- + H_2O \tag{2.2}$$

$$Si-O-Si+2OH^- \longrightarrow Si-O^- + {}^-O-Si+H_2O \tag{2.3}$$

Depending on the amount of hydroxyl ions available, this process will repeat many times, fragmenting the once three dimensional silica framework into separate groups, of variable sizes, with Si-O^- groups [14]. The negative charge of the silicate anions can be balanced by sodium and potassium, which are available in the pore solution [3],[12]. For example, in the case of sodium, the following reaction takes place:

$$Si-O^- + Na^+ \longrightarrow Si-O...Na \tag{2.4}$$

Some of the incorporated sodium (or potassium) ions might later be replaced by calcium ions and return to the pore solution, in a process called "alkali recycling" [3]:

$$2Si-O...Na+Ca^{++} \longrightarrow 2Na^+ + Si-O...Ca...Si-O \tag{2.5}$$

In addition, calcium ions also balance the negative charge of the silicate anions:

$$2Si - O^{-} + Ca^{++} \longrightarrow Si - O...Ca...O - Si \tag{2.6}$$

Finally, an amorphous or poorly crystalline alkali silica gel is formed. It is believed that the presence of calcium is necessary for the gel to be formed - otherwise, only the dissolution of silica takes place (e.g. [15],[16]). The composition of the ASR gel varies with time and location in the concrete element. The gel inside of cracks has a higher calcium content than the gel in the aggregate, whereas the opposite trend is observed regarding silicon concentrations [17],[18]. Nevertheless, the ASR gel generally has a high silica content, lower calcium content and low alkali content. The silica and calcium levels are highly variable while alkalis are found in relatively constant levels [18].

The gel is usually located around the reactive aggregate particle, if the latter is entirely composed by reactive silica [3],[19]. However, it can also be located within the aggregate particle, when the aggregate is composed of reactive silica distributed in a matrix of non-reactive material or in the presence of micro-cracks. In these cases, the pore solution diffuses into the aggregate, where the reaction takes place [3].

2.1.2. EXPANSION MECHANISM OF ASR

DIFFERENT mechanisms have been proposed in order to explain concrete expansion due to ASR throughout the years. Hansen [20] proposed that the hardened cement paste around reactive aggregate particles would act as a semi-permeable membrane. It would allow water, hydroxyl ions and alkali ions to pass through, but it would prevent the diffusion of larger silicate ions. This way, osmosis would occur: water would be drawn into the alkali-silicate gel and it would build up a hydraulic pressure against the cement paste. Eventually, the osmotic pressure would lead to the expansion and cracking of the cement paste.

Similarly, Chatterji et al. [21] attributed expansion to the different transport rates of species (water, sodium, calcium and hydroxyl ions) quickly moving into the reactive aggregate and silicon ions slowly moving outwards. Consequently, the accumulation of species in the particle would lead to the generation of expansive force.

The absorption theory defends that ASR expansion would be caused by water absorption of the gel [22]. In this theory, as the gel absorb water, it swells. Once the it reaches a certain level of swelling, internal stresses would be developed, resulting in expansion and cracking of the concrete. The magnitude of the expansion would depend on the volume fraction of the gel and its physical properties [22]. On the other hand, Powers and Steinour [23] proposed that both absorption and osmosis theories are fundamentally in harmony. According to the authors, expansion is caused by swelling of the gel due to water absorption, if the gel is solid. However, if the gel is liquid or plastic, expansion is caused by the action of hydraulic (osmotic) pressures.

Prezzi et al. [24] developed a model based on the electrical double-layer theory. When the silica dissolution takes place, its surface becomes negative. The model defends that an electrical double layer of cations from the pore solution (i.e. sodium, potassium and calcium ions) is formed to balance the negative charge. The repulsion effects of the double-layer lead to the expansion of the gel.

Garcia-Diaz et al. [25] proposed that the ASR expansion is caused by the de-polymerization

of Q_4 [1] silica tetrahedrons (siloxane bonds) into Q_3 sites, during the attack of the siloxane bonds by hydroxyl ions. The transition causes swelling and micro-cracking of the aggregate and increases its specific pore volume up to seven times.

2.2. MEASURES TO PREVENT ASR

FOUR components are essential for the development of ASR [2], [3], [14], [28], [29], [30]:

- Critical amount of reactive silica
- Sufficiently alkaline pore solution
- Source of soluble calcium (e.g. portlandite) to form deleterious gel
- Sufficient moisture

Limiting the availability of one or more of those components will prevent deleterious ASR expansion in new concrete. Using non-reactive aggregate seems to be the most straightforward method to avoid ASR. However, this method is frequently impractical, due to limited availability in several places [3], [11]. In addition, cases have been reported of aggregates that showed to be ASR reactive in the field even though they were classified as non-reactive by laboratory tests [11].

The alkalinity of the pore solution can be limited by using low alkali cement (less than 0.60% sodium oxide equivalent (Na_2O_{eq}) [2], limiting the alkali content of the concrete mixture and by using sufficient amounts of supplementary cementitious materials [30]. Even though the use of low alkali cements has demonstrated to be effective, there have been occasional reports of deleterious expansion in concretes with such cements [30]. In addition, this measure might not be effective if there are other sources of alkalis, such as aggregates, admixtures or external sources (e.g. seawater or de-incing salts)[11], [30].

When limiting the alkali content of the concrete mixture, not only the alkalis from cement are considered, but also other sources are taken into account. This measure is acknowledged the most easily applied and monitored of all methods[3]. For aggregates of medium reactivity, the limit is typically between 2.5 – 3.0 kg/m^2 Na_2O_{eq} [29],[30]. Although considering sources of alkalis other than the cement is a good practice, it is not clear how much of the total content of alkalis from such sources is leachable. Rajabipour et al.[3] recommend that, in structures with high risk of ASR, the limitation of alkali content should be considered in combination with the application of other measures.

The use of supplementary cementitious material (SCM), such as low lime fly ash, silica fume and blast furnace slag, is the most common measure to control ASR in new structures [3], [30]. These materials control ASR development by decreasing the pH of the pore solution (due to alkali binding alkali), consuming portlandite and reducing mass transport (due to pore refining) [3], [29], [31], [32]. There is also evidence that the

[1] Q_n, with $n = 0..4$, is a notation for a silicon tetrahedron with four oxygen attached; n indicates the number of 'Si'units connected through the oxygens to an individual silicon atom (forming Si-O-Si bonds) [25], [26], [27].
[2] $\%Na_2O_{eq} = \%Na_2O + 0.658\%K_2O$

aluminum present in some SCM (such as fly ash and metakaolin) may have beneficial effects mitigating ASR development [33], [34]. The proportion of SCM necessary to prevent deleterious expansion depends on the type of SCM and on the reactivity of the aggregate [30].

There is evidence that at relative humidity (R.H.) values below 80%, ASR expansion is reduced or suppressed [8]. The access of water to the concrete structure can be reduced by external cladding or tanking (protection that uses a waterproof barrier). However, this is not an effective method in cold and very humid environment. Surface treatments, such as coatings and impregnations (such as silanes and siloxanes) aim to prevent the ingress of water at the same time it allows internal moisture, in the form of vapor, to escape [35]. Nevertheless, the application of such products has exhibited variable performance and it is not regarded as a preventive method against ASR expansion [30].

Finally, the addition of lithium compounds in the concrete mix is regarded as an effective means of controlling ASR deleterious expansion [3],[4],[30]. This last preventive measure will be discussed in more details in the following subsection.

2.2.1. EFFECTS OF LITHIUM ADMIXTURES AGAINST ASR

THE incorporation of lithium based admixtures has been investigated since the 1950's. McCoy and Cadwell [36] reported the beneficial effects of the addition of lithium salts in the reduction or prevention of ASR deleterious expansion in mortar bars containing Pyrex glass as aggregate. Their investigation studied over 100 different compounds and lithium salts (LiCl, Li_2CO_3, LiF, Li_2SiO_3, $LiNO_3$ and Li_2SO_4) were the most effective in mitigating ASR expansion. The minimum lithium to alkali (sodium and potassium) dosage molar ratio ($\frac{[Li]}{[K]+[Na]}$) to suppress the reaction was 0.74.

Since then, several authors (e.g. [37], [38],[39]) have studied the influence of the addition of various lithium salts on the expansive behavior of concretes and mortars composed with different reactive aggregates.

The amount of lithium to prevent ASR deleterious expansion strongly depends on the nature of the aggregate, the alkali content and the type of lithium compound [4],[40],[41]. In high alkali content concrete, the minimum lithium to alkali molar ratio necessary to prevent expansion varies between 0.67 and 1.20, for different combinations of reactive aggregate, alkali content and lithium compound [40]. If the dosage of lithium is insufficient, higher levels of expansion can be observed, when compared to control samples (without lithium). This is known as the "pessimum effect" and is probably caused by the increase of alkalinity with the addition of certain lithium compounds, especially LiOH [40].

Among all lithium salts investigated, $LiNO_3$ is the preferred one. It does not increase the alkalinity of the pore solution, as it has neutral pH and it is highly soluble [4],[30],[40]. Indeed, commercially available lithium-based admixtures to prevent ASR expansion are $LiNO_3$ solutions (e.g. Sika®Control ASR and Lifetime ®N admixture).

Although the benefits of the addition of lithium compounds against ASR expansion in new concrete has been acknowledged for years, the mechanisms involved are not still fully understood. According to Rajabjpour et al. [3], Feng et al. [40] and Folliard et al. [42], the main proposed mechanisms include:

- Alteration of ASR gel composition into a less expansive product by lithium;

- Reduction of the dissolution rate of silica by lithium;
- Lithium may hinder the formation of ASR gel by decreasing the ASR gel repolymerization;
- The repulsive forces between colloidal particles of the ASR gel may be reduced by lithium.

2.3. SUGGESTED INTERVENTIONS AGAINST ASR

THE intervention methods for ASR detected in existing structures can be divided into two categories: those that deal with the symptoms and measures that address the causes of ASR (that is, that interfere with the mechanism of the reaction) [4], [28].

Methods that minimize or manage the symptoms include crack filling, cutting and applying restraint or confinement. Crack caulking/filling can recover the integrity of cracked concrete and protect the structure against the ingress of deterioration agents (e.g. water, external alkalis, chlorides). Flexible grouts or caulking are generally more effective in filling the cracks [4],[35].

Cutting joints is helpful in relieving the stresses generated by ASR. This method has been applied in various massive hydraulic structures, such as dams. As this measure does not stop (or reduce) ASR expansion, it is common that new joints need to be cut again after some time [4],[35].

The application of restraint or confinement (e.g. enclosing of the affected element by new non-reactive concrete or fiber-reinforced polymers, applied stress or reinforcement) has shown to be effective in reducing ASR expansion [3],[35]. This method affects the structural behavior of the construction and requires detailed structural analysis before the implementation of the measure [35]. Figure 2.3 shows a foundation elements receiving post-stressed reinforcement in order to mitigate ASR.

Amongst the approaches that address the causes of ASR are the use of coatings and penetrating sealants, cladding and drains or treatment with lithium compounds. Methods such as the application of coatings, cladding and drains as a mitigation measure aim to reduce the access to water, as previously discussed. Improving drainage may redirect the water away from an ASR affected structure. The application of cladding may be interesting; however, the remaining moisture in the structure might be sufficient for ASR development [35]. Although the use of coatings and penetrating sealants (such as silanes and siloxanes) is not recommended as a preventive measure by RILEM [30], their application on ASR affected concrete is regarded as effective in reducing further expansion by other authors [35], [44], [45].

Figure 2.4 shows the comparison between two sections, one treated with silane and the control, three years after the application. It is possible to observe that the treatment prevented further expansion and cracking. Nevertheless, there are limitations. In massive concrete structures or structures that are fully submerged, for example, it is unlikely that a topical treatment will decrease the relative humidity of the core. In concrete with large width cracks, it is necessary to close those cracks before the treatment [35],[44].

Treatment of ASR affected concrete with lithium compound solutions has been investigated by various authors. Applying lithium solutions by methods such as immersion, ponding or wet and dry cycles is effective in reducing further ASR expansion in

Figure 2.3: Post-tensioned reinforcement on a foundation element affected by ASR. In this case, Dywidag ST 85-105 steel rods were placed in parallel to the longest sides of the element. The tension was distributed to the concrete block through three metallic profiles placed on the shortest sides. The concrete used to encapsulate the element had non-reactive aggregate and the addition of micro silica, in order to avoid ASR[43].

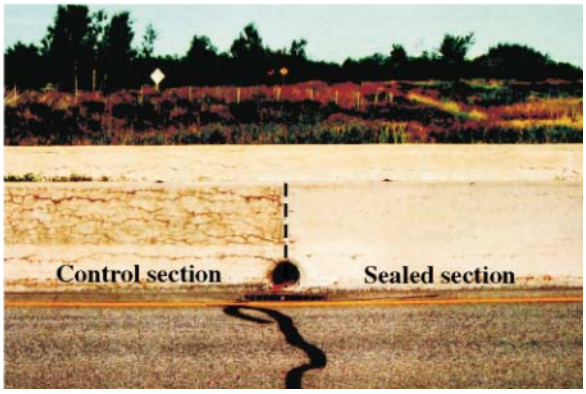

Figure 2.4: Comparison between silane-sealed and unsealed sections. The control section has far more cracks than the treated one. The photo is from three years after the application of silane[44].

small laboratory specimens [28], [46], [47]. Stark [28] dried the specimens for a day and soaked them for two days in saturated LiOH, Li_2CO_3 and LiF solutions. In all cases, the remaining expansive behavior was significantly reduced, when compared to the control.

Thomas and Stokes [46] investigated the penetration depth of lithium ions in specimens that were submitted to different treatments, using 30% $LiNO_3$ solution: immersion, wet and dry cycles and vacuum impregnation. Immersion was the method that led to lowest contents of lithium, whereas vacuum impregnation led to the best results in terms of lithium content and depth of impregnation (of at least 30 mm). Even though wet and dry cycles resulted in lithium impregnation of only the first 20-25 mm, the treatment reduced expansion, when compared to the untreated case. Kawamura and Kodera [47] treated mortar specimens by immersion in 0.5 M LiOH solution at different ages. The treatment is effective in reducing the remaining expansion. However, the authors obtained similar results by immersion in water, which could indicate that the reaction was affected by leaching of sodium and potassium rather than by the ingress of lithium.

On the other hand, there is little information on the effectiveness of this type of treatment in structures in the field [35]. Stokes et al. [48] presented the case of topical application (spraying) of a 30% $LiNO_3$ on an ASR affected pavement during three years. Cores were extracted and lithium concentration profiles were obtained. In uncracked concrete, lithium reached penetrations of 20-30 mm. In moderately cracked concrete, lithium was found until the deepest analyzed portion (50 mm), indicating that possibly even further penetration took place. It is not clear though whether lithium was found at deeper portions in the region between cracks. After the three years of treatment, untreated sections presented higher levels of deterioration than the treated ones.

Folliard et al. [49] reported field application of lithium treatment in various structures affected by ASR. A pavement section was treated by topical applications of 30% $LiNO_3$ solution, as show in Figure 2.5. Limited lithium penetration was observed. In fact, the authors pointed out that only the first 4 mm had received enough lithium to suppress the reaction.

Another case reported by Folliard et al. [49] was the treatment of highway barriers with 30% $LiNO_3$ solution by topical applications and vacuum impregnation, shown in Figure 2.6. Again, lithium penetration was limited and only the first 2-4 mm of the structure received enough lithium to avoid further expansion. Information regarding the expansive behavior of those elements during over five years was published in another work [45] and neither treatment method was effective in reducing expansion.

Vacuum impregnation was also applied to a bridge column [49] and, although the penetration was higher than in the cases previously discussed, it was still limited to the first 10-15 mm. The region in the first 8-10 mm had enough lithium to suppress ASR, according to the authors. Nevertheless, as Drimalas et al. [45] later reported, the treatment was ineffective in preventing further expansion in the treated columns.

Electrochemical lithium treatments resulted in deeper penetrations and higher lithium concentrations when compared to the methods previously discussed [46], [50], [49]. Figure 2.7 shows the comparison between vacuum impregnation and electrochemical treatment regarding lithium concentration and it is clear that the use of current led to much higher lithium contents. In the following section, investigations on electrochemical lithium treatments will be discussed.

Figure 2.5: Topical application (spraying) of $LiNO_3$ solution to an ASR affected pavement [49].

(a) (b)

Figure 2.6: Treatment of highway barriers by topical application (a) and vacuum impregnation (b)[49].

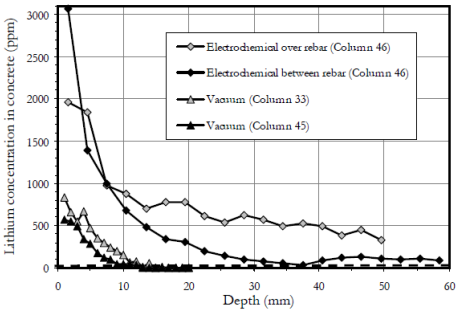

Figure 2.7: Lithium concentrations obtained after electrochemical treatment and vacuum impregnation of bridge columns[49].

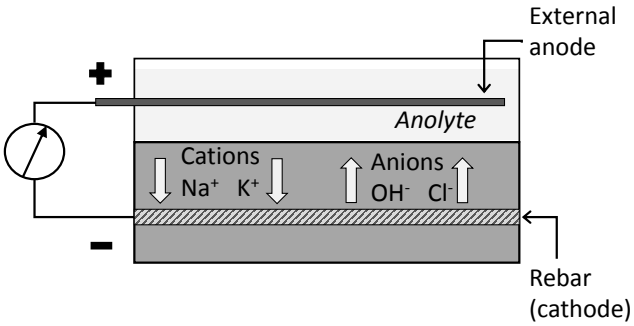

Figure 2.8: Schematic diagram of the ionic movement during ECE. Positive ions move towards the cathode (negative electrode), whereas negative ions move in direction of the anode (positive electrode).

2.4. ELECTROCHEMICAL TREATMENT AGAINST ASR

IONIC migration is the movement of ions in solution due to an electrical field. The velocity in which the ion moves, as well the direction, depend on its characteristics, such as charge and size, and on the strength of the electrical field. Positive ions migrate towards the negative electrode (cathode) and the negative ones go in the opposite direction, attracted by the anode [51].

In concrete structures the application of an electrical field to transport ions is the principle behind electrochemical chloride extraction (ECE). Generally, during this treatment, an electrical field is imposed between the reinforcing steel and an external electrode immersed in an anolyte solution. Chloride ions are forced out of the concrete, attracted by an external anode. A schematic diagram with the ionic movement during ECE is shown in Figure 2.8.

The use of an electrical field to transport lithium ions into concrete was first suggested by Page [52] in order to avoid ASR development induced by the alkalization of the region around the rebar in structures under ECE. Whitmore and Abbot [53] described the application of modified ECE to two bridge decks in the 90's. The treatment procedure was the same as for usual ECE, except that instead of water, a lithium borate (Li_3BO_3) solution was used as anolyte solution. The treatment lasted eight weeks. Dust samples were collected from the first 32 mm of one of the decks and analyzed for lithium content. The lowest concentration was obtained at 19 to 32 mm from the surface and was 203 ppm. The authors made a rough estimation of the target concentration and that would be 80 ppm. Therefore, the results showed that lithium migration was achieved in a relatively short time of treatment. Nevertheless, neither the maximum depth of penetration nor the effects of the treatment on ASR were investigated.

Matsumoto et al. [54] evaluated the effect of lithium migration on carbonated and ASR affected concrete. ASR reactive concrete prisms were cast with a reinforcement bar placed longitudinally, as shown in the scheme of Figure 2.9. They went under accelerated carbonation for up to five months and then received the electrochemical treatment for one or three weeks, under current density of 1.0 A/m^2 (in relation to concrete surface). The reinforcement bar was used as cathode and the anolyte solutions were a 2 N

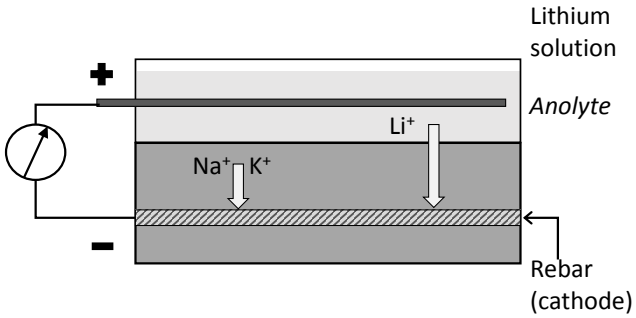

Figure 2.9: Schematic diagram of a lithium migration test using reinforcement bar as electrode.

Li_3BO_3 solution or a 1 N Na_2CO_3 solution. The latter is usually used in realkalization treatments. After the treatment, the specimens were placed under ASR accelerating conditions (40 °C / R.H. 95%) for one year. Results show that both solutions worked well against carbonation. The specimens treated with Li_3BO_3 had $\frac{[Li]}{Na}$ molar ratios above 1.0 in the region near the surface. However, in the area around the rebar, much lower $\frac{[Li]}{Na}$ ratios were found. Nevertheless, the use of Li_3BO_3 led to lower levels of expansion when comparing to the specimens treated with Na_2CO_3. Interestingly, even though the longer treatment led to higher levels of lithium ingress, the influence of the treatment duration could not be observed on the expansion behavior. Finally, it is unclear whether lithium reduced the expansion or the extra sodium injected during the treatment with Na_2CO_3 aggravated the problem.

The effect of ASR expansion (and cracking) on lithium migration was investigated by Thomas and Stokes [46]. In their work, ASR reactive concrete cylinders (50 mm of height) were cast and submitted to ASR accelerating conditions (storage over water at 38 °C) until different levels of expansion and cracking were achieved, as shown in Table 2.1. Then, the specimens were vacuum impregnated with limewater and placed in a two-chamber migration cell, similar to the one prescribed by ASTM C 1202 [55], as shown in the scheme of Figure 2.10. In this type of set-up, not only lithium is transported into the specimen, but also sodium and potassium ions are forced to leave the specimen, which also contributes to reducing further ASR expansion.

The catholyte was a mixed solution of 0.3 M KOH and 0.1 NaOH saturated with $Ca(OH)_2$, whereas the anolyte consisted of a 30% $LiNO_3$ solution. The voltage of 20 V was applied and the duration of the experiment varied between 35 and 101 days, depending on the expansion level. Lithium concentration in the catholyte was monitored and it showed that the higher the pre-existing level of expansion (and cracking) of the specimens, the faster lithium could reach the catholyte chamber. After testing, lithium concentration profiles in the specimen were obtained. Interestingly, the specimen with the highest expansion (and the most visible cracks) had highest content of lithium, despite the shortest migration time. Nevertheless, significant lithium content was detected throughout all samples.

A number of other studies were also conducted in two-chamber set-ups, similar to

Table 2.1: Expansion and cracking of tested specimens over time (adapted from [46]).

Curing time [1](days)	Expansion (%)	Cracking	Duration of test (days)
28	0.018	No visible cracking	101
70	0.061	Hair cracks	42
112	0.107	Significant map cracking (crack width up to 1 mm)	35

[1] Period of exposure to ASR accelerating conditions prior to testing.

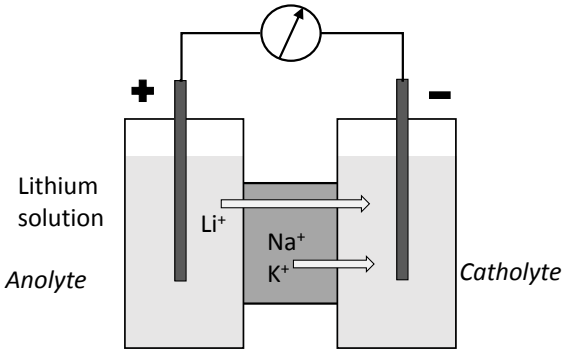

Figure 2.10: Schematic diagram of two-chamber migration set-up.

the one in Figure 2.10. In a preliminary study of migration of lithium ions, Pacheco and Polder [56] tested non-reactive mortar samples of water to cement ratio (w/c) ratio of 0.5. The specimens were cylinders with 100 mm of diameter and 50 mm of height. The anolyte was a 1 M $LiNO_3$ solution and a 0.3 M solution of NaOH was the catholyte. The migration mechanism was evaluated in tests with applied voltages of 20 and 40 V, for 28 days. Some samples were also tested at 40 V for 7 days. During the tests, the passing current was recorded and, once they were finished, lithium concentration profiles of the specimens were obtained.

Results showed that the lithium content after the test depended on the time and applied voltage. Nevertheless, the concentration of lithium decreased towards the catholyte regardless of the conditions of the test. Some specimens had $LiNO_3$ added to the fresh mixture, with $\frac{[Li]}{[Na_2O_{eq}]}$ ratio of 1.0, to be considered as reference. The measured concentration of lithium in those specimens was 600 ppm. After four weeks of treatment, the content of lithium in the first 10 mm was between 600 and 900 ppm. The maximum concentration was obtained in the test with applied voltage of 40 V during four weeks and it was about 1000 ppm in the first 5 mm. Nevertheless, even in this case, only the first 10 mm had a concentration above 600 ppm. The authors observed an increase of specimen resistance during the test. However, 24 hours after the end of the experiment, the resistances decreased to values close to what was initially observed. They suggested that this variation might be related the evolution of gas bubbles at the electrode and/or to changes in the pore solution composition.

Lee et al. [57] investigated the influence of the thickness of the specimens on lithium ion migration in a two-chamber set-up. For that, concrete discs with 100 mm of diameter and thickness varying from 50 to 200 mm were tested at the age of 28 days. In the concrete mixture, reactive sandstone was used as aggregate, the Na_2O_{eq} was adjusted to 1.25% by addition of NaOH and the w/c was 0.6.

The specimens were tested under constant current density of 9.0 A/m^2 during 30 days. A solution of 1 N LiOH and a saturated solution of $Ca(OH)_2$ were used as electrolytes. During the test, sodium and lithium contents in the cathodic cell solution were measured. The results showed the sodium ions were removed from the specimens and accumulated in the catholyte during the experiment. The sodium content of the specimens after the treatment decreased to values lower than 3.0 kg/m^3 Na_2O_{eq}. Therefore, in their work, the removal of sodium alone would be enough to prevent or reduce further ASR. Regarding the movement of lithium ions, the authors concluded that the time for the ions to pass through the sample was directly proportional to its thickness. The average $\frac{[Li]}{[Na]}$ molar ratios of all samples, regardless the size, were higher than 2.0, above the known mitigation values. However, most lithium ions were concentrated in the first 25 – 30 mm from the exposed surface. It is noteworthy that $CaCO_3$ crystals blocking the pores were found in all specimens, leading to the increase of resistivity of the samples during the test. In order to evaluate the effect of the treatment on the expansive behavior, treated specimens were submitted to ASR accelerating conditions (38 °C and 100% R.H.) for one year and the results indicate reduction of rate of expansion.

Instead of evaluating the treatment of cast specimens, Santos Silva et al. [50] tested cores from concrete railway sleepers, which were cracked by ASR and delayed ettringite formation. Some cores went under the electrochemical treatment while others were submitted to different mitigation techniques such as the application of different coatings, immersion in 30% $LiNO_3$ solution and wet and dry cycles with 30% $LiNO_3$ solution. Regarding the electrochemical method, cores with length of 50 mm and diameter of 74 mm were treated in two-chamber set-ups for a week under 20, 40 and 60 V. In this study, the electrolytes were water and a 30% $LiNO_3$ solution. Like in other studies, the authors observed the influence of the applied voltage on the efficacy of the ionic transport – the higher was the voltage, the higher were the levels of ionic transport. The alkali removal from the cores was also noted. In comparison to immersion or wet and dry cycles, migration was the method that led to higher lithium transport in both concentration and depth of penetration. The effect of the electrochemical treatment on the expansion behavior was evaluated on cores treated under 60 V. After the treatment, they were placed in a fog chamber at 20 °C and 95% R.H for 180 days. The results indicated that the electrochemical treatment had better effect on the expansion than the application of coatings. However, untreated samples were not evaluated, making it difficult to analyze the efficacy of the treatments.

The behavior of the sodium, potassium and lithium ions in mortar under an electrical field was investigated by Liu et al. [58], also in a two-chamber set-up. The electrolytes were 1 N LiOH solution and a saturated $Ca(OH)_2$ solution. The mortar was produced with reactive meta sandstone, w/c of 0.5 and the total Na_2O_{eq} was 11.37 kg/m^3. The specimens were cylinders with diameter of 100 mm and 50 mm of height and were cured for three months at 23 °C and 100% R.H. before being tested. Five different voltages were

used, 12, 18, 24, 30 and 40 V, and the tests stopped once the flow of lithium had reached steady state (approximately 33 days for the test at 40 V and 50 days for the rest).

The authors observed that the removal time of sodium and potassium ions depended on the applied voltage. They also noted that the time for lithium ions to go through the sample decreased when the applied voltage increased. Interestingly, the specimen treated under 24 V had higher levels of lithium after the treatment then the one treated under 30 V. The concentration data for the experiment with 40 V was not reported. The alkali contents of all other specimens after the treatment were less than 0.6 kg/m^3 and the average $\frac{[Li]}{[Na+K]}$ ratios were above 9. Once again, it must be noted that most ions were concentrated in the first 30 mm from the exposed surface.

Wang et al. [59] investigated the effect of the anolyte solution on lithium migration. The concrete mixture had reactive metasandstone and the alkali content was increased to 1.25% Na_2O_{eq} by NaOH addition. Concrete cylinders (100 mm in diameter and 50 mm in height) were tested in two-chamber set-ups after 28 days of curing (23 °C and 100% R.H.). Constant current density of 9.0 A/m^2 was applied during 30 days. The investigated anolyte solutions were 1 N LiOH, 1 N $LiNO_3$, oversaturated Li_2CO_3 and oversaturated $Li_2B_4O_7$ whereas the catholyte was a saturated $Ca(OH)_2$ solution in all cases. The authors observed increase in resistivity in the tests with LiOH and $LiNO_3$ solutions. In the case of LiOH, they attributed it to the formation of $CaCO_3$ crystals on the specimen on the cathodic side, while in the case of $LiNO_3$, a "sticky reddish brown precipitate" was formed on the anodic side of the specimen. Nevertheless, those cases presented the highest levels of lithium in the specimen after the test. In addition, sodium was removed from the specimens and the remaining Na_2O_{eq} was below 1.0 kg/m^3 in all cases. The specimens had $\frac{[Li]}{Na}$ molar ratios above 1.90 in all regions after migration. Regarding the expansive behavior one year after the experiment, all treated specimens presented less expansion than the control and 1 N LiOH was the most effective solution.

Lizarazo-Marriaga et al. [60] evaluated the efficiency of the electrochemical treatment in mortar bars of 25 mm x 25 mm x 290 mm. The mixes were prepared according to the ASTM 1260 [61] mortar bar test and a reactive Colombian aggregate and a blended limestone cement (Na_2O_{eq} of 0.57%) were used. After curing in water at 80 °C for 24 hours, two specimens received the treatment for four days, before being placed under ASR accelerating conditions (as prescribed by the ASTM 1260, the specimens were immersed in a 1 N NaOH solution at 80 °C). The control specimens were placed in ASR accelerating environment after curing. A two-chamber set-up was used with a 30% $LiNO_3$ solution as anolyte and a 0.3 M KOH and 0.1 NaOH mix solution as catholyte. One set of specimens was treated under 15 V and the other under 20 V. Results show that treated specimens exhibited less expansion than the control cases and the application of a higher voltage was more effective.

As in the case for ECE treatment, lithium based electrochemical treatment of existing structures might use the reinforcement bars are electrodes. Therefore, it is reasonable to perform laboratory investigations with the use reinforced concrete specimens. In this kind of arrangement, lithium ions from the electrolyte migrate in towards the direction of the reinforcement bar, as shown in Figure 2.9. As the cathode is placed inside the concrete, sodium and potassium cations are not expected to be removed, as it was observed in the two-chamber set-up. In fact, those ions will accumulate in the area around the

steel bar.

Ueda et al. [62] applied the electrochemical treatment to concrete prismatic specimens (100 x 100 x 200 mm) with a steel bar located at the center of the cross-section. In the concrete mixture, reactive silica sand with opal composition mixed with non-reactive sand (in the weight ratio of 0.061) was used as fine aggregate, the coarse aggregate was non-reactive and the Na_2O_{eq}content of the mixture was 8.0 kg/m^3 (increased by NaCl addition). After curing for 28 days at 20 °C, the specimens went through the electrochemical treatment. Once the treatment was finished, some samples were exposed to ASR accelerating conditions (40 °C, R.H.: 95%) for 160 days. In this work, the electrolyte was LiOH, in two different concentrations (2 and 5 N) and three treatment duration (4, 8 and 12 weeks) were evaluated. Current was applied between the bar (working as cathode) and an external anode placed near the exposed surface and the current density was kept constant at 1.0 A/m^2. After the tests, it was observed that sodium and potassium ions tend to accumulate near the cathode and most of lithium ions did not go farther than 20 mm from the exposed surface. In the region near to the anolyte, the $\frac{[Li]}{[Na]}$ molar ratio was above 1.0 in all cases. However, it greatly dropped in the region close to the rebar.

Interestingly, the authors commented that the electrolyte concentration and treatment period did not greatly influence the penetration of lithium ions. That fact might be explained by the low current density used. On the other hand, when evaluating the expansion behavior after treatment, the authors pointed out that the treatment with 5.0 N LiOH solution was more effective than when the solution of lower concentration was used.

In Ueda et al. [63] similar set-ups were used. However, different treatment conditions were investigated. Concrete prisms (100 x 100 x 300 mm) were cast with an embedded steel bar in the middle of the cross-section. Concrete with different w/c ratios (0.45 and 0.60) were studied. The fine portion of the aggregate was non-reactive. The coarse aggregate, on the other hand, was composed by reactive and non-reactive aggregate, mixed in the pessimum weight ratio of 6:4. NaCl was added to the mixing water in order to adjust the total alkali content of the mixture to 8.0 kg/m^3. They were cured for 28 days in wet conditions. The untreated cases were placed directly in ASR accelerating environment (40 °C, R.H.: 95%). After curing, the other specimens were treated and then placed under ASR accelerating conditions. The specimens were treated under 0.5, 1.0 or 2.0 A/m^2 for 4, 8 or 16 weeks. The anolyte was a mixed solution of 5 N LiOH and 0.1 N H_3BO_3 and its temperature was controlled at 20 °C or 40 °C.

Once again, sodium and potassium ions accumulated in the region around the rebar. This effect was more pronounced when higher temperature was applied. Higher temperature also affected the transport of lithium, leading to higher concentrations and penetration depth. It is worth noting that hardly any lithium was found close to the rebar in all cases – in that region, $\frac{[Li]}{[Na]}$ was much lower than 1.0. In contrast, the areas close to the exposed surface presented $\frac{[Li]}{[Na]}$ ratios above 3.0. Nevertheless, all treated cases, regardless of the treatment conditions, exhibited reduced expansion when compared to untreated specimens. The authors pointed out that the suppression effects are more noticeable in the region near to the surface exposed to the anolyte.

Mortar discs were cast with similar mixture as the concrete prisms, but without the

coarse aggregate. They were tested in two-chamber set-ups, in order to obtain the effective diffusion coefficient. The experimental conditions were similar to the ones used in the treatment of the prismatic specimens, except that the catholyte was a saturated $Ca(OH)_2$ solution. Results showed that higher applied current density and longer migration period led to higher coefficients.

In an attempt at obtaining higher levels of lithium penetration, Ueda et al. [64] added a surface-active agent (SAA) to the anolyte solution, in order to reduce the surface tension of the solution. The surface-active agent used in this study was a co-polymer of ethylene oxide and propylene oxide generally used to reduce drying shrinkage in concrete. This investigation was conducted with prismatic concrete specimens (100 x 100 x 300 mm) with a steel bar embedded at the center of the square section. The concrete mixture had w/c of 0.6 and non-reactive sand as fine aggregate. As the coarse aggregate a mixture of reactive (andesite) and non-reactive aggregate was used, at the pessimum weight ratio of 6:4, like in the previous study. NaCl was dissolved into the mixing water so that the total alkali content was adjusted to 8.0 kg/m^3. The specimens were cured for 28 days in wet condition before treatment.

The applied current density was 2.0 A/m^2 and the anolyte solutions were 5.0 N LiOH, 0.5 N Li_2CO_3 and each solution with 5% of the surface-active agent. The anolyte solutions 0.5 N Li_2CO_3 and 0.5 N Li_2CO_3 + surface active agent were evaluated at different temperatures, 20 and 40 °C. Some of the specimens were placed under ASR accelerating conditions (40 °C, R.H.: 95%) for two months before the treatment. The treatment lasted eight weeks. After treatment, all specimens were kept on environment for ASR acceleration. The results showed little influence of the surface-active agent in the transport of lithium. On the other hand, the increase in temperature of the 0.5 N Li_2CO_3 led to higher lithium content and depth of penetration. At 20°C the $\frac{[Li]}{[Na]}$ molar ratio was above 1.0 near to the exposed surface and it greatly dropped in the area around the rebar. However, the increase in temperature led to higher concentrations of lithium around the rebar – even this region, $\frac{[Li]}{[Na]}$ ratio was above 1.0. Regarding the expansive behavior, all cases had lower expansion rate than the non-treated case. The reduction was less noticeable in the specimens that were kept in ASR accelerating conditions prior to treatment. The beneficial effect of increased temperature was also mentioned in another study [65], where similar results were reported.

In another work, Ueda et al. [66] studied the influence of temperature on lithium migration with different lithium salts solutions as anolytes. Concrete prisms (100 mm x 100 mm x 300 mm) were cast with a rebar in the middle of the cross-section, like in previous works. The fine and coarse aggregate portions were both composed by reactive and non-reactive aggregate at the pessimum weight ratio of 3:7. The w/c ratio was 0.55 and NaOH was added to the mixture in order to increase the total alkali content to 10.0 kg/m^3. The specimens were cured in wet conditions at 20 °C for 28 days before treatment. The applied current was 1.0 A/m^2 and the treatment lasted eight weeks. The investigated anolyte solutions were 10% LiOH, 1.2% Li_2CO_3, 23% Li_2SiO_4 and 30% $LiNO_3$. All solutions were heated up to 30 °C. $LiNO_3$ was also tested at 40 °C. After treatment, once again, the specimens were kept in ASR accelerating conditions (40 °C, R.H.: 95%). Untreated specimens were placed under such conditions directly after curing.

Results indicated that when the anolyte temperature was 30 °C, the penetration depth

of lithium was around 25 mm, regardless of the anolyte solution. However, when the anolyte was heated up to 40 °C, higher content and penetration depth of lithium are found. In addition, when higher temperature was applied, there was less accumulation of sodium and potassium around the rebar, according to the authors. They believe that the increase of temperature caused a decrease of the transference number [3] of sodium and potassium. All treated cases had lower longitudinal (parallel to the reinforcement bar) expansion than non-treated cases. However, in the case of expansion on the vertical direction, only $LiNO_3$ (at both temperatures) and Li_2CO_3 treatment suppressed the expansive behavior. Overall, the treatment with $LiNO_3$ at 40 °C was the most effective in suppressing ASR expansion in both directions.

The specimens treated with $LiNO_3$ at 30 and 40 °C (1.0 A/m^2 for eight weeks) and untreated were split open and the analysis results were reported in another paper [67]. A white product was found around the rebar of specimens treated with $LiNO_3$ at 40 °C, which contained over 10% of Li_2O. The analysis of the white product showed that the treatment led to the formation of product with lower CaO/SiO_2 ratio, when compared to products found in a non-treated specimen. According to the authors, this could mean that the rigidity of the gel was reduced. The authors suggested that the product found in the treated specimens would be a lithium containing gel with low expansion capacity.

A different type of anode system was investigated by Ueda et al.[68] . Again, prismatic reinforced concrete specimens (100 x 100 x 300 mm) were used. However, a ductile fiber reinforced cementitious composite (DFRCC) layer containing lithium with an embedded steel mesh was the anode. In the concrete mixture, reactive coarse aggregate and non-reactive fine aggregates were used, in the ratio of 7:3 and the total alkali content of the concrete raised to 8.0 kg/m^3 by NaCl addition. Two different lithium salts (LiOH and $LiNO_3$) were investigated as admixtures in the DFRCC layer. After 28 days of curing at 20 °C, the reinforced beams were immersed in the electrolyte (0.1 M Li_3BO_3) and the electric current between the anodic layer and the reinforcement bar was supplied. Two different current densities were applied: 0.05 A/m^2 during 16 weeks and 1.0 A/m^2 for eight weeks. After the tests, a high alkali concentration near the cathode was observed and the lithium ions mainly concentrated near the exposed surface, in the first 20 mm of the concrete beam, regardless of the intensity of the current. In fact, only the region close to the exposed surface had $\frac{[Li]}{[Na]}$ above slightly 1.0. Nevertheless, it was highlighted that the lithium penetration due to migration was not much higher than the transport due to diffusion.

Bentivegna et al. [69] studied the treatment of large-scale reinforced cylindrical concrete columns (0.61 m in diameter and 1.22 m in height). The specimens were cast with reactive aggregate and sufficient alkali in order to be expansive and result in cracking. After achieving the expansion of 0.1%, two specimens were submitted to the treatment for five weeks. The reinforcement was used as cathode and a $LiNO_3$ solution as anolyte. As usual in the case of actual columns, the reinforcement was close to the surface of the cast elements, as shown in Figure 2.11 (a).

As result of the test, most of lithium ions concentrated on the first 20 mm. The authors considered that 100 ppm of lithium would be enough to suppress ASR expansion

[3] The transference number of an ion is the ratio of the current carried by that ion in relation to the total current. It depends on the concentration and mobility of all ions present[51].

(a) (b)

Figure 2.11: (a) The reinforcement arrangement used by Bentivegna et al. [69] in their laboratory tests and (b) the field application of the electrochemical lithium treatment on a bridge column [69])

and pointed out that only the first 40 mm from the surface would then be treated. They also observed the accumulation of sodium and potassium ions close to the reinforcement, which could increase ASR gel formation in that region. The expansion behavior was monitored for over a thousand days and the treated and untreated specimens exhibited similar trends – the treatment was considered unsuccessful.

In the same paper, Bentivegna et al. [69] described the field trial treatment of columns of a bridge affected by ASR in Houston, US. In contrast to other field cases [53], the mitigation of ASR was the primary goal of this work. Two columns were treated for five weeks, with a $LiNO_3$ solution as anolyte. The level of the applied current (or voltage) was not reported. However, the authors reported that a constant current was applied during the treatment. In order to obtain migration not only through the surface, holes were drilled to a depth of several centimeters behind the rebar. Into them, extra anodes and irrigation tubes were inserted to provide impregnation from inside the rebar cage. The arranged set-up is shown in Figure 2.11 (b). The final effects were evaluated by the monitoring of both expansion and propagation of the cracking. According the authors, the treatment did not reduce the expansion or cracking. In fact, cracks were noted in treated columns after five years. The accumulation of sodium and potassium close to the reinforcement, reported elsewhere [70], [49], may be responsible for the failure of the method in this case, as the accumulation might have led to the increase of ASR gel formation. Bentivegna et al. [69] also highlighted that the electrochemical procedure was a time-consuming and high-cost mitigation method and concluded it does not seem to be a viable mitigation technique.

Tables 2.2 and 2.3 show a summary of the various experimental conditions applied in the studies here described.

Table 2.2: Experimental conditions of lithium migration studies

Study	Specimen	Applied current density/ voltage	Av. passing current density	Duration	Set-up	Anolyte solution
Whitmore and Abbot [53]	ASR affected concrete structures	Not informed		8 weeks	Rebar as cathode	Li_3BO_3
Matsumoto [54]	Carbonated and ASR reactive concrete (100×100 x200 mm)	1 A/m^2		1 and 3 weeks	Rebar as cathode	2 N Li_3BO_3
Thomas and Stokes [46]	ASR reactive concrete (∅ 100 mm, h 50 mm)	20 V		35 - 101 days, depending on cracking level	Two-chamber set-up	30% $LiNO_3$
Pacheco and Polder [56]	Standard mortar (∅ 100 mm, h 50 mm)	20 and 40 V	4 - 15 A/m^2, depending on applied voltage	1 and 4 weeks	Two-chamber set-up	1 M $LiNO_3$
Lee et al. [57]	ASR reactive concrete (∅ 100 mm, h 50 - 200 mm)	9 A/m^2		30 days	Two-chamber set up	1 N LiOH
Santos Silva et al. [50]	ASR reactive concrete cores (∅ 74 mm, h 50 mm)	20, 40 and 60 V		1 week	Two-chamber set-up	30% $LiNO_3$
Liu et al. [58]	ASR reactive mortar (∅ 100 mm, h 50 mm)	12, 18, 24, 30 and 40 V	3.9 -21.8 A/m^2, depending on applied voltage	50 days – except for 40 V (33 days)	Two-chamber set-up	1 N LiOH
Wang et al. [59]	ASR reactive concrete (∅ 100 mm, h 50 mm)	9 A/m^2		30 days	Two-chamber set-up	1 N LiOH, 1 N $LiNO_3$, oversat. Li_2CO_3 and oversat. $Li_2B_4O_7$

Table 2.3: Experimental conditions of lithium migration studies (continuation).

Study	Specimen	Applied current density/ voltage	Duration	Set-up	Anolyte solution
Lizarazo-Marriaga et al. [60]	ASR reactive mortar (25 x 25 x 290 mm)	15 and 20 V	4 days	Two-chamber set-up	30% $LiNO_3$
Ueda et al. [62]	ASR reactive concrete (100 x 100 x 200 mm)	1 A/m^2	4, 8 and 12 weeks	Rebar as cathode	2 and 5 N LiOH
Ueda et al. [63]	ASR reactive concrete (100 x 100 x 300 mm)	0.5, 1 and 2 A/m^2	4, 8 and 16 weeks	Rebar as cathode	Mixture of 5 N LiOH and 0.1 N H_3BO_3 at 20 °C and 40 °C
Ueda et al. [64]	ASR reactive concrete (100 x 100 x 300 mm)	2 A/m^2	8 weeks	Rebar as cathode	5.0 N LiOH, 0.5 N Li_2CO_3, 5.0 N LiOH + 5% of SAA (at 20 °C and 40 °C) and 0.5 N Li_2CO_3 + 5% of SAA (at 20 °C and 40 °C)
Ueda et al. [65]	ASR reactive concrete (100 x 100 x 300 mm)	2 A/m^2	8 weeks	Rebar as cathode	0.5 N Li_2CO_3 at 20 °C , 30 °C and 40 °C
Ueda et al. [66], [67]	ASR reactive concrete (100 x 100 x 300 mm)	1 A/m^2	8 weeks	Rebar as cathode	10% LiOH , 1.2% Li_2CO_3, 23% Li_2SiO_4 and 30% $LiNO_3$ at 30 °C. 30% $LiNO_3$ at 40 °C
Ueda et al. [68]	ASR reactive concrete (100 x 100 x 300 mm)	0.05 and 1 A/m^2	16 and 8 weeks	Rebar as cathode. A DFRCC layer with lithium and embedded steel mesh as anode.	LiOH and $LiNO_3$ in the DFRCC layer
Bentivegna et al. [69]	ASR reactive reinforce concrete (∅ 0.61 m, h 1.22 m)	Not informed	5 weeks	Rebar as cathode	$LiNO_3$
Bentivegna et al. [69]	ASR affected concrete bridge columns	Not informed	5 weeks	Rebar as cathode	$LiNO_3$

2.5. CONCLUDING REMARKS

From the review above, it is clear that the development of innovative ASR treatment methods is necessary. Moreover, it can be seen that some principles of lithium migration and its effect on concrete affected by ASR are still not fully understood. The variability amongst the experimental procedures adopted by the several mentioned authors makes it difficult to compare the results. Caution should be taken when evaluating the various results.

The first striking difference is the type of set-up used and its effect on the behavior of sodium and potassium. The use of external electrodes in two-chamber types of migration cells allows the removal of alkalis. Therefore, in experiments of this type, the treatment is rewarded with two beneficial actions regarding ASR control - the impregnation of lithium and the reduction of the total amount of sodium and potassium. On the other hand, when using the reinforcement bar as cathode, alkalis accumulate in that area, increasing the alkalinity of the pore solution. The accumulation should not be neglected, as it may accelerate ASR development in that region. In fact, this means that the use of external electrodes (both anode and cathode) may be preferred in future applications of the treatment of large-scale structural elements.

Regarding the parameters that control the migration of lithium ions, it is generally agreed that the applied voltage and time of the test influence the rate of penetration and the final concentration profile. Nevertheless, most of the present studies have not been able to enhance the maximum penetration depth, leaving areas beyond the first 30-40 mm relatively untreated. Also, the influence of other parameters such as the type and concentration of lithium solution used and lithium binding are still not clear.

It is interesting to note that, in the papers reviewed, little or nothing has been said about the pore structure of the material. As mentioned before, the ionic transport through concrete or mortars depends on the tortuosity of the path and comparing results without the characterization of the pore structure can lead to unreliable conclusions. A similar remark can be made concerning the pore solution composition. Resistance measurements bring information on the pore structure and pore solution and are important in order to better understand ionic transport

Another important aspect is the $\frac{[Li]}{[Na_2O_{eq}]}$ molar ratio that should be reached in order to mitigate deleterious ASR expansion in the case of existing structures. Some of the studies previously discussed compared the ratios obtained during the electrochemical treatment of hardened concrete with values from the literature for preventing the reaction on new concrete. The literature values were obtained from the case when the lithium salt is incorporated into the fresh mixture and the mechanism of action of lithium ions on ASR in hardened concrete might be different. Also, the amounts involved are not necessarily the same - the addition of lithium salts in fresh mixture may have a different effect on binding. It could be that lower levels of lithium transported into hardened concrete are enough to mitigate ASR. Understanding the mitigation mechanism during the treatment of existing structures is needed.

REFERENCES

[1] L. M. S. Souza and R. B. Polder, *Studies on electrochemical lithium migration for remediation of alkali-silica reaction at macro level in concrete structures,* in *Proceedings of the Fifth International PhD Student Workshop on Durability of Reinforced Concrete. From Composition to Service Life Design* (VTT Technical Research Centre of Finland, 2012) pp. 50–62.

[2] A. Poole, *Introduction to alkali-aggregate reaction in concrete,* (Blackie, London, 1992) pp. 1–29.

[3] F. Rajabipour, E. Giannini, C. Dunant, J. H. Ideker, and M. D. Thomas, *Alkali-silica reaction: Current understanding of the reaction mechanisms and the knowledge gaps,* Cement and Concrete Research **76**, 130 (2015).

[4] M. D. Thomas, B. Fournier, K. J. Folliard, J. H. Ideker, and Y. Resendez, *The Use of Lithium to Prevent or Mitigate Alkali-Silica Reactions in Concrete Pavements and Structures*, Tech. Rep. FHWA-HRT-06-133 (Federal Highway Administration, 2007).

[5] T. E. Stanton, *Expansion of concrete through reaction between cement and aggregate,* Transactions of The American Society of Civil Engineers **107**, 54 (1942).

[6] D. J. Deschenes, O. Bayrak, and K. J. Folliard, *ASR/DEF-damaged bent caps: shear tests and field implications*, Master's thesis, University of Texas at Austin (2009).

[7] K. J. Folliard, M. D. Thomas, and K. E. Kurtis, *Guidelines for the use of lithium to mitigate or prevent ASR*, Tech. Rep. FHWA-RD-03-047 (Federal Highway Administration, 2003).

[8] D. Stark, *The handbook for the identification of alkali-silica reactivity in highway structures*, Tech. Rep. SHRP-C-315 (Strategic Highway Research Program, 1991).

[9] N. Hasparyk, *Investigação de concretos afetados pela reação álcali-agregado e caracterização avançada do gel exsudado (in Portuguese)*, Ph.D. thesis, Universidade Federal do Rio Grande do Sul. Escola de Engenharia (2005).

[10] D. Hülsenberg, A. Harnisch, and A. Bismarck, *Microstructuring of glasses* (Springer, 2008).

[11] X. Feng, *Effects and Mechanisms of Lithium Nitrate on Controlling Alkali-silica Reaction*, Ph.D. thesis, University of New Brunswick (2008).

[12] L. D. Glasser and N. Kataoka, *The chemistry of 'alkali-aggregate' reaction,* Cement and Concrete Research **11**, 1 (1981).

[13] L. D. Glasser, *Osmotic pressure and the swelling of gels,* Cement and Concrete Research **9**, 515 (1979).

[14] H. F. Taylor, *Cement chemistry* (Thomas Telford, 1997).

[15] S. Diamond, *ASR - another look at mechanisms,* in *Proceedings of the 8th International conference on alkali-aggregate reaction* (1989) pp. 83–94.

[16] A. Leemann, G. Le Saout, F. Winnefeld, D. Rentsch, and B. Lothenbach, *Alkali–silica reaction: the influence of calcium on silica dissolution and the formation of reaction products,* Journal of the American Ceramic Society **94**, 1243 (2011).

[17] T. Knudsen and N. Thaulow, *Quantitative microanalyses of alkali-silica gel in concrete,* Cement and Concrete Research **5**, 443 (1975).

[18] J. Lindgård, Ö. Andiç-Çakır, I. Fernandes, T. F. Rønning, and M. D. Thomas, *Alkali–silica reactions (ASR): literature review on parameters influencing laboratory performance testing,* Cement and Concrete research **42**, 223 (2012).

[19] F. Glasser, *Chemistry of the alkali-aggregate reaction,* (Blackie, London, 1992) pp. 30–53.

[20] W. Hansen, *Studies relating to the mechanism by which the alkali-aggregate reaction produces expansion in concrete,* in *ACI Journal Proceedings*, Vol. 40 (ACI, 1944).

[21] S. Chatterji, A. Jensen, N. Thaulow, and P. Christensen, *Studies of alkali-silica reaction.Part 3. Mechanisms by which NaCl and Ca(OH)$_2$ affect the reaction,* Cement and Concrete Research **16**, 246 (1986).

[22] D. W. Hobbs, *Alkali-silica reaction in concrete* (Telford London, 1988).

[23] T. C. Powers and H. H. Steinour, *An interpretation of some published researches on the alkali-aggregate reaction. Part i - The chemical reactions and mechanism of expansion,* in *ACI Journal Proceedings*, Vol. 51 (ACI, 1955).

[24] M. Prezzi, P. Monteiro, and G. Sposito, *Alkali-silica reaction, Part I: Use of the double-layer theory to explain the behavior of reaction-product gels,* ACI materials journal **94** (1997).

[25] E. Garcia-Diaz, J. Riche, D. Bulteel, and C. Vernet, *Mechanism of damage for the alkali–silica reaction,* Cement and Concrete Research **36**, 395 (2006).

[26] D. J. Belton, O. Deschaume, and C. C. Perry, *An overview of the fundamentals of the chemistry of silica with relevance to biosilicification and technological advances,* FEBS Journal **279**, 1710 (2012).

[27] J. F. Schneider, N. P. Hasparyk, D. A. Silva, and P. J. Monteiro, *Effect of lithium nitrate on the alkali-silica reaction gel,* Journal of the American Ceramic Society **91**, 3370 (2008).

[28] D. Stark, B. Morgan, and P. Okamoto, *Eliminating or minimizing alkali-silica reactivity*, Tech. Rep. SHRP-C-343 (Strategic Highway Research Program, 1993).

[29] T. G. Nijland and W. A. de Bruijn, *New dutch guideline on asr-prevention,* Heron **47**, 87 (2002).

[30] P. J. Nixon and I. Sims, *RILEM Recommendations for the Prevention of Damage by Alkali-Aggregate Reactions in New Concrete Structures: State-of-the-Art Report of the RILEM Technical Committee 219-ACS*, Vol. 17 (Springer, 2015).

[31] S. M. Shafaatian, A. Akhavan, H. Maraghechi, and F. Rajabipour, *How does fly ash mitigate alkali–silica reaction (ASR) in accelerated mortar bar test (ASTM C1567),* Cement and Concrete Composites **37**, 143 (2013).

[32] M. Thomas, *The effect of supplementary cementing materials on alkali-silica reaction: A review,* Cement and Concrete Research **41**, 1224 (2011).

[33] J. Duchesne and M.-A. Bérubé, *Long-term effectiveness of supplementary cementing materials against alkali–silica reaction,* Cement and concrete research **31**, 1057 (2001).

[34] W. Aquino, D. Lange, and J. Olek, *The influence of metakaolin and silica fume on the chemistry of alkali–silica reaction products,* Cement and Concrete Composites **23**, 485 (2001).

[35] B. Fournier, M.-A. Berube, K. J. Folliard, and M. Thomas, *Report on the diagnosis, prognosis, and mitigation of alkali-silica reaction (ASR) in transportation structures,* Tech. Rep. FHWA-HIF-09-004 (Federal Highway Administration, 2010).

[36] W. McCoy and A. Caldwell, *New approach to inhibiting alkali-aggregate expansion,* in *ACI Journal Proceedings*, Vol. 47 (ACI, 1951).

[37] M. Lawrence and H. Vivian, *The reactions of various alkalis with silica,* Australian Journal of applied science **12**, 96 (1961).

[38] R. L. Hooper, P. J. Nixon, and M. D. Thomas, *Considerations when specifying lithium admixtures to mitigate the risk of ASR,* in *Proc. 12 th Int. Conf. on Alkali-Aggregate Reaction in Concrete* (2004) pp. 554–563.

[39] A. Leemann, L. Lörtscher, L. Bernard, G. Le Saout, B. Lothenbach, and R. M. Espinosa-Marzal, *Mitigation of ASR by the use of $LiNO_3$ - characterization of the reaction products,* Cement and Concrete Research **59**, 73 (2014).

[40] X. Feng, M. Thomas, T. Bremner, B. Balcom, and K. Folliard, *Studies on lithium salts to mitigate ASR-induced expansion in new concrete: a critical review,* Cement and Concrete Research **35**, 1789 (2005).

[41] C. Tremblay, M. Bérubé, B. Fournier, and M. Thomas, *Performance of lithium-based products against ASR: effect of aggregate type and reactivity, and reaction mechanisms,* in *Proceedings of the 7th CANMET/ACI International Conference on Recent Advances in Concrete Technology (Suppl. Papers)* (2004) pp. 247–267.

[42] K. J. Folliard, M. D. Thomas, B. Fournier, K. E. Kurtis, and J. H. Ideker, *Interim recommendations for the use of lithium to mitigate or prevent alkali-silica reaction (ASR),* Tech. Rep. FHWA-HRT-06-073 (Federal Highway Administration, 2006).

[43] E. A. d. O. Gomes, *Recuperação estrutural de blocos de fundação afetados pela reação álcali-agregado - a experiência do Recife (in Portuguese)*, Master's thesis, (Universidade Católica de Pernambuco (2008).

[44] M.-A. Bérubé, D. Chouinard, M. Pigeon, J. Frenette, L. Boisvert, and M. Rivest, *Effectiveness of sealers in counteracting alkali-silica reaction in plain and air-entrained laboratory concretes exposed to wetting and drying, freezing and thawing, and salt water,* Canadian Journal of Civil Engineering **29**, 289 (2002).

[45] T. Drimalas, K. Folliard, M. Thomas, B. Fournier, and A. Bentivegna, *Study of the effectiveness of lithium and silane treatments on field structures affected by ASR,* in *Proceedings, 14th International Conference on Alkali-Aggregate Reaction* (2014).

[46] M. Thomas and D. Stokes, *Lithium impregnation of ASR-affected concrete: preliminary studies,* in *Proceedings of the 12th International Conference on Alkali-Aggregate Reaction in Concrete* (2004) pp. 659–667.

[47] M. Kawamura and T. Kodera, *Effects of externally supplied lithium on the suppression of ASR expansion in mortars,* Cement and concrete research **35**, 494 (2005).

[48] D. Stokes, J. Pappas, M. Thomas, and K. Folliard, *Field cases involving treatment or repair of ASR-affected concrete using lithium,* in *Proceedings of the 6th CANMET/ACI International Conference on Durability of Concrete* (2002) pp. 631–642.

[49] K. J. Folliard, M. D. Thomas, J. H. Ideker, B. East, and B. Fournier, *Case studies of treating asr-affected structures with lithium nitrate,* in *Proceedings of the 13th International Conference on Alkali-Aggregate Reaction in Concrete* (2008) pp. 90–99.

[50] A. Santos Silva, M. Salta, M. Melo Jorge, M. Rodrigues, and A. Cristino, *Research on the suppression expansion due to ASR. Effect of coatings and lithium nitrate,* in *Proceedings of the 13th International Conference on Alkali-Aggregate Reaction in Concrete* (2008).

[51] L. Bertolini, B. Elsener, P. Pedeferri, E. Redaelli, and R. B. Polder, *Corrosion of steel in concrete: prevention, diagnosis, repair*, 2nd ed. (John Wiley & Sons, 2013).

[52] C. Page, *Interfacial effects of electrochemical protection methods applied to steel in chloride-containing concrete,* in *Proceedings of International Conference on Rehabilitation of Concrete Structures* (1992) pp. 179–187.

[53] D. Whitmore and S. Abbott, *Use of an applied electric field to drive lithium ions into alkali-silica reactive structures,* in *Proceedings, 11th International Conference on Alkali-Aggregate Reaction* (2000) pp. 1089–1098.

[54] K. I. Matsumoto, T. Ueda, M. Ashida, and T. Miyagawa, *Study on realkalization with electrolyte containing lithium ion,* International Journal of Modern Physics B **17**, 1446 (2003).

[55] ASTM-C1202-05, *Standard test method for electrical indication of concrete's ability to resist chloride ion penetration,* (2005).

[56] J. Pacheco and R. B. Polder, *Preliminary study of electrochemical lithium migration into cementitious mortar,* in *2nd International Symposium on Service Life Design for Infrastructures* (RILEM Publications SARL, 2010) pp. 1093–1100.

[57] C. Lee, C. Liu, and W. Wang, *Effect of the distance between electrodes on the performance of using electrochemical technique to repair the concrete damaged by AAR,* in *Proceedings of the 13th International Conference on Alkali-Aggregate Reaction in Concrete* (2008) pp. 234–2459.

[58] C.-C. Liu, W.-C. Wang, and C. Lee, *Behavior of cations in mortar under accelerated lithium migration technique controlled by a constant voltage,* Journal of Marine Science and Technology **19**, 26 (2011).

[59] W. Wang, C. Lee, C. Liu, and C. Lee, *Effect of the electrolyte on the performance in electrochemical repairing technique for the concrete affected by ASR,* in *Proceeding of the 14th International Conference on Alkali-Aggregate Reaction* (2012).

[60] J. Lizarazo-Marriaga, J. Lozano, J. Silva, L. Fonseca, G. Hermida, and P. Claisse, *A novel assessment of the electrochemical lithium impregnation treatment used to mitigate alkali-silica reaction in concrete,* Concrete Solutions 2014 , 205 (2014).

[61] ASTM-C1260, *Standard test method for potential alkali reactivity of aggregates (mortar-bar method),* (2007).

[62] T. Ueda, Y. Yoshida, K. Yamaguchi, and M. Ashida, *Effect of electrochemical penetration of lithium ions on ASR expansion of concrete,* in *Proceedings of the third international conference on engineering materials* (2005).

[63] T. Ueda, Y. Yoshida, K. Yamaguchi, and M. Ashida, *Electrochemical migration of lithium ions into hardened concrete and ASR expansion after treatment,* Proceedings of structural faults & repair-2006 (2006).

[64] T. Ueda, Y. Baba, and A. Nanasawa, *Effect of electrochemical penetration of lithium ions on concrete expansion due to ASR,* Journal of Advanced Concrete Technology **9**, 31 (2011).

[65] T. Ueda, Y. Baba, and A. Nanasawa, *Penetration of lithium into ASR affected concrete due to electro-osmosis of lithium carbonate solution,* Construction and Building Materials **39**, 113 (2013).

[66] T. Ueda, J. Kushida, M. Tsukagoshi, and A. Nanasawa, *Influence of temperature on electrochemical remedial measures and complex deterioration due to chloride attack and ASR,* Construction and Building Materials **67**, 81 (2014).

[67] T. Ueda, A. Nanasawa, and M. Tsukagoshi, *Influence of electrochemical lithium penetration from various kinds of lithium solution on ASR expansion of concrete,* in *Proceedings of the 4th International Conference on Concrete Repair, Rehabilitation and Retrofitting* (CRC Press, 2015).

[68] T. Ueda, T. Kameda, T. Maeda, and A. Nanasawa, *Suppression of ASR expansion due to electrochemical penetration of lithium supplied by DFRCC anode system,* in *Proceedings of the 6th International Conference on Concrete under Severe Conditions* (2010) pp. 1229–1236.

[69] A. Bentivegna, E. Giannini, and K. Folliard, *Use of electrochemical migration to mitigate alkali-silica reaction in large scale concrete structures,* Concrete Solutions (2011).

[70] E. R. Giannini, *Field Studies of Mitigation Strategies for Alkali-Silica Reaction in Hardened Concrete*, Master's thesis, University of Texas at Austin (2009).

3

LITHIUM MIGRATION IN MORTAR SPECIMENS

Parts of this chapter have been published in Souza et al., Durability of Reinforced Concrete from Composition to Protection, 2015 [1]; Souza et al., Concrete Repair, Rehabilitation and Retrofitting IV: Fourth International Conference on Concrete Repair, Rehabilitation and Retrofitting, 2015 [2] and Souza et al., Proceedings of the First Concrete Innovation Conference, 2014 [3].

3.1. INTRODUCTION

DRIVING lithium ions into concrete by means of an electrical field was first suggested by Page [4]. The author theorized that, if a lithium solution was used as anolyte during an electrochemical chloride extraction treatment of a structure, lithium ions would migrate towards the reinforcing steel and mitigate the effects of ASR. Since then, a number of different studies have been published, with divergent conclusions, as presented in the literature review. Fully understanding the principles behind lithium migration is necessary in order to best interpret those conclusions.

It is generally agreed that the applied voltage (or current density) and time of the treatment positively influence the rate of penetration and the final lithium concentration profile. Nevertheless, the most appropriate set of treatment conditions, which balances out benefits and side effects, has not systematically been investigated yet.

In this chapter, an experimental study on the effect on migration of the type of lithium compound used in the anolyte will be presented. From this investigation, the lithium solutions that provided the best ingress were chosen to be evaluated in longer experiments. Thus, a study on the effect of time on the treatment will be discussed. Finally, the position of the cathode, placed inside or outside the treated material, will be addressed.

3.2. EFFECT OF ANOLYTE SOLUTION ON MIGRATION

IN the various studies on lithium migration presented in the literature review, several different lithium salts are used in the anolyte solution, at different concentrations. However, little has been discussed on the reason behind the choice of those solutions or on whether the choice would influence the final results. In fact, Ueda [5] investigated the effect of different lithium compounds, however the concentration of the anolyte solutions was not discussed. In this section, the influence of different lithium solutions on migration will be addressed. Li_2CO_3, LiOH and $LiNO_3$ were the lithium salts chosen to be tested at various concentrations. LiOH and $LiNO_3$ were considered because of their high solubility in water. Although Li_2CO_3 has very low solubility in water, Ueda [6] noted in his work that Li_2CO_3 solution leads to higher effective diffusion coefficient than LiOH (when tested in two-chamber set-ups).

3.2.1. EXPERIMENTAL PROCEDURE

MATERIALS AND SPECIMEN PREPARATION

MORTAR specimens were prepared with water to cement ratio (w/c) of 0.5 and sand to cement proportion of 3:1. The mixing procedure followed the standard EN 196 1:2005. The air void content was 1.0% (NEN-EN 12350-7) and the flow value, obtained by the flow table test (NEN-EN 12350-5), was 270 mm.

Ordinary Portland cement type CEM I 42.5 N, commercially available in the Netherlands (ENCI), was used. Its chemical composition is shown in Table 3.1. In addition, CEN standard sand with D_{max} of 2.00 mm (according to EN 196 1:2005) and deionized water were used. Cylindrical specimens, with diameter of 98 mm and height of 50 mm, were cast and cured in a fog room ($20.0 \pm 2.0\,^{\circ}C$ and R.H. of $96 \pm 2\%$) for 36 days before the beginning of the experiment.

Table 3.1: Cement composition, wt. % of cement.

CaO	SiO_2	Al_2O_3	Fe_2O_3	SO_3	MgO	P_2O_5	K_2O	TiO_2	Na_2O	Other	L.O.I [1]
65.00	18.33	4.42	3.38	3.01	2.02	0.57	0.46	0.37	0.28	0.53	1.60

[1] L.O.I.: loss on ignition

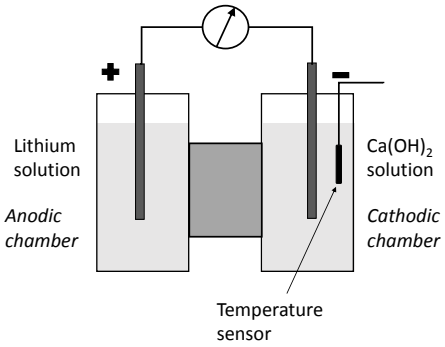

Figure 3.1: Schematic diagram of the experimental set-up. Each electrolyte chamber contained 270 ml of solution.

METHODS

LITHIUM migration testing was performed in the set-up described by ASTM 1202 - Standard Test Method for Electrical Indication of Concretes Ability to Resist Chloride Ion Penetration [7]. As shown in the scheme of Figure 3.1, a specimen was placed between two acrylic chambers filled with solution, each with a stainless steel mesh as electrode. Each chamber contained 270 ml of electrolyte solution. Once the electric potential was applied between the electrodes, cations were attracted by the cathode (negative electrode), whereas anions moved in the opposite direction, towards the anode (positive electrode). Two models of cells were used. They were identical, except for the presence of ventilation holes in the type I, as shown in Figure 3.2. The experiments were carried out in a climate controlled laboratory, at 20.0 ± 2.0 °C and R.H. of 50 ± 5%. Figure 3.1 (c) shows eight cells connected to a power source during an experiment.

Saturated $Ca(OH)_2$ solution (0.02 M) was used as catholyte in all tests. The anolytes, on the other hand, were lithium solutions of different compounds, at different concentrations, as shown in Table 3.2. The highest concentration of each lithium compound solution is its saturation (or near saturation) concentration. Lithium compounds with higher solubility were also tested in lower concentrations, as the table shows. Each solution was tested with two replicates, during one week under 40 V (eletric field of 0.8 V/mm). This voltage was chosen as it is the usual maximum voltage used in the field in treatments such as electrochemical chloride removal [8].

Passing current and catholyte temperature were continuously monitored and recorded by a data logger (with accuracy of 1×10^{-6} mA and 1×10^{-6} °C, respectively), while electrical resistance of the specimens and electrolyte pH were measured four times during the experiments. The electrical resistance was measured with a LCR meter, at 120 Hz in re-

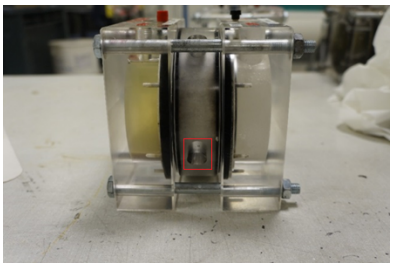

(a)

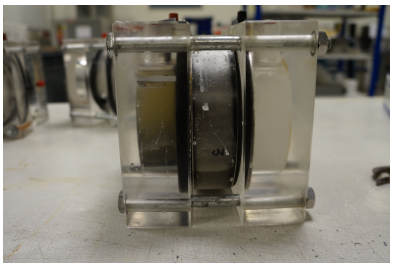

(b)

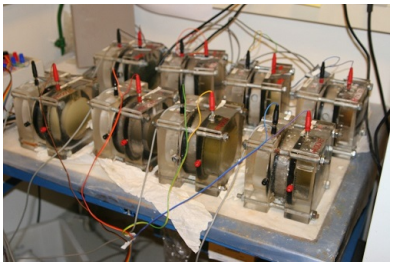

(c)

Figure 3.2: The two types of migration cells - type I, with ventilation holes in the rings around the specimen (a) and type II, without ventilation holes (b); and migration cells during experiment (c).

Table 3.2: Lithium solutions used as anolytes.

Salt	Concentration (M)	Salt	Concentration (M)
Li_2CO_3	0.2 (saturated)	$LiNO_3$	0.2
LiOH	0.2	$LiNO_3$	4.9
LiOH	4.9 (near saturation)	$LiNO_3$	7.8 (near saturation)

sistance mode, with accuracy of 0.1 Ω. From the resistance, the specimen resistivity can be calculated with Equation 3.1 [9], assuming that the resistance outside the specimens is zero:

$$\rho = \frac{RA}{L} \tag{3.1}$$

where R is the electrical resistance (Ω), A is the specimen surface area (m^2) and L is the thickness of the specimen (m). Care should be taken when interpreting resistivity values, as they are strongly affected by temperature variations. Increase in temperature leads to drop in resistivity and vice versa. In fact, temperature may influence up to 5% with every K degree of variation [9].

The pH values of the electrolytes were obtained with a pH-meter (with accuracy of 0.01), when it was possible. In the case of high pH or high lithium concentration, pH test

strips were used (with accuracy of 0.5 or 1, depending on the pH level) [1] Electrolyte samples were collected three times during the test and were analyzed by inductively coupled plasma optical emission spectroscopy (ICP-OES), in order to obtain the concentration of sodium, potassium, lithium and calcium (the latter only in anolyte). The detection limits were 0.02 mg/l for potassium and 0.05 mg/l for lithium, sodium and calcium. Standard solutions were used for control. Most concentration measurements had variations below 4% and the error bars were omitted from the graphs.

Ionic concentration profiles were obtained after the end of the test. To obtain these, the specimens were ground in a profile grinder in steps of 5.0 mm. The obtained powder (10-20 g) was then dissolved in boiling 3.0 M HNO_3 (100 ml) and filtered to obtain a clear solution. When filtering, the filtrate was washed with four parts of 10 ml of 1.0 M HNO_3. The obtained clear solution was then analyzed by ICP-OES for lithium, sodium and potassium.

3.2.2. RESULTS AND DISCUSSION

In Figure 3.3 (a) it is possible to observe the current density that passed through all specimens during the migration experiment. The test with $LiNO_3$ – 4.9 M (2) presented connection problems, as can be seen in the current density plot. The general behavior can be divided into three parts: in the first couple of hours, there is a rapid current increase, followed by a slower drop until around the third day. Finally, the current density stabilizes until the end of tests in the majority of the cells. This initial behavior was also noted by other authors [11],[12] and it is believed to be due to the initial incomplete saturation of the specimens [11]. The overall trend is quite similar to what was reported by Liu et al. [12]. The temperature of the catholyte during the experiment can be seen in Figure 3.3 (b). In all cells, there was an increase in temperature, in particular, in the first few hours. This increase influenced the resistivity values, as will be further discussed.

The total charge that passed through the specimens can be calculated by the integration of their current plots, as shown in Equation 3.2:

$$Q = \int_0^T i(t)\,dt \tag{3.2}$$

where Q is the charge that passed through the specimens (in C), i is the current (in A), T is the total time of the experiment (in s) and t is time (in s).

Table 3.3 presents the total charges that passed through the cells. The specimen LiOH 0.2 M (I) presented problems during the experiment, which will be further discussed, and its passing charge (78 kC) was not considered in the table. Two solutions exhibited deviations of above 10% between replicates, $LiNO_3$ 4.9 M and LiOH 4.9 M. In the first case, connection problems in one of the cells explain that variation. However, that is not the case with the last one. Overall, solutions with concentrations up to 4.9 M presented

[1] In highly alkaline solutions (pH > 11), the pH electrode becomes responsive to other ions such as sodium and lithium. This error, known as alkaline error, leads to readings that are lower than the actual pH. On the other hand, when analyzing highly concentrated solutions, there might be diffusion of ions in the reference electrolyte and in the analyzed solution. This leads to a diffusion potential different from zero, which alters the reading value [10].

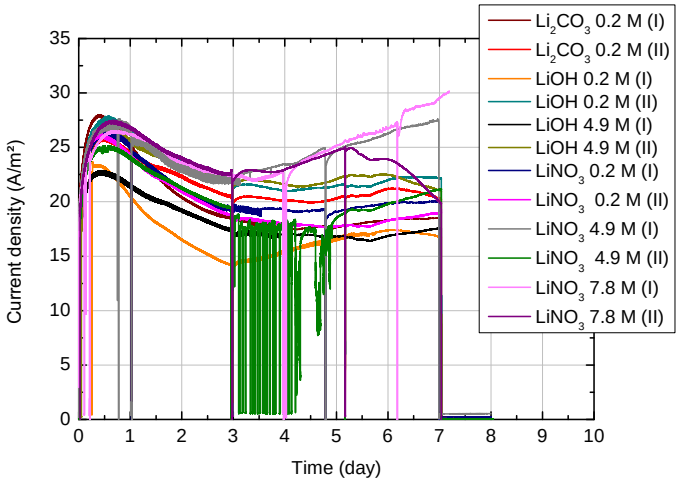

(a)

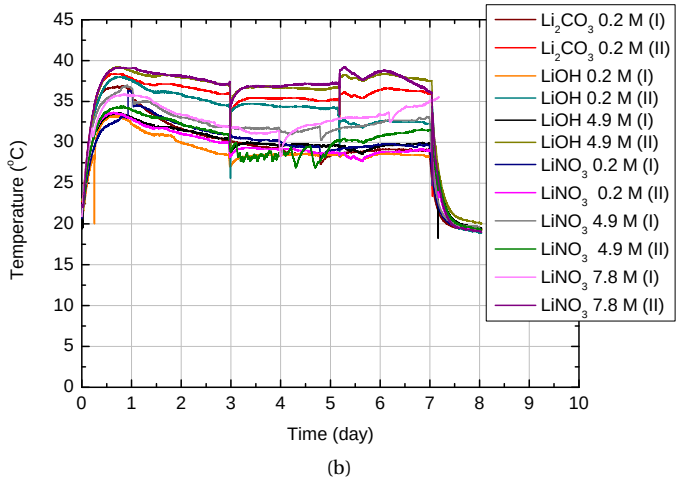

(b)

Figure 3.3: Passing current density (a)and temperature (b) during the experiment.

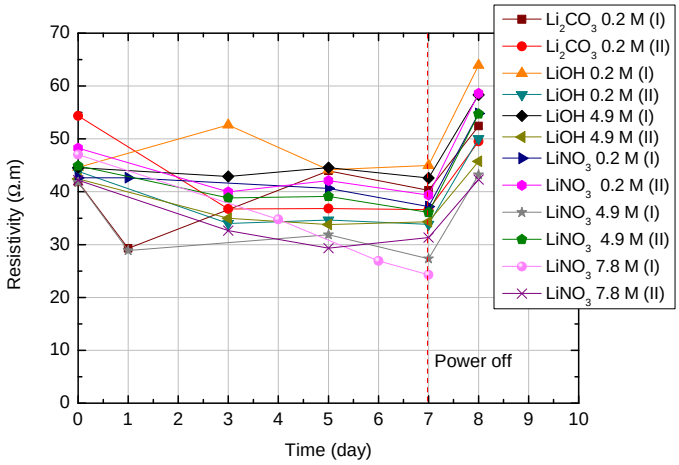

Figure 3.4: Resistivity variations during the experiment.

similar passing charges while the ones with 7.8 M had the highest charges. It is interesting to note that, when comparing solutions of different compounds, but with same concentration, charge values did not vary by more than 5%, indicating that the type of compound does not play an important role on the charge.

In Figure 3.4, specimen electrical resistivity variations during the experiment are shown. A summary is presented in Table 3.4. The measurement on the eighth day was performed after 24 hours without power, at room temperature. The average initial resistivity was 45 ± 4 Ω.m. During the migration experiment, the increase in temperature noted in Figure 3.3 led to resistivity values lower than initially observed. Once the power was turned off and the cells cooled down to room temperature, the resistivity values were overall higher than the initial ones and the average was 52 ± 7 Ω.m. This indicates that non-reversible modifications in pore structure and/or pore solution composition may have taken place. Liu at al. [12] observed the same behavior in their migration experiments. In fact, studies [13], [14], [15] have pointed out that the application of current on concrete may lead to lower porosity and higher resistivity.

Variations in pH in catholyte and anolyte are related to the cathodic and anodic reactions, respectively, as shown in the equations below. The cathodic reaction is shown

Table 3.3: Passing charges during the experiment. The average between replicates and between specimens tested with solutions with the same concentration are presented.

Concentrations	0.2 M			4.9 M		7.8 M
Lithium compound	Li_2CO_3	LiOH	$LiNO_3$	LiOH	$LiNO_3$	$LiNO_3$
Charge (kC)	95	104	93	93	100	112
CV (%)	4	-	2	11	12	3
Av. charge (per conc.) (kC)		93			97	112
CV (%)		2			3	3

Table 3.4: Average (Av.) resistivity values at different moments of the experiment.

	Li_2CO_3 0.2 M		LiOH 0.2 M [a]		$LiNO_3$ 0.2 M		Average per concentration	
	Av. ($\Omega.m$)	CV (%)	Av. ($\Omega.m$)	CV (%)	Av. ($\Omega.m$)	CV (%)	Av. ($\Omega.m$)	CV(%)
Initial	48	13	44	-	45	6	46	4
Middle	40	9	35	-	41	2	40	2
End	38	5	35	-	38	2	39	1
After 24 h	51	3	50	-	57	3	55	5
	LiOH 4.9		$LiNO_3$ 4.9 M					
	Av. ($\Omega.m$)	CV (%)	Av. ($\Omega.m$)	CV (%)			Av. ($\Omega.m$)	CV (%)
Initial	44	3	43	4			44	0
Middle	39	14	36	10			37	5
End	39	11	32	14			35	10
After 24 h	52	12	49	12			51	3
	$LiNO_3$ 7.8 M							
	Av. ($\Omega.m$)	CV (%)					Av.($\Omega.m$)	CV (%)
Initial	45	5					45	5
Middle	32	9					32	9
End	28	13					28	13
After 24 h	42	- [b]					42	-

[a] Specimen LiOH 0.2 M (I) was not considered in the calculation of the average.
[b] Specimen $LiNO_3$ 7.8 M (I) was not measured after 24 h. Thus, it was not considered in the calculation of the average.

in Equation 3.3 and produces hydroxyl ions, leading to an increase of pH. The reaction that takes place at the anode depends on the pH of the solution: if it is basic, Equation 3.4 occurs. Otherwise, Equation 3.5 happens. Either way, the anodic reactions decrease the pH of the solution.

$$2H_2O + 2e^- \longrightarrow 2OH^- + H_2 \tag{3.3}$$

$$2OH^- \longrightarrow H_2O + \frac{1}{2}O_2(g) + 2e^- \tag{3.4}$$

$$H_2O \longrightarrow 2H^+ + \frac{1}{2}O_2(g) + 2e^- \tag{3.5}$$

Figure 3.5 presents the pH variations in catholyte (a) and anolyte (b) solutions during the experiment. Initially, the catholyte solutions exhibited a pH around 12 and, throughout the test, their pH increased very slightly. Even though hydroxyl ions were produced at the cathode (Equation 3.3), they were also transported through the specimen, in the direction of the anode. The progress of the anolyte pH, on the other hand, as shown in Equations 3.4 and 3.5, depended on the initial value. The passing charge and the buffer capacity of the solution also influenced the pH – the higher the passing charge in $LiNO_3$ solutions, for example, the more rapid and stronger was the acidification of the solution. All $LiNO_3$ solutions were initially nearly neutral and they presented the highest pH drops during the test. In fact, the anodes of those cells presented corrosion, due to the low pH and strong anodic polarization. Figure 3.6 shows one of those very corroded anodes. Both LiOH - 4.9 M solutions had very basic initial pH (14) and it remained until the end of the experiment. It is interesting to notice that, although Li_2CO_3 and LiOH – 0.2 M had

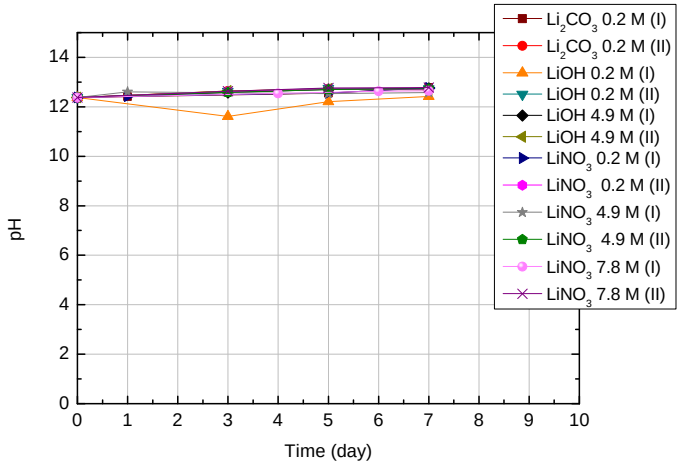

(a)

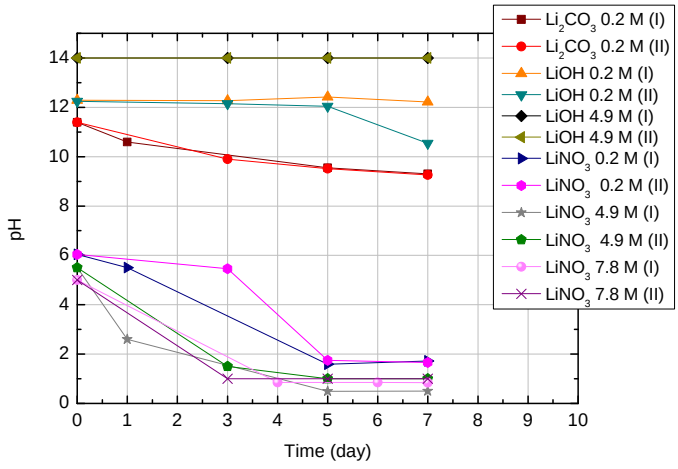

(b)

Figure 3.5: pH variations in catholyte and anolyte during the experiments.

Figure 3.6: Corroded anode of a cell that contained a $LiNO_3$ solution.

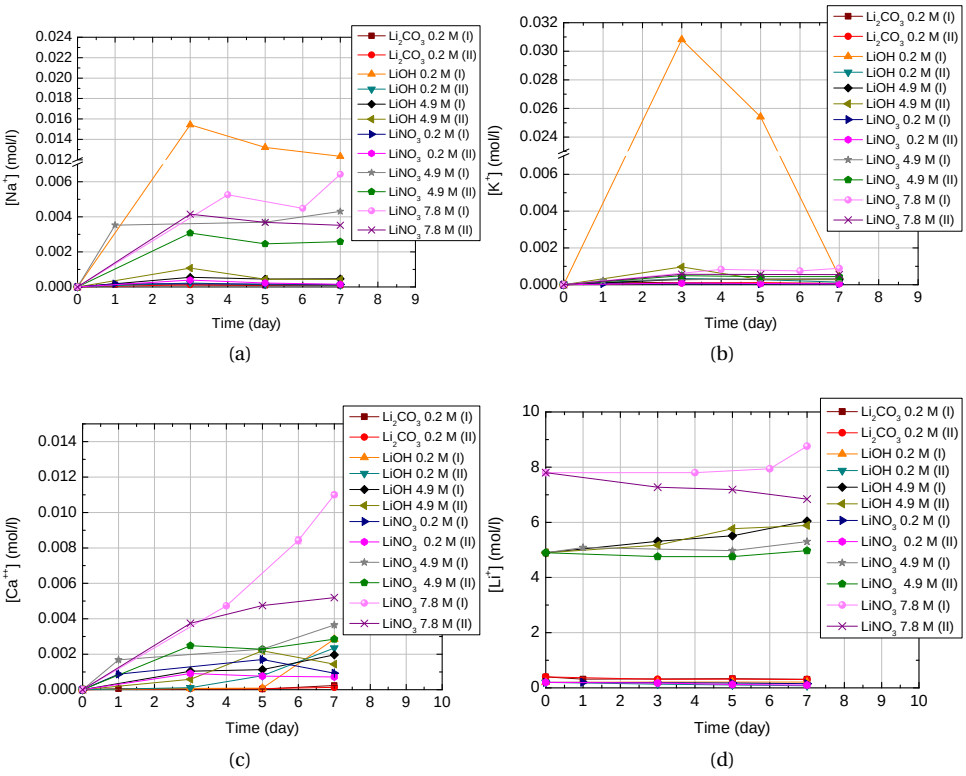

Figure 3.7: Variations in concentration in anolyte solutions of sodium (a), potassium (b), calcium (c) and lithium (d). The vertical scale for sodium and potassium concentrations were modified.

close initial pH, LiOH solutions had better buffer capacity and the pH showed a slower decrease.

Chemical compositions of anolyte solutions can be seen in Figure 3.7. Sodium, potassium and calcium ions move from the specimen to the anolyte due to diffusion and dissolution of the hydrated phases. The latter happened especially in the cells with $LiNO_3$ 4.9 and 7.8 M solutions, because of the acidification of the anolyte. Acids, with pH below 4.5, severely attack concretes (or mortars), by dissolving $Ca(OH)_2$ and removing calcium ions from hydrated silicates and aluminates [16], [17]. This explains why the $LiNO_3$ anolytes presented higher concentrations of those three ions - especially calcium. Lithium concentration in the anolyte was supposed to decrease, as lithium ions are transported into the specimen. Nevertheless, in some tests, that was not the case. This is probably because of changes in the volume of water by evaporation. This means that the concentrations presented for the other ions are likely to be overestimated.

As expected, sodium and potassium concentrations in the catholytes increased with time, as those ions left the pore solution of the specimens, as shown in Figure 3.8. Potassium ions left the specimen faster, especially in the first days, because of its higher ionic

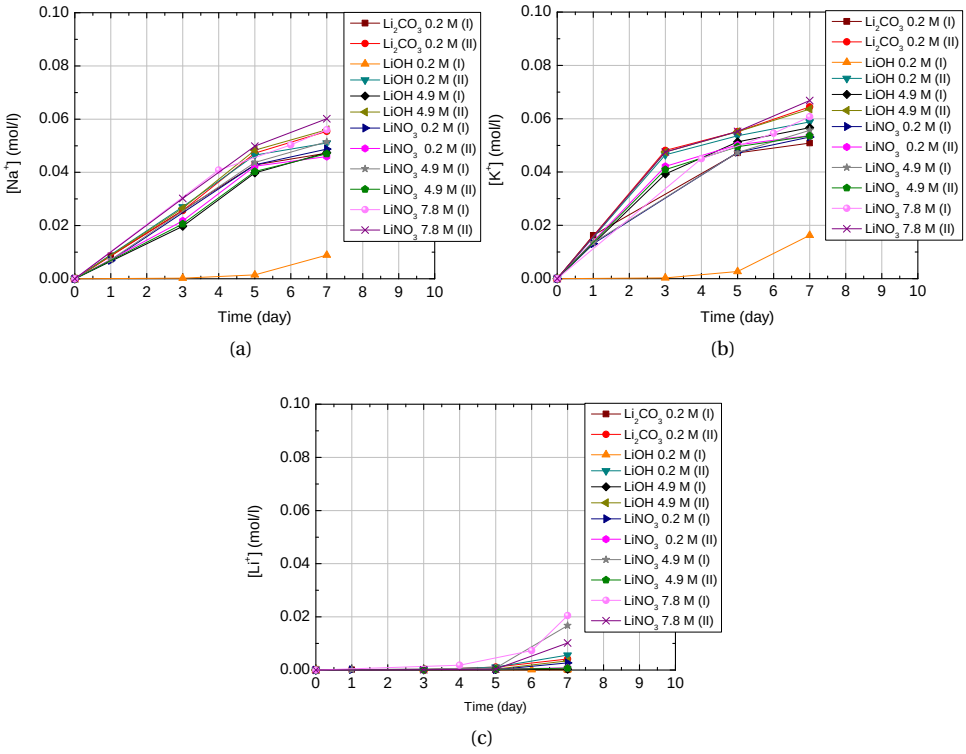

Figure 3.8: Variations in concentration in catholye solutions of sodium (a), potassium (b) and lithium (c).

mobility and higher concentration in the pore solution. Once again, the cell LiOH 0.2 M (I) presented different behavior from the other cells, with much lower concentrations of potassium and sodium in the catholyte.

Figure 3.8 shows the detectable amounts of lithium concentration in the catholyte. For most cells, it took at least 5 days for lithium ions to reach the cathodic chamber. The cells with $LiNO_3$ 4.9 and 7.8 M presented the highest levels of lithium in the catholyte.

Figure 3.9 exhibits total sodium and potassium concentration profiles in the specimens after the experiment. The control case is the initial level of those ions, from a specimen that did not go through the test. As the concentrations were obtained from ground specimens, ions from the pore solution or bound and/or adsorbed to the solid phases are not distinguished. As expected, all specimens showed lower concentrations of sodium and potassium than the control. Furthermore, the profiles were more or less constant for most specimens (LiOH 4.9 M (1) presented profiles that increased towards the cathode). This may indicate that all free sodium and potassium ions had left the specimen by the end of the test and the ones that were measured were actually bound and/or adsorbed to solid phases. In fact, Liu et al. [12] obtained the same type of constant profile, after longer experiments. In addition, they also monitored the sodium and potassium concentrations in the catholyte and noted that, after some time, they became constant

until the end of the experiment. The authors then concluded that all free sodium and potassium had left the specimens.

Lithium concentration profiles in the specimen are shown in Figure 3.10. The profiles exhibit the same basic shape, in which the concentration is higher close to the anode and it decreases towards the cathode. A sharp concentration front would be expected for a migration experiment through a porous medium [11]. However, this was not the case. In fact, other authors have found the same type of profile in their works (e.g. [11],[12],[6]).

In the first 10 mm from the anode, all specimens that were treated with lithium solutions with 4.9 M and 7.8 M presented higher lithium content. However, in deeper layers, the cases LiOH 4.9 M (I) and $LiNO_3$ 4.9 M (II) exhibited lower levels. In fact, LiOH 4.9 M (I), in the last 25 mm, presented the lowest lithium concentrations. This is probably related to the elevated sodium and potassium levels in the same specimen in that region (Figure 3.9). It is worth noting that the final resistivity values of these specimens are amongst the highest in Figure 3.4. The increase in resistivity may explain their lithium profiles. Interestingly, beyond the first 10 mm, the specimen Li_2CO_3 0.2 M (I) presented higher lithium content than the other cases with lithium solution at 0.2 M, probably due to its lower initial resistivity (Figure 3.4). The average amounts of lithium in the specimens can be seen in Table 3.5. Although some variations between replicates are fairly high, the overall trend indicates that the specimens with highest lithium contents had been treated with lithium solutions with concentrations of 4.9 or 7.8 M.

Table 3.5: Average concentration of lithium in the specimens after experiments.

Concentrations	0.2 M			4.9 M		7.8 M
Lithium compound	Li_2CO_3	LiOH	$LiNO_3$	LiOH	$LiNO_3$	$LiNO_3$
Average Li (wt. % of cement)	0.12	0.09	0.07	0.15	0.17	0.22
CV (%)	23.6	-	6.0	27.0	2.2	16.4
Av. per conc. (wt. % of cement)		0.09		0.16		0.22
CV (%)		29.5		18.9		16.4

Figure 3.11 shows the lithium to sodium plus potassium molar ratio ($\frac{[Li]}{[Na+K]}$) in the specimens after test. When lithium is used as admixture, it is known that the ratio to prevent deleterious ASR expansion depends on the type of lithium compound and aggregate. It is generally accepted that the minimum ratio varies from 0.65 to 1.00 [18]. If the upper limit is considered, only the specimen $LiNO_3$ 7.8 M (I) is fully treated, with $\frac{[Li]}{[Na+K]}$ above 1.0 in all regions. Most specimens would be treated until 35 mm from the anode, while LiOH 4.9 M (I) and $LiNO_3$ 4.9 M (II), only until 25 mm. Nevertheless, results should be interpreted with care - the mechanism to stop ASR expansion is not necessarily the same that takes place when lithium admixtures are used. It is possible that, in the case of treatment, other $\frac{[Li]}{[Na+K]}$ ratios should be reached in order to stop (or reduce) ASR expansion.

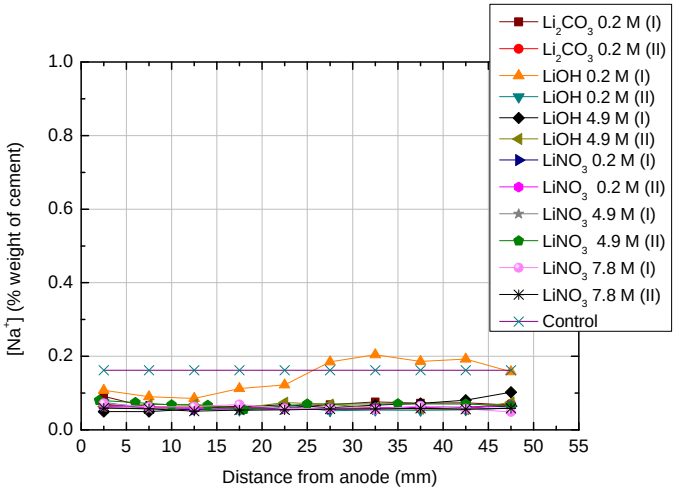

(a)

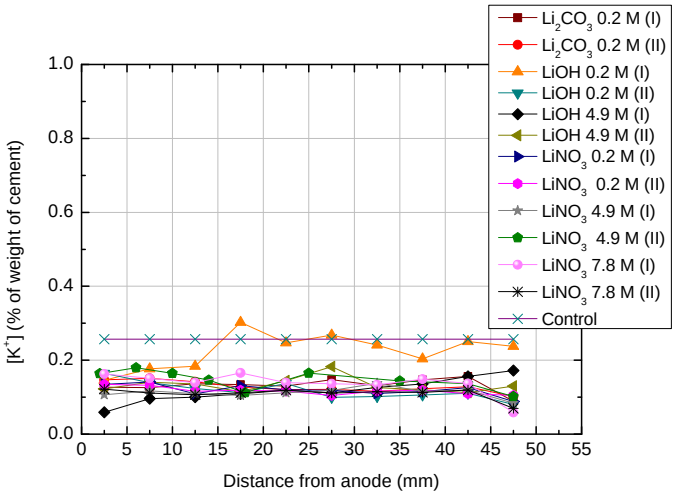

(b)

Figure 3.9: Sodium (a) and potassium (b) concentration profile in the specimen after test.

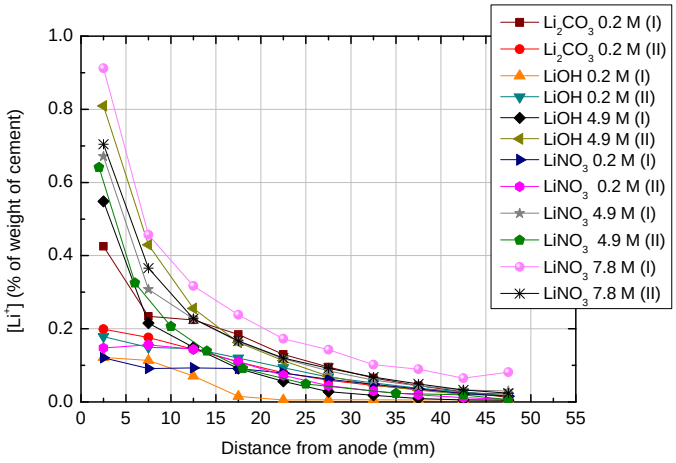

Figure 3.10: Lithium concentration profile in the specimen after test.

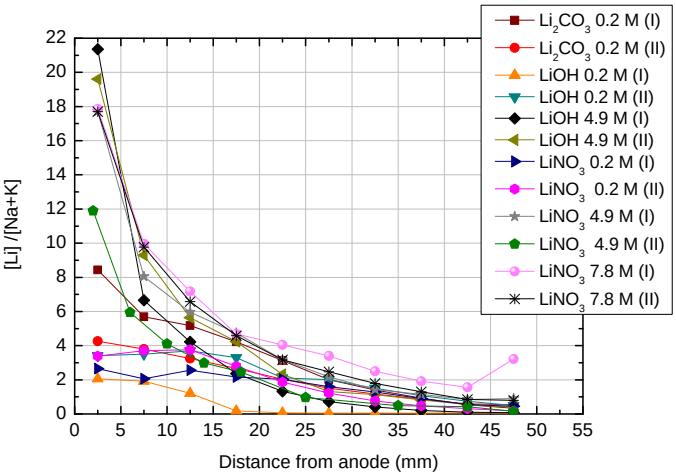

Figure 3.11: Lithium to alkalis molar ratio in the specimen after test.

Regarding the specimen LiOH 0.2 M (I), most results deviated greatly from all other experiments, indicating that problems might have occurred during the test. Indeed, until day three, the catholyte pH decreased, when it was expected to increase, while the opposite behavior was observed in the anolyte solution (Figure 3.5). Also, the concentrations of sodium and potassium in the anolyte solution (Figure 3.7 a and b) were much higher than what was found in all other cases and their peaks were on day three. These results indicate that the power source might have been mistakenly connected in the reversed direction until the third day of experiment. During that time, sodium and potassium were transported to the lithium solution and lithium ions did not migrate into the specimen due the effect of the electrical field. After the third day, when the connection was probably fixed, sodium and potassium concentrations in the anolyte start to decrease, whereas they start to build up in the catholyte solution (Figure 3.8). The effects of the delayed lithium migration into the specimen can also be observed in the lithium profile in the specimen (Figure 3.10) - there is detectable lithium only in the first 20 mm from the anode. In addition, the sodium and potassium concentration profiles (Figure 3.9) show that only the ions from the initial layers have been removed. Interestingly, the area from which sodium and potassium have been removed coincides with the area impregnated by lithium, indicating that the alkali removal may be necessary so that lithium impregnation can take place.

3.2.3. CONCLUSIONS

THE following conclusions can be drawn from this section:

- The concentration of the anolyte, rather than the type of salt in it, plays a role on the passing charge and on lithium content in the specimen. The higher is the concentration the more lithium goes into the mortar. $LiNO_3$ 7.8 M solutions were the ones that presented the highest levels of lithium after the experiment.
- Migration, under the tested conditions (for a week under 40 V), led to increase of resistivity of the specimens.
- The use of $LINO_3$ solutions led to the acidification of the anolyte solution. Although, under visual inspection, the specimens did not show deterioration, the chemical compositions of the anolyte indicate that acid attack took place in those cases. In addition, the low pH and the high anodic polarization caused the corrosion of the anodes.
- Most, if not all, free sodium and potassium left the specimen during the one week experiments and it took around five days for lithium to go through the specimen and arrive in the catholyte solutions of most cells.

3.3. EFFECT OF TIME ON MIGRATION

IN the previous section, the experiments only lasted a week, as the main goal was to observe the effect of different anolytes. However, electrochemical treatments, such as chloride removal, usually last six to ten weeks [8]. In this section, the effects of longer treatment periods (four and eight weeks)on migration will be investigated.

3.3.1. EXPERIMENTAL PROCEDURE

MATERIALS AND SPECIMEN PREPARATION

LIKE in the previous section 3.2, cylindrical specimens (diameter of 98 mm and height of 50 mm) were cast with water to cement ratio (w/c) of 0.5 and sand to cement proportion of 3:1, following the same mixing procedure. The specimens were again cured for 36 days in a fog room (20.0 ± 2.0°C and R.H. of $96 \pm 2\%$). Ordinary Portland cement type CEM I 42.5 N (Table 3.1) was used. Also, CEN standard sand with D_{max} of 2.00 mm (according to EN 196 1:2005) and deionized water were use, as before.

METHODS

AS previously, the experiments were performed in the two-chamber set-up described by ASTM 1202 [7], shown in Figure (3.1). Again, two models of cells were used (see Figure 3.2). In order to avoid the electrode corrosion observed in the previous experiments, titanium meshes with iridium/tantalum oxide coating were used as anodes (Figure 3.12).

Once again, saturated $Ca(OH)_2$ solution (0.02 M) was used as catholyte in all tests. Based on the previous results, $LiNO_3$ 7.8 M and LiOH 4.9 M solutions were chosen to be used as anolytes, as they provided the highest levels of lithium penetration. The experiments lasted four or eight weeks and the applied voltage was 40 V (0.8 V/mm). Those periods were selected because they are in the usual range of durations of electrochemical treatments of concrete structures [8]. Each experimental condition was tested with two replicates – each replicate in one type of cell, as shown in Table 3.6.

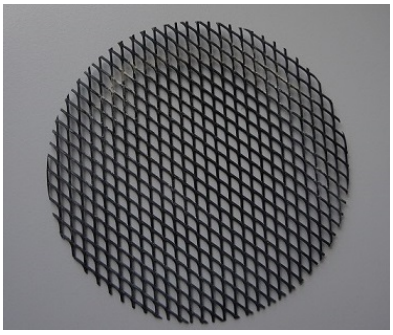

Figure 3.12: Titanium mesh used at anode (100 mm in diameter).

As in the past experiments, passing current and catholyte temperature were continuously recorded by a data logger. Electrical cell resistance and electrolyte pH were measured at least once a week, following the same procedures as before. At that time, elec-

Table 3.6: Experimental conditions for each case.

Cell type	Anolyte solution	Duration
I	LiOH 4.9 M	4 weeks
	$LiNO_3$ 7.8 M	4 weeks
	LiOH 4.9 M	8 weeks
	$LiNO_3$ 7.8 M	8 weeks
II	LiOH 4.9 M	4 weeks
	$LiNO_3$ 7.8 M	4 weeks
	LiOH 4.9 M	8 weeks
	$LiNO_3$7.8 M	8 weeks

trolytes were sampled in order to obtain their sodium, potassium, lithium and calcium (the latter only in anolyte) concentrations by ICP-OES. In order to avoid variations in volume due to evaporation that in previous experiments, the electrolyte solutions were filled up with deionized water before sampling.

After the experiment, the specimens were sliced in steps of approximately 5.0 mm and the slices were ground in a micro ball mill. Then, the powder was dissolved in 3.0 M HNO_3, as previously, and the obtained solution was analyzed by ICP-OES for lithium, sodium and potassium concentrations.

3.3.2. RESULTS AND DISCUSSION

CURRENT density plots are shown in Figure 3.13. For the first week, all cells but one ($LiNO_3$ 7.8 M 4w (I)) presented behavior very similar to what was observed in the previous experiments. The cell $LiNO_3$ 7.8 M 4w. (I) behaved differently due to connection problems, which were solved in the first week. In that cell, the voltage was inverted for two days. When the problem was observed, the electrolyte solutions were changed and the experiment started again. Some of the cells type II, without ventilation holes, had passing currents that reached the limits of the power supply. The cell LiOH 4.9 M 4w. (II) was the first that presented the problem. Around day 16, the limit was reached and the power was shut off. The issue was not noted for about 35 hours and, during that time, the system had no current. After that, the cell was connected to an alternative power source. The same happened with cell LiOH 4.9 M 8 w (II), which had no power for 40 hours, until being reconnected to another source. In the case of the cells $LiNO_3$ 7.8 M 4 w. (II) and $LiNO_3$ 7.8 M 8 w. (II), once the current reached values close to the limit, they were connected to other supplies.

After about ten days, two groups of trends can be observed. The tests performed in the cells type II then presented steadily increasing current densities, that peaked at different moments and decreased until stable levels. Those cells also presented very elevated temperatures (see Figure 3.14), following the current density trends. Indeed, at their peaks, temperatures above 80 °C were reached. Such high current densities and temperatures are not desirable – even though they might lead to high levels of lithium penetration, they may also affect the pore structure and mineralogy (e.g. ettringite is

known to decompose to form monosulfate hydrate at temperatures above 65 °C [16]) of the specimens.

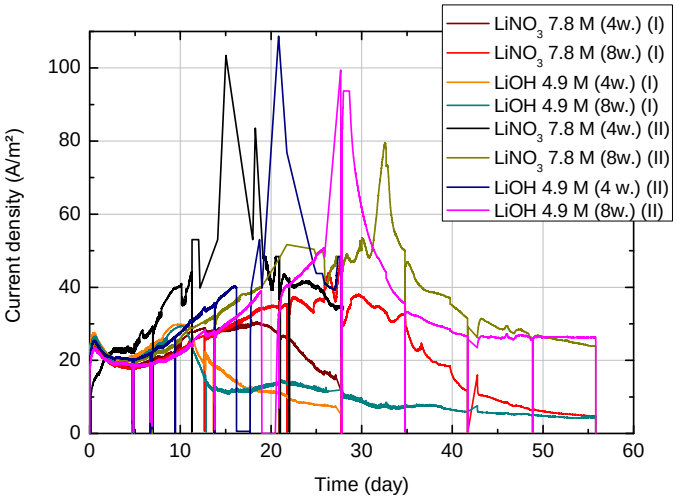

Figure 3.13: Passing current density during longer experiments.

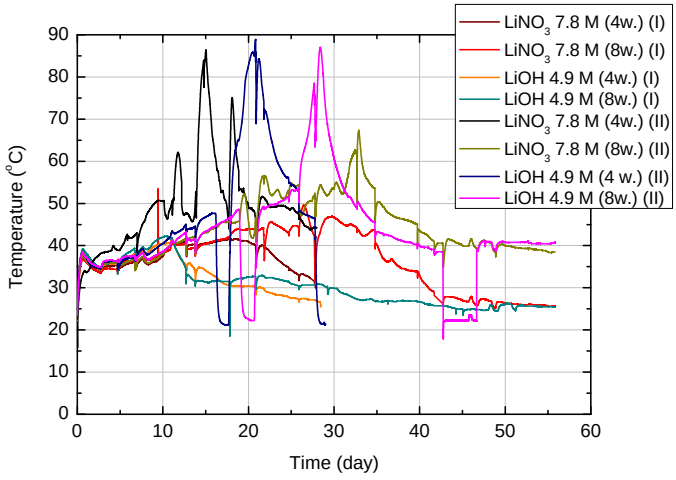

Figure 3.14: Temperature variations during longer experiments.

The specimens in cells type I (with ventilation holes) on the other hand, presented lower levels of current density. After ten days, their currents decreased or slowly increased until a stable value and dropped after some days. Once again, catholyte temperature followed the current trend for these cells and the maximum temperatures were below 50 °C. The presence of ventilation holes probably prevented these cells from heating up as much as the cells without ventilation did.

Table 3.7: Passing charges during experiment.

		Charge (kC)
Cells type I	$LiNO_3$ 7.8 M 4 w. (I)	423
	$LiNO_3$ 7.8 M 8 w. (I)	807
	LiOH 4.9 M 4 w. (I)	313
	LiOH 4.9 M 8 w. (I)	426
Cells type II	$LiNO_3$ 7.8 M 4 w. (II)	770
	$LiNO_3$ 7.8 M 8 w. (II)	1283
	LiOH 4.9 M 4 w.(II)	672
	LiOH 4.9 M 8 w. (II)	1171

The charges that passed through the specimens are shown in Table 3.7. Following the same trend observed in the current density plots, the specimens tested in cells type II had much higher current density than the ones in cells type I.

The specimen electrical resistivity behavior during the experiment is shown in Figure 3.15. Initially, the average resistivity was 44 ± 4 Ω.m. Once the experiment started, most specimens had a resistivity drop until a minimum value followed by an increase. The moment of the minimum value varied from cell to cell. This behavior is in accordance to the temperature trends of most cases. After the experiment duration, four or eight weeks, the power was shut off and, 24 hours later, specimen resistivities were one again measured and the average value was 40 ± 6 Ω.m, showing a slight decrease in relation to the initial value. This is an indication that non-reversible changes in pore structure and/or pore solution may have taken place. Nevertheless, these results are different from what was observed in the experiments of the previous section (3.2). It is possible that the higher levels of temperature and current may have affected the pore structure and/or pore solution in a different way.

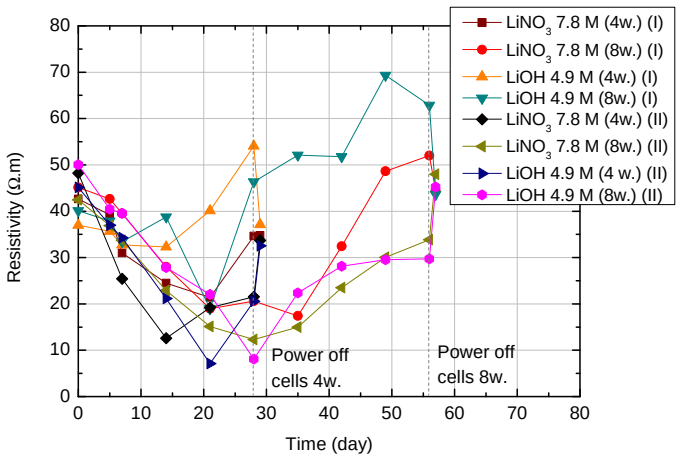

Figure 3.15: Electrical resistivity variations during longer experiments.

Table 3.8: Average resistivity values at different moments of the longer experiments.

	$LiNO_3$ 7.8 M 4 w.		LiOH 4.9 M 8w.	
	Av. (Ω.m)	CV (%)	Av. (Ω.m)	CV(%)
Initial	45	6	41	10
Middle (day 14)	19	32	27	21
End	28	23	37	45
After 24 h	34	1.6	35	7
	$LiNO_3$ 7.8 M 8 w.		LiOH 4.9 M 8 w.	
	Av. (Ω.m)	CV (%)	Av. (Ω.m)	CV (%)
Initial	44	3	45	11
Middle (day 28)	17	25	27	70
End	43	21	46	36
After 24 h	46	4	44	2

Table 3.8 shows the average resistivity values during the experiment. During treatment, the variations between replicates are fairly high, due to the differences in temperature between type I and type II cells. However, 24 hours after the end of migration, when all specimens are at room temperature, variations between replicates are lower than 7%. This indicates that possible non-reversible alterations in pore structure and/or pore solution did not depend on the type of cell used.

Variations in anolyte pH are shown in Figures 3.16. The pH of all anolyte solutions dropped in the first week, as observed in previous experiments. In the case of the LiOH solutions, the pH stabilized at 13 until the end of the tests. On the other hand, the $LiNO_3$ solutions became very acidic. Consequently, the surface of the specimens in contact with the anolyte solution was attacked, as shown in Figure 3.17. The acidification of the anolyte and the deterioration of the specimen is obviously a side effect to be avoided. The pH of the catholyte solutions was measured by two methods: using a pH-meter and using pH test strips and the results are shown in Figure 3.18. The initial measurements made with the pH-meter are correct. However, as lithium arrives in the catholyte, its concentration builds up; once a certain threshold is reached, alkaline error occurs and the readings become lower than the actual pH. This explains the drop observed in the pH-meter measurements after day 15. This effect was not noted in the previous section due to the limited concentration of lithium in those catholytes. Therefore, the values obtained with the pH test strips, shown in Figure 3.18 should be considered. Once again, a slight increase in pH was observed when a higher increase was expected.

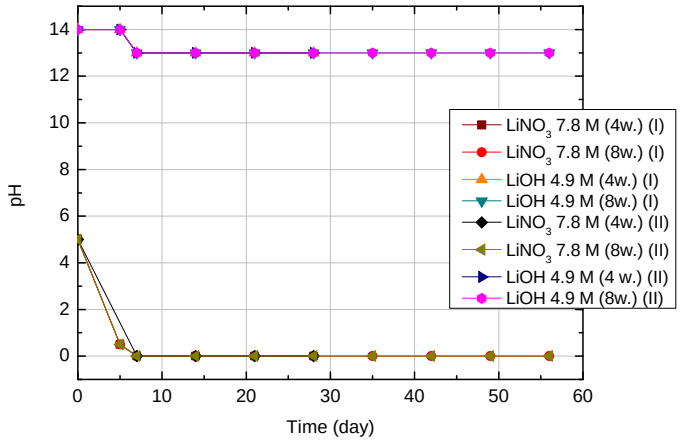

Figure 3.16: Anolyte pH variations during longer experiments. The plots from the experiments with $LiNO_3$ are overlapped as well as the plots from the tests with LiOH.

Figure 3.17: The anolyte surface of the specimen $LiNO_3$ 7.8 M 4w.(I). The surface was deteriorated by the acidic anolyte solution.

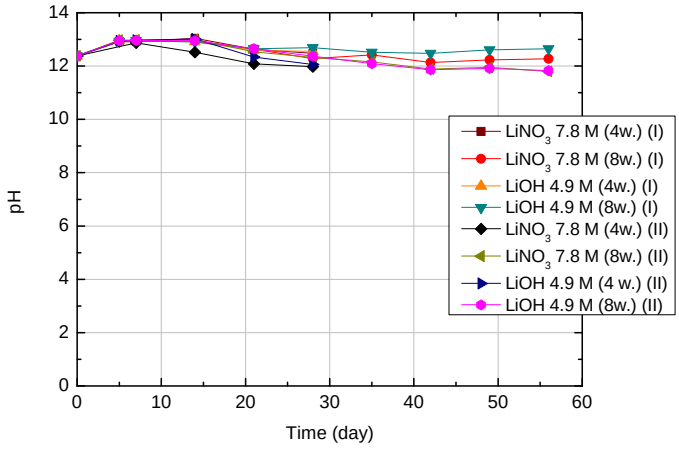

(a)

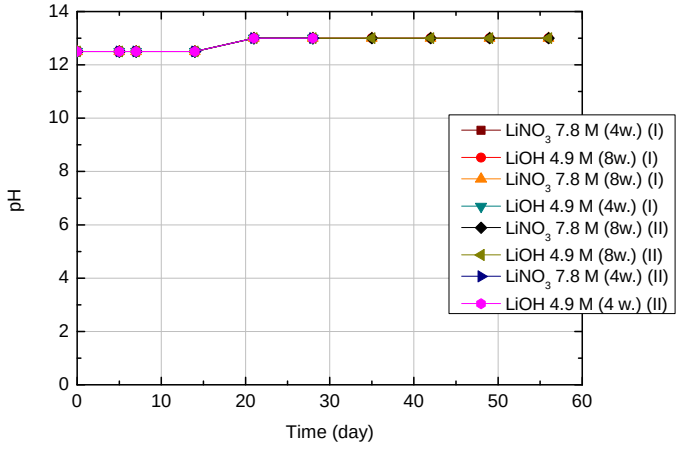

(b)

Figure 3.18: Catholyte pH variations during longer experiments measured with pH-meter (a) and pH strips (b). The plots shown in (b) are overlapped, as all experiments had the same pH values measured.

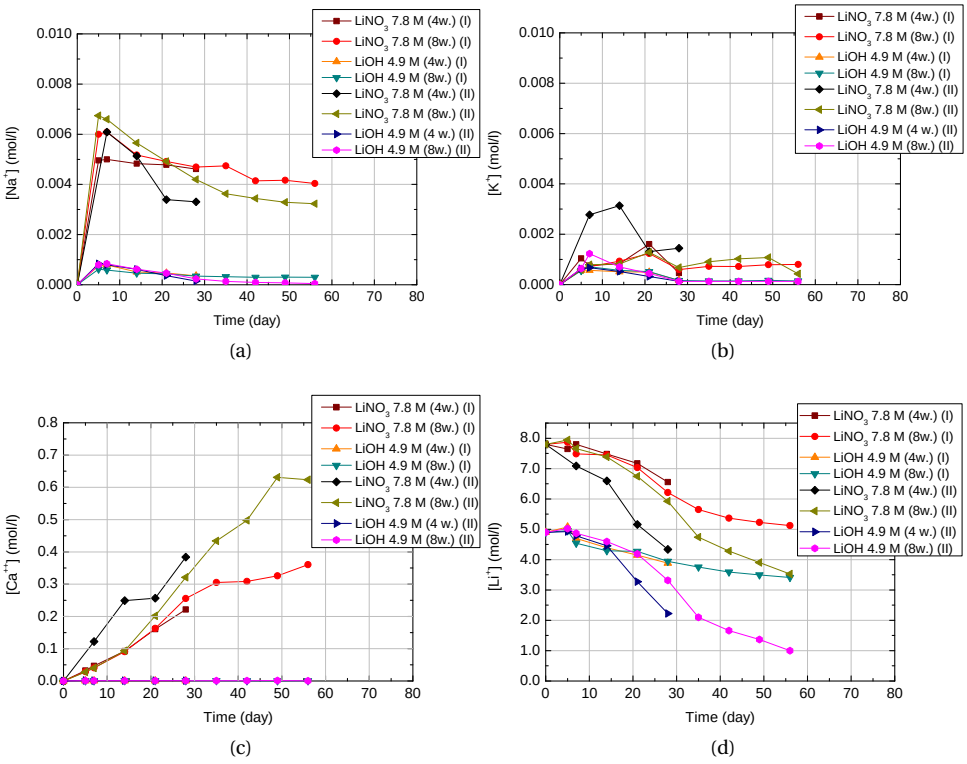

Figure 3.19: Sodium (a), potassium(b) calcium(c) and lithium (d) concentrations in the anolyte solutions during longer experiments.

Figure 3.19 shows the chemical composition of the anolyte solutions during the experiment. Sodium, potassium and calcium ions leave the specimen due to diffusion but also due to the dissolution of hydrated phases. The latter is especially seen in the cases where $LiNO_3$ was the anolyte and acid attack took place. Indeed, calcium concentrations are much higher in those solutions, due to the dissolution of $Ca(OH)_2$ and/or removal of calcium from hydrated phases [16]. Among replicates, the ones that had higher passing charge presented higher concentrations. Similar behavior can be observed in the sodium and potassium plots – the cells with $LiNO_3$ presented the highest concentrations. Interestingly, in those cases, sodium concentrations were higher than potassium whereas in the cells with LiOH, the levels of those ions are similar.

As for the lithium concentrations in the anolytes, as expected, they decrease with time – the cells that had the highest passing currents are the ones that presented the lowest final concentrations. It is noteworthy that, although a longer migration period did lead to more lithium going into the specimens, most ions left the anolyte in the first 35 days – after that, lithium migration rate decreases.

The chemical compositions of the catholyte solutions are shown in Figure3.20. Sodium

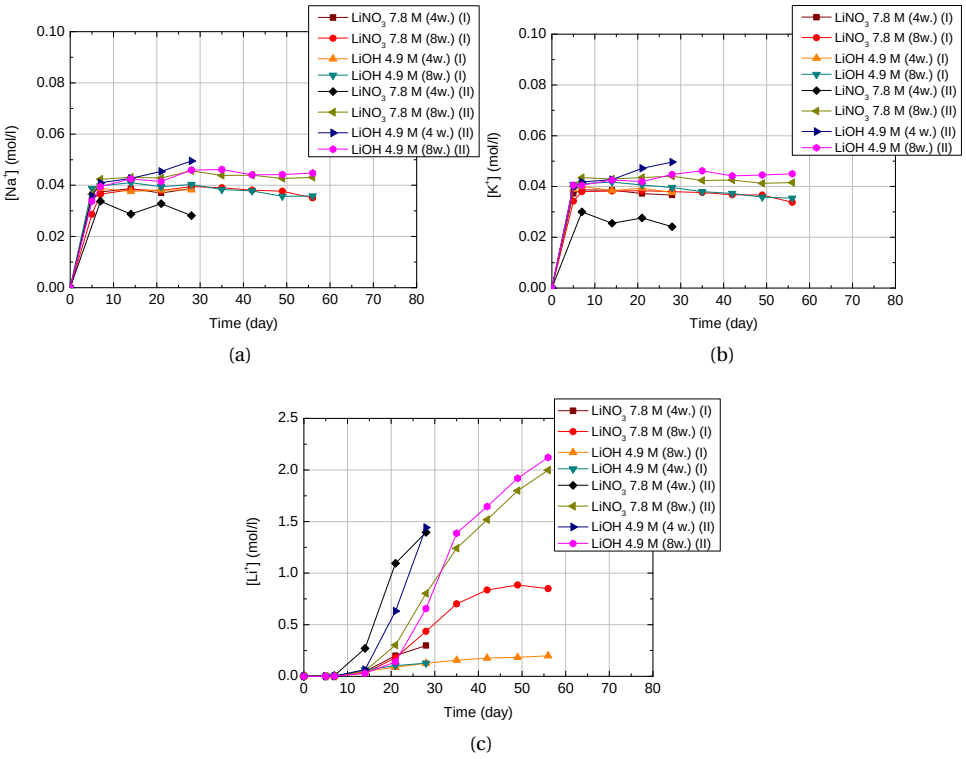

Figure 3.20: Sodium (a), potassium(b) and lithium(c) concentrations in the catholyte solutions during longer experiments.

and potassium concentrations increase in the first week and then become somewhat constant. This indicates that most of those ions left the pore solution in the first days. Also during those first days, lithium ions start to reach the catholyte, at very low concentrations (in the order of 10^{-3} mol/l). After the first week, the concentration of lithium started to build up. Once again, the cells that presented the highest passing charges were the ones with the highest lithium concentrations in the catholyte.

Sodium and potassium total concentration profiles in the specimens at the end of the test are shown in Figure 3.21. As commented for the catholyte concentration plots (Figure 3.20), most free sodium and potassium ions left the specimen in the first week. Therefore, the sodium and potassium found in the ground specimens after the test are likely to be chemically bound. Indeed, the almost constant and similar profiles, regardless of the experimental conditions, are an indication of that.

Lithium concentration profiles (see Figure 3.21), on the other hand, were quite different, depending on the experimental conditions. Overall, the specimens treated with $LiNO_3$ solution presented higher lithium content than the ones treated with LiOH. Two distinct groups can be noted, depending on the type of cell the specimens were tested in. In general, specimens tested in cells type I had lower lithium content than their repli-

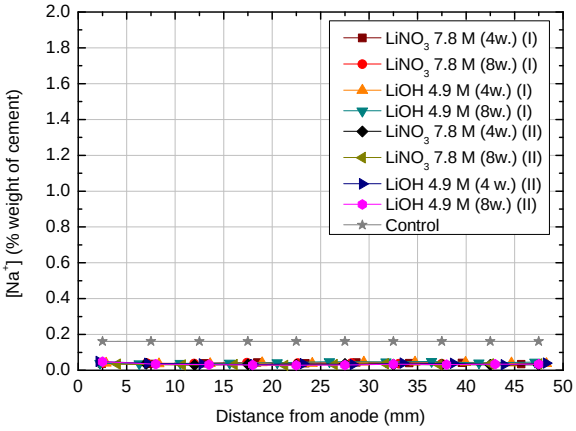

(a)

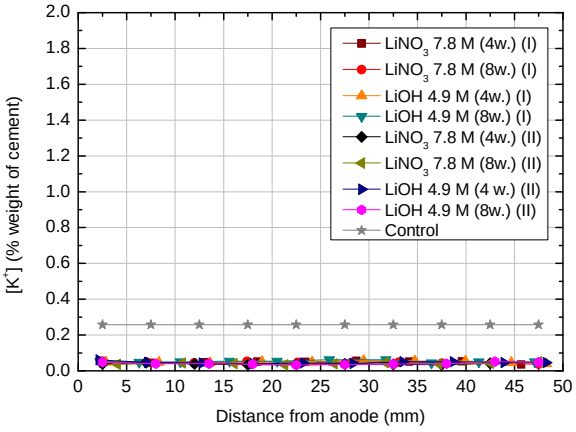

(b)

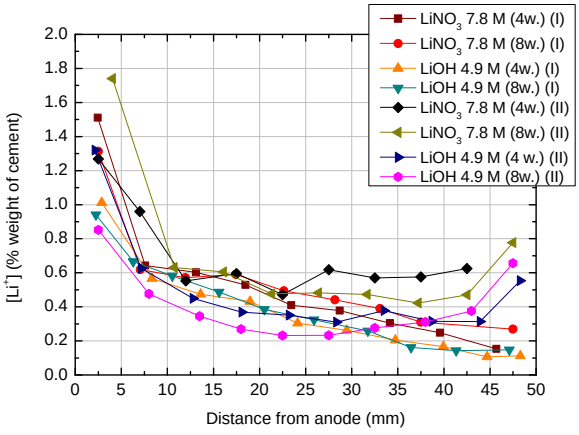

(c)

Figure 3.21: Sodium (a), potassium(b) and lithium(c) concentrations profiles in the specimens after longer experiments.

cates from cells type II, which is in accordance to the amount of passing charge. The shape of the profile also varied according to the type of cell. Although all profiles had a sharp decrease in the initial 10 mm, specimens tested in cells type I had profiles with a decreasing trend towards the catholyte. Differently, the profiles of specimens tested in cell II were somewhat flat in the middle, with increase in the final 10 mm. This different shape of profile could be due to reduced binding. In the case of chlorides, binding capacity is reduced with increase in temperature [19], [20]. If this is also true for lithium ions, the higher temperatures observed in cells type II could be responsible for lower lithium binding capacity of those specimens. In this case, more lithium ions would be free to be transported from the specimen to the catholyte. In addition, cells type II present the highest concentrations of lithium in the catholyte, which may explain the increase in concentration in the last 10 mm of the specimens. Further investigation on lithium binding is necessary in order to elucidate whether this is the case.

Table 3.9 shows the average lithium content in the specimens. The effect of time is hardly seen in the lithium profiles in specimens tested in cells type I (see Figure 3.22 (a)). Both specimens tested with LiOH had very similar profiles (and lithium content) while the one tested with $LiNO_3$ for eight weeks had slightly higher lithium content than the one tested for four weeks.

On the other hand, in the case of cells type II (see Figure 3.22 (b)), the profiles of specimens tested with the same lithium salt were not so close. In fact, in the case of $LiNO_3$ (II), although the specimen tested for eight weeks had higher concentrations in the first 10 mm, in the regions towards the cathode, the one tested for four weeks presented higher content. In the case of the specimens treated with LiOH, the one tested for four weeks had higher lithium content until 40 mm from the anode, while in the final 10 mm, the one tested for longer period presented more lithium. Either way, having higher lithium content in specimens treated for four weeks is surprising. As the specimens tested for longer period presented higher passing charge, they were expected to present higher lithium concentrations. However, once again, the effect of temperature on lithium binding could have played a role. The specimen tested for eight weeks was exposed to higher temperatures (in average 12 °C higher than the cells (I) with LiOH) for longer periods than the specimen treated for four weeks. Overall, these results show that the rate of lithium penetration decreases with time (or passing charge). This is probably due to the fact that the concentration of lithium in the anolyte solutions drops throughout the test.

The lithium to alkalis molar ratios ($\frac{[Li]}{[Na+K]}$) throughout the specimens after the experiments are shown in Figure 3.23. All specimens show $\frac{[Li]}{[Na+K]}$ far above the minimum ratio ($\frac{[Li]}{[Na+K]}$ = 1.0) required to prevent ASR deleterious expansion in all regions. However, as mentioned in the previous section, the reference minimum $\frac{[Li]}{[Na+K]}$ ratio for preventing ASR expansion in new structures is not necessarily the same as the one needed to stop the reaction in existing constructions.

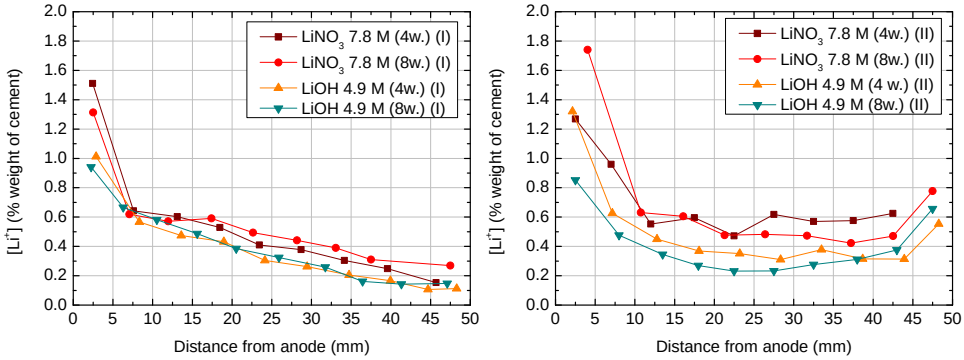

Figure 3.22: Lithium concentration profiles in the specimens tested in cells type I (a) and in cells type II (b)

Table 3.9: Average lithium content in specimens after experiments.

Specimen	Average Li (%wt. of cement)
$LiNO_3$ 7.8 M (4w.) (I)	0.51
$LiNO_3$ 7.8 M (8w.) (I)	0.53
LiOH 4.9 M (4w.) (I)	0.39
LiOH 4.9 M (8w.) (I)	0.39
$LiNO_3$ 7.8 M (4w.) (II)	0.68
$LiNO_3$ 7.8 M (8w.) (II)	0.73
LiOH 4.9 M (4w.) (II)	0.48
LiOH 4.9 M (8w.) (II)	0.41

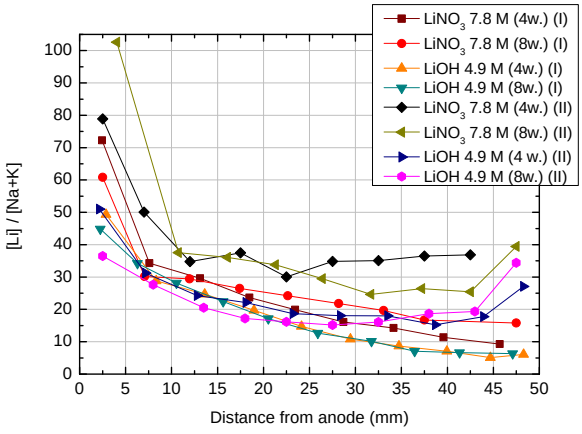

Figure 3.23: Lithium to alkali ratio in specimens after longer treatments.

3.3.3. CONCLUSIONS

The following conclusions can be drawn from this section:

- Specimens tested in cells without ventilation holes presented the highest values of current density. In fact, in those cells, very high levels of current density and temperature (above 100 A/m^2 and 80 °C, respectively) were reached.
- Even though lower levels of current density and temperature were reached in the cells with ventilation holes, those values were still high enough to possibly cause deterioration to concrete or mortar.
- When $LiNO_3$ 7.8 M was used as anolyte, the acidification of the solution and the prolonged exposition to it led to the deterioration of the surface of the specimens. The use of a basic anolyte, such as LiOH 4.9 M, avoided the attack.
- Most sodium and potassium ions were removed from the pore solution in the first week, for most cells.
- Specimens tested for eight weeks did not exhibit much higher lithium content than those tested for four weeks. This means that the efficiency of the treatment decreases over time and this is probably related to the fact that lithium content in the anolyte solution decreases throughout the experiment.
- When comparing specimens tested with the same type of cell, $LiNO_3$ led to higher levels of lithium penetration.

3.4. EFFECT OF EMBEDDED CATHODE ON MIGRATION

IN the previous sections, a two-chamber set-up was used to investigate lithium migration. In this type of set-up, the cathode is placed externally to the specimen, which allows to the removal of alkali ions. In the case of real structures, however, as for chloride extraction treatment, the reinforcement might be used as cathode. The use of embedded rebar as cathode might alter the lithium migration process and lead to undesirable side effects, such as the accumulation of alkali ions in the region around it (which may possibly induce further ASR development in the area). In this section, the use of embedded as cathode will be investigated.

3.4.1. EXPERIMENTAL PROCEDURE

Figure 3.24: Specimen with embedded titanium mesh. The wire coming out of the specimen on the left is from the embedded mesh.

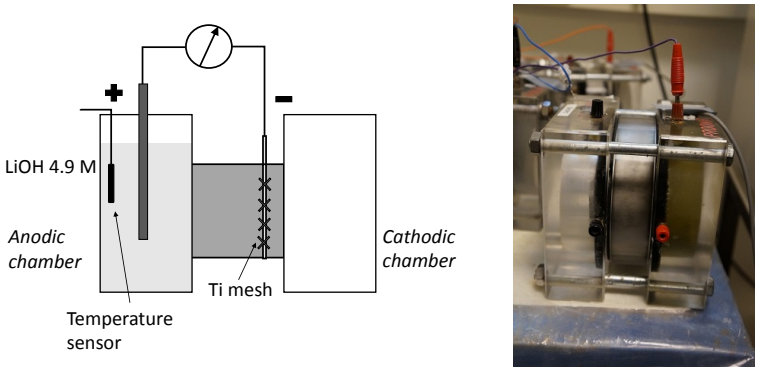

(a) (b)

Figure 3.25: Diagram of the experimental set-up (a) and experimental set-up (b).

MATERIALS AND SPECIMEN PREPARATION

MORTAR cylinders (diameter of 98 mm and 60 mm of height) were cast with a titanium mesh at 10 mm from one of the surfaces, as shown in Figure 3.24. The mesh was embedded to represent the situation when a reinforcement bar would be used as cathode in a structure under treatment. The mortar mixture was the same previously used. Once again, the specimens were cured for 36 days in a fog room ($20.0 \pm 2.0\,^{\circ}C$ and R.H. of $96 \pm 2\%$).

METHODS

THE two chamber set-up previously described was used. Each specimen was positioned between two chambers – one with lithium solution and the other remained empty, working only as support for the specimen (Figure 3.25). For these experiments, LiOH 4.9 M was chosen, in order to avoid the acidification of the anolyte and the deterioration of the specimen. The chamber with electrolyte received a titanium mesh with iridium/tantalum oxide coating that worked as anode and the embedded titanium mesh in the specimens were used as cathodes. Again, two types of cells were used: type I cells had ventilation holes, while the type II did not (Figure 3.11).

The experiments lasted four or eight weeks and the applied voltage was 15 or 25 V (electric field of 0.3 or 0.5 V/mm). Lower values of voltage were chosen in order to avoid the very high currents and temperatures observed in section 3.3. Passing current and anolyte temperature were constantly recorded by a data logger. Anolyte pH and specimen electrical resistance were measured once a week, by the same procedures previously described. At those occasions, the anolyte solutions were sampled in order to obtain sodium, potassium, lithium and calcium concentrations, by ICP-OES. Like in the experiments in section 3.3, the anolyte chambers had their solution levels completed with deionized water before sampling, to avoid the influence of evaporation. After the tests, images from the specimens were made in a X-ray computed tomography scanner, in order to check for debonding of the mesh. The images were made in a macro CT-scanner similar to the ones used for medical applications. The resolution on the horizontal place (the place of each slice) was of 3.0 mm and the resolution on the vertical direction was of 1.0 mm.

Finally, as previously, the mortar cylinders were cut in slices of approximately 5.0 mm, which were ground in a micro ball mill. The obtained powder was then dissolved in 3.0 M HNO_3 and the final solution was filtered following the same procedure previously described. The obtained clear solutions were analyzed by ICP-OES for lithium, sodium and potassium concentrations.

3.4.2. RESULTS AND DISCUSSION

CURRENT density plots are shown in Figure 3.26. The cells exhibited rapid increase in current density in the first hours and reached a maximum value in less than 12 hours, similarly to what was observed in previous experiments. After that, the current density dropped steadily until about day 30, when it stabilized until the end of the experiment (in the case of the cells tested for eight weeks). When comparing the cells under the same level of voltage, it can be noted that cells in the set-up type II presented higher current density than those in the set-up type I - and the difference was more pro-

nounced when the applied voltage was higher. It is worth noting that specimens under 25 V had current densities above 10 A/m^2 for the first days, and subsequently dropped to lower values, whereas for the cells under 15 V, that level was not reached – the maximum current density for those cells was around 8 A/m^2. It is generally accepted that current densities higher than 10 A/m^2 may lead to concrete (or mortar) deterioration [8].

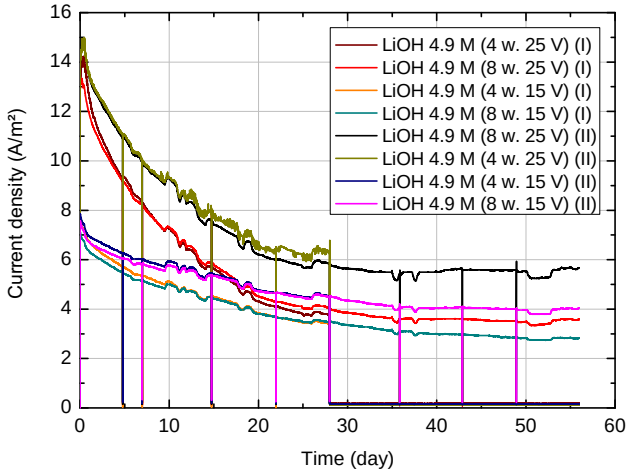

Figure 3.26: Current density plots in the experiments with embedded cathode.

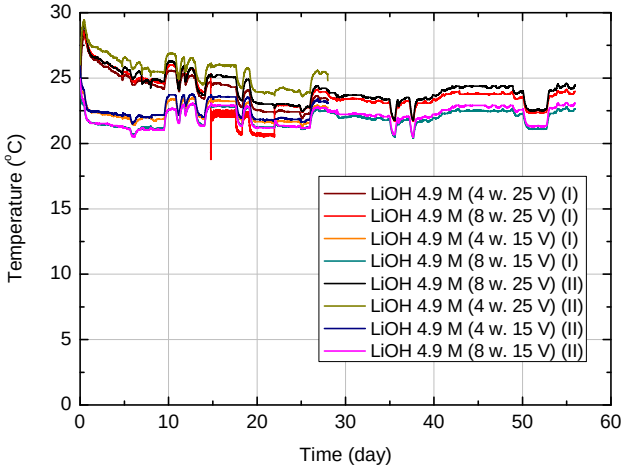

Figure 3.27: Anolyte temperature plots in the experiments with embedded cathode.

Applying lower voltage had desired effect on the temperature of the systems. Figure 3.27 shows the anolyte temperatures, which were all below 30 °C. From day 14 until day 20, the cell LiOH 4.9 M (8 w. 25V I) did not have its anolyte temperature measured due to problems with the temperature sensor. The temperature of the anolytes follow the same

Table 3.10: Passing charges for the experiments with embedded cathode.

Cells	Charge (kC)
LiOH 4.9M 4w 25V (I)	123
LiOH 4.9M 8w 25V (I)	186
LiOH 4.9M 4w 15V (I)	88
LiOH 4.9M 8w 15V (I)	138
LiOH 4.9M 4w 25V (II)	159
LiOH 4.9M 8w 25V (II)	253
LiOH 4.9M 4w 15V (II)	103
LiOH 4.9M 8w 15V (II)	172

trend as the current density plots. The cells under 25 V had the highest temperatures and, for the same voltage level, the set-ups type I presented slightly lower values. This happened most likely due to the presence of ventilation holes in ring around the specimen. Lower temperatures led to higher resistivity values and, finally, to lower current densities. Table 3.10 shows the passing charges. As expected, higher voltage and longer period of test led to higher charge. In addition, specimens tested in set-ups type II had higher passing charge than the ones tested in cells type I.

Electrical resistivity values during the experiment are shown in Figure 3.28. Table 3.11 shows the average values between replicates at different moments of the experiments. Initially, the specimens presented average resistivity of 35 ± 1 Ω.m. The specimens tested in cells type I (either for four or eight weeks) presented increasing resistivity until the end of the experiment. The ones tested in set-up type II had increasing values for the first four weeks and then their resistivity stabilized until the end of the eight weeks. The difference in behavior between specimens in different types of cells is evident in the variations between replicates (Table 3.11). For the same level of applied voltage, specimens tested in set-ups type I presented greater increments in resistivity than the ones tested in cells type II.

Within the same type of set-up, the cells that received higher voltage had higher resistivity by the end of the experiment. At the end of the tests, the current was turned off and resistance was measured after 24 hours. Interestingly, the resistivities did not return to the initial values, indicating that the variations during the experiment were not a mere effect of temperatures. This indicates that there were, in fact, irreversible changes in the pore structure and /or in the pore solution composition. One possibility could be that the production of H_2 on the titanium mesh in the specimens, due to cathodic reaction (3.3), led to development of pressure that resulted in local debonding. In order to check for development of cracking around the mesh, the specimens were analyzed by computerized tomography (CT). No debonding or cracking were detected at the resolution used in this analysis. Figure 3.29 shows CT scan images from the region around the mesh of the specimen LiOH 4.9 M (8w. 25 V).

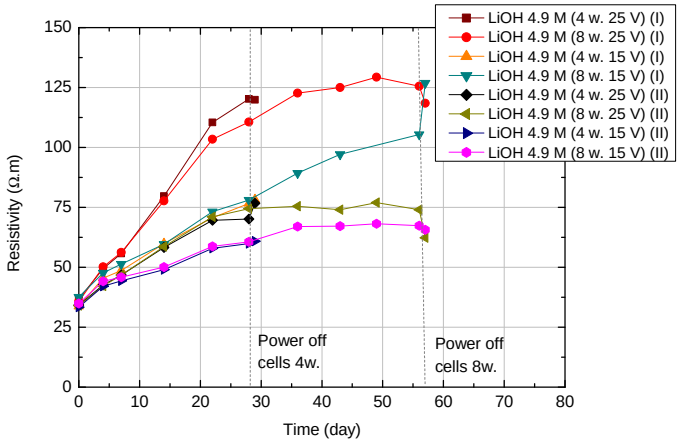

Figure 3.28: Cell resistivity behavior during experiments with embedded cathode.

Table 3.11: Average resistivity values at different moments of the experiments with embedded cathode.

	LiOH 4.9 M (4 w. 25 V)		LiOH 4.9 M (4 w. 15 V)	
	Av. (Ω.m)	CV (%)	Av. (Ω.m)	CV (%)
Initial	36	4	34	1
Middle (14 days)	69	16	55	10
End	95	26	68	12
After 24 h	98	22	70	13
	LiOH 4.9 M (8 w. 25 V)		LiOH 4.9 M (8 w. 15 V)	
	Av. (Ω.m)	CV (%)	Av. (Ω.m)	CV (%)
Initial	35	2	36	4
Middle (28 days)	93	20	69	13
End	100	26	86	22
After 24 h	90	31	96	32

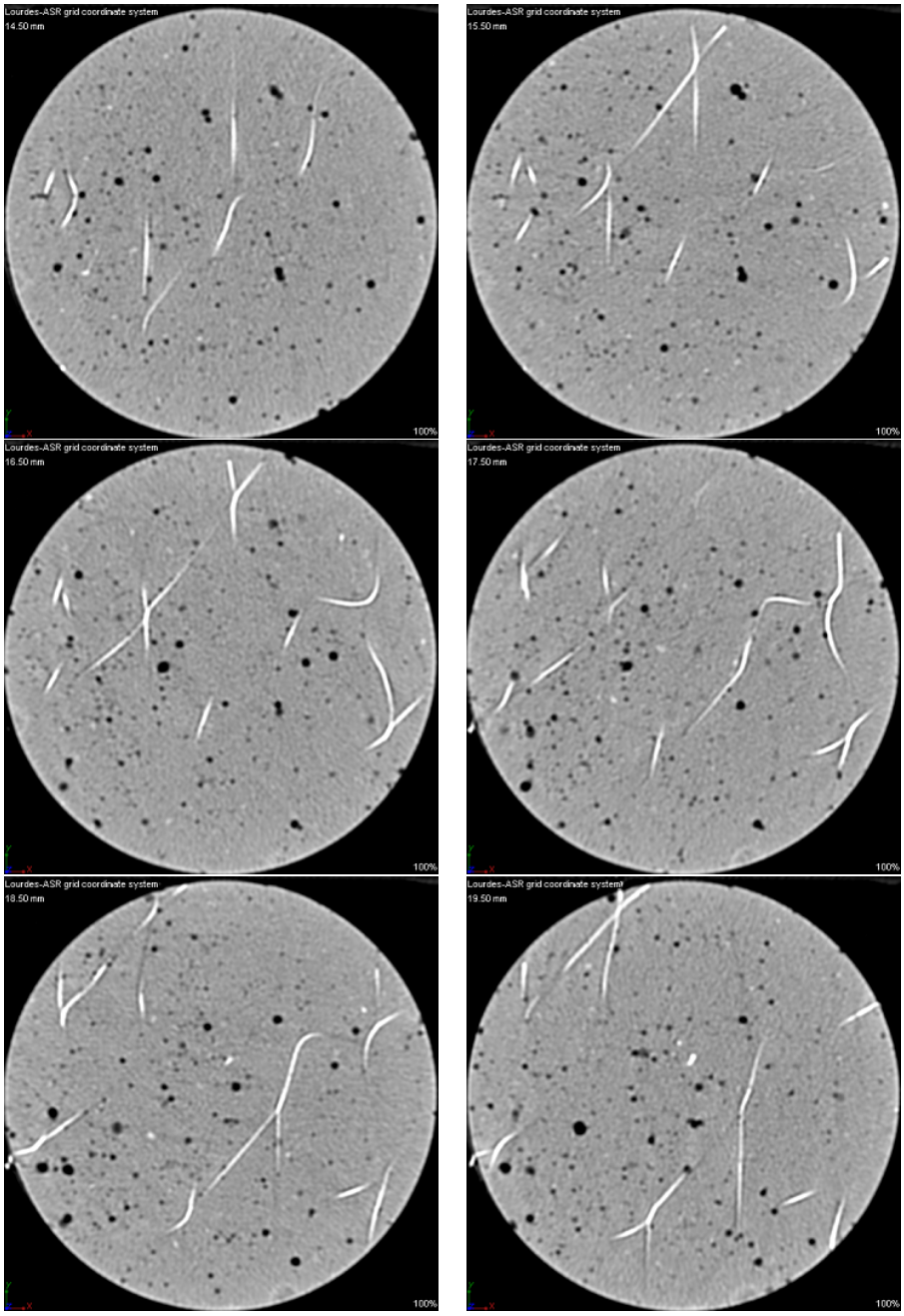

Figure 3.29: Images obtained by computerized tomography of the region around the titanium mesh in specimen LiOH 4.9 M (8w. 25 V). The clear areas are the mesh. No debonding or cracking can be detected.

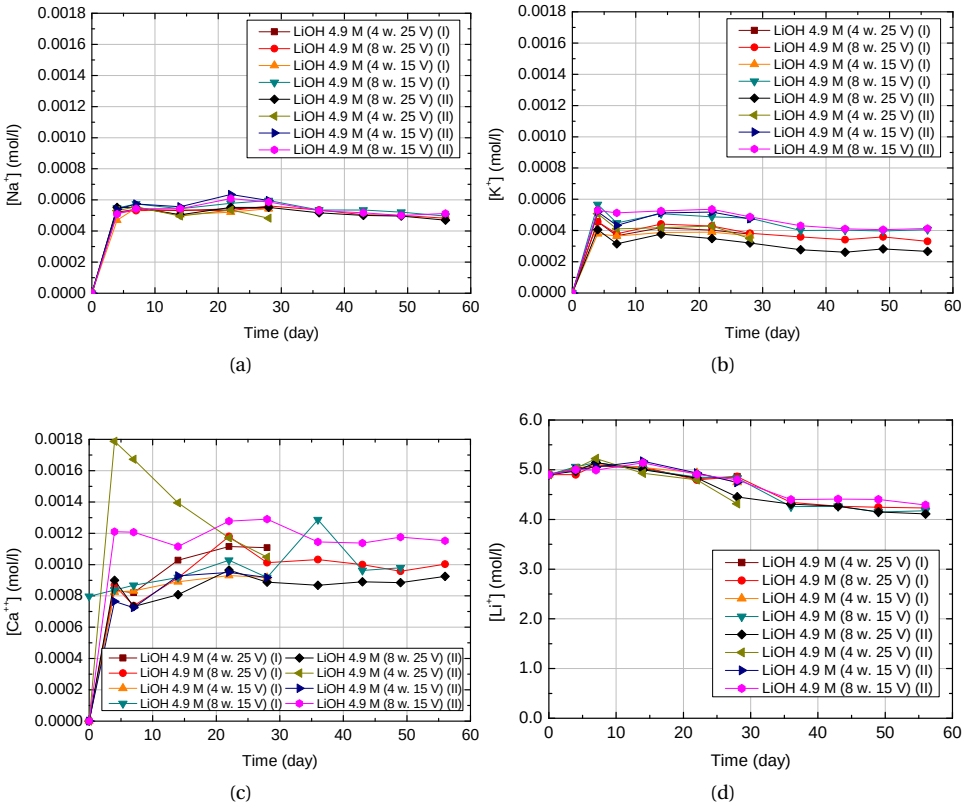

Figure 3.30: Sodium (a), potassium (b), calcium (c) and lithium (d) concentrations in anolyte solutions during experiments with embedded cathode.

The pH of the anolyte solution of all cells remained 14 throughout the test, due to the high buffer capacity of the initial solution. Figure 3.30 presents the chemical composition of the anolyte solutions during the experiment. Sodium, potassium and calcium ions leached from the specimen by diffusion and dissolution during the first couple of days and reached constant levels throughout the tests (Figure 3.30 a, b and c). There is no correlation between passing charges and final level of those concentrations. Lithium ions left the anolyte into the specimen, as expected (Figure 3.30 d). Overall, the specimens with the highest passing charges are the ones with the lowest final lithium concentrations in the anolyte, as expected.

Sodium and potassium concentration profiles in the specimen can be seen in Figure 3.31. As expected, sodium and potassium ions were attracted by the cathode and concentrated in the area around it. Overall, the concentrations in the region until 35-40 mm from the anode are close to the ones found in the profiles from section 3.3. This indicates that most (if not all) free sodium and potassium were removed from that area. And the specimens with the highest passing charge had profiles shifted towards the cathode.

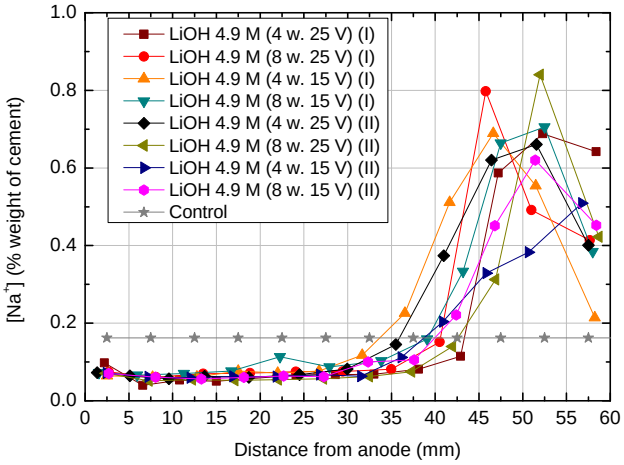

(a)

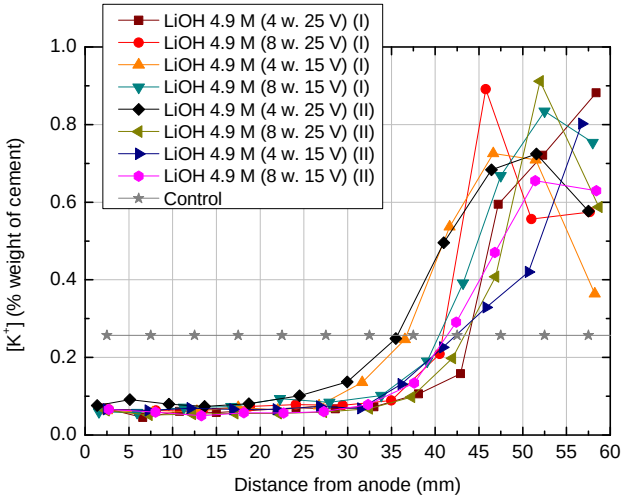

(b)

Figure 3.31: Sodium (a)and potassium (b) in the specimens tested with embedded cathode. The mesh is situated at 50 mm from the anode.

Lithium profiles are shown in Figure 3.32. The specimens with highest passing charges are the ones in which lithium was able to reach deeper layers. In fact, the total lithium content in the specimens, shown in Table 3.12, can be correlated to the passing charges. Nevertheless, in most specimens, lithium ions did not reach deeper layers. Lithium to alkali molar ratios ($\frac{[Li]}{[Na+K]}$) throughout the specimens can be seen Figure 3.33. No specimen had $\frac{[Li]}{[Na+K]}$ above 1.0 in all regions. In fact, most specimens only reach that value in the first 25-35 mm from the anode.

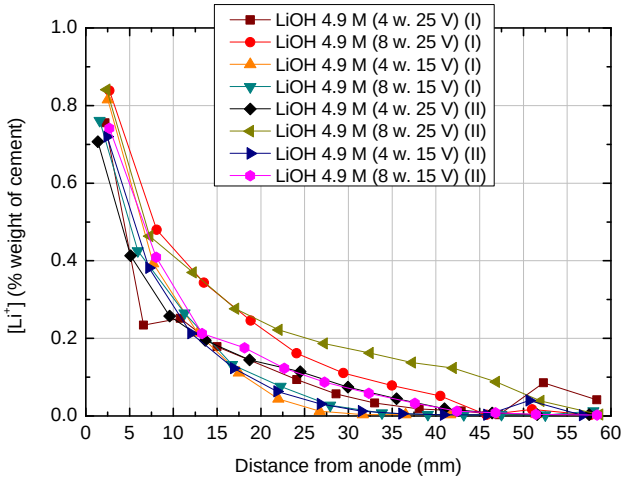

Figure 3.32: Lithium profiles in the specimens tested with embedded cathode.The mesh is situated at 50 mm from the anode.

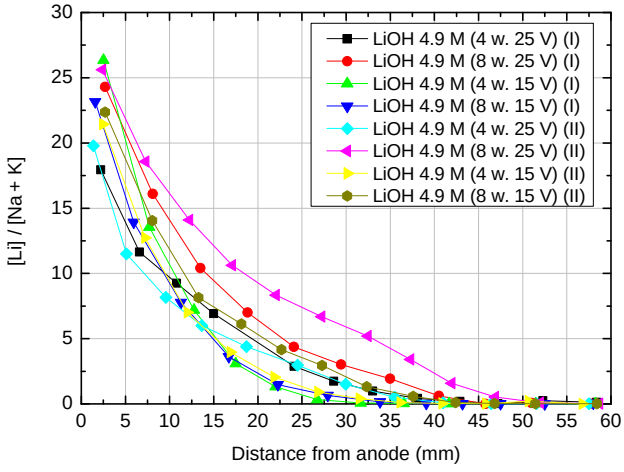

Figure 3.33: Lithium to alkalis molar ratio in the specimen tested with embedded cathode.The mesh is situated at 50 mm from the anode.

Table 3.12: Average lithium content in specimens after testing.

Specimen	Average Li (%wt. of cement)
LiOH 4.9M 4w 25V (I)	0.13
LiOH 4.9M 8w 25V (I)	0.20
LiOH 4.9M 4w 15V (I)	0.13
LiOH 4.9M 8w 15V (I)	0.13
LiOH 4.9M 4w 25V (II)	0.13
LiOH 4.9M 8w 25V (II)	0.23
LiOH 4.9M 4w 15V (II)	0.13
LiOH 4.9M 8w 15V (II)	0.15

3.4.3. CONCLUSIONS

The following conclusions can be drawn from this section:

- As expected, cells under 25 V presented higher current density and passing charge than the cells under 15 V. In addition, once again the ventilation holes in the cells influenced the results - cells with no ventilation holes presented higher passing charge.
- Limiting the value of the applied voltage resulted in much lower temperatures and current densities than the ones observed in the previous experiments.
- The resistivity values after 24 h of all specimens were significantly higher than the initial ones, indicating that non-reversible changes to the pore structure and/or pore solution composition may have taken place. Debonding of the titanium mesh was not observed in images obtained by computerized tomography.
- Sodium and potassium ions accumulated in the region close to the titanium mesh. Moreover, very few or no lithium ions arrived in that region.
- As sodium and potassium ions accumulate around the cathode, hydroxyl ions produced by the cathodic reaction (Equation 3.3) are likely to accumulate in that region, in order to electrically balance the positive charge of the alkalis. In the case of the treatment of ASR affected concrete using the reinforcement as cathode, the increase in alkali and hydroxyl concentrations in that area is likely to locally induce further formation of ASR gel (if enough reactive silica is still present in the system). In fact, Bentivegna et al. [21] mentioned that the alkali accumulation around the reinforcement combined with the lack of lithium ion in that area after treatment were probably the cause for the remaining expansive behavior. In their experiments, treated columns had expansion levels similar or greater than the untreated ones. Therefore, the accumulation of alkalis near the cathode is a potentially dangerous side effect, if not enough lithium ions reach that area, in order to mitigate further expansion.

REFERENCES

[1] L. M. Souza, R. B. Polder, and O. Çopuroğlu, *Influence of anolyte on lithium migration in concrete,* in *Durability of Reinforced Concrete from Composition to Protection* (Springer, 2015) pp. 27–34.

[2] L. M. S. Souza, R. B. Polder, and O. Çopuroğlu, *Lithium migration in mortar specimens with embedded cathode,* in *Concrete Repair, Rehabilitation and Retrofitting IV: Proceedings of the 4th International Conference on Concrete Repair, Rehabilitation and Retrofitting (ICCRRR-4), 5-7 October 2015, Leipzig, Germany* (CRC Press, 2015) p. 39.

[3] L. M. S. Souza, R. B. Polder, and O. Çopuroğlu, *Investigation on lithium migration for treating alkali-silica reaction affected concrete,* in *Proceedings of the 1st Concrete Innovation Conference, CIC 2014, Oslo, Norway, June 11-13, 2014. Authors version* (NCF, 2014).

[4] C. Page, *Interfacial effects of electrochemical protection methods applied to steel in chloride-containing concrete,* in *Proceedings of International Conference on Rehabilitation of Concrete Structures* (1992) pp. 179–187.

[5] T. Ueda, A. Nanasawa, and M. Tsukagoshi, *Influence of electrochemical lithium penetration from various kinds of lithium solution on ASR expansion of concrete,* in *Proceedings of the 4th International Conference on Concrete Repair, Rehabilitation and Retrofitting* (CRC Press, 2015).

[6] T. Ueda, Y. Baba, and A. Nanasawa, *Penetration of lithium into ASR affected concrete due to electro-osmosis of lithium carbonate solution,* Construction and Building Materials **39**, 113 (2013).

[7] ASTM-C1202-05, *Standard test method for electrical indication of concrete's ability to resist chloride ion penetration,* (2005).

[8] L. Bertolini, B. Elsener, P. Pedeferri, E. Redaelli, and R. B. Polder, *Corrosion of steel in concrete: prevention, diagnosis, repair*, 2nd ed. (John Wiley & Sons, 2013).

[9] R. B. Polder, *Test methods for on site measurement of resistivity of concrete - a RILEM TC -154 technical recommendation,* Construction and building materials **15**, 125 (2001).

[10] W. Boyes, *Instrumentation reference book* (Butterworth-Heinemann, 2009).

[11] J. Pacheco and R. B. Polder, *Preliminary study of electrochemical lithium migration into cementitious mortar,* in *2nd International Symposium on Service Life Design for Infrastructures* (RILEM Publications SARL, 2010) pp. 1093–1100.

[12] C.-C. Liu, W.-C. Wang, and C. Lee, *Behavior of cations in mortar under accelerated lithium migration technique controlled by a constant voltage,* Journal of Marine Science and Technology **19**, 26 (2011).

[13] P. Banfill, *Re-alkalisation of carbonated concrete - effect on concrete properties,* Construction and Building Materials **11**, 255 (1997).

[14] M. Siegwart, J. F. Lyness, and B. J. McFarland, *Change of pore size in concrete due to electrochemical chloride extraction and possible implications for the migration of ions,* Cement and Concrete Research **33**, 1211 (2003).

[15] D. Koleva, O. Copuroglu, K. van Breugel, G. Ye, and J. De Wit, *Electrical resistivity and microstructural properties of concrete materials in conditions of current flow,* Cement and Concrete Composites **30**, 731 (2008).

[16] H. F. Taylor, *Cement chemistry* (Thomas Telford, 1997).

[17] A. M. Neville, *Properties of concrete*, 5th ed. (Pearson, 2011).

[18] X. Feng, M. Thomas, T. Bremner, B. Balcom, and K. Folliard, *Studies on lithium salts to mitigate ASR-induced expansion in new concrete: a critical review,* Cement and Concrete Research **35**, 1789 (2005).

[19] H. Zibara, *Binding of external chlorides by cement pastes*, Ph.D. thesis, University of Toronto (2001).

[20] C. Larsen, *Effect of type of aggregate, temperature and,* in *RILEM International Workshop on Chloride Penetration into Concrete* (RILEM Publications SARL, 1995) pp. 27–35.

[21] A. Bentivegna, E. Giannini, and K. Folliard, *Use of electrochemical migration to mitigate alkali-silica reaction in large scale concrete structures,* Concrete Solutions (2011).

4

MODELING OF LITHIUM MIGRATION IN MORTAR

Parts of this chapter have been published in Souza et al., Study on lithium migration for electrochemical treatment of concrete affected by alkali-silica reaction, 2014 [1]

4.1. INTRODUCTION

NUMERICAL modeling can be a useful tool in understanding mechanisms and principles behind ionic migration in cement-based materials. In fact, in the past years, a variety of models has been proposed, mostly to describe the transport (ingress or removal) of chloride in concrete. Even though most models use the mass balance equation (Nernst-Planck) to describe the movement of species in solution, different approaches are employed.

Many studies only consider the ion of interest - the effect of the interaction between species is neglected and one mass balance equation is used (e.g. [2],[3], [4]). On the other hand, simulations that take into consideration different ions in the pore solution (e.g. sodium, potassium, hydroxyl) become more complex, as they demand a separate mass balance equation for each species. Moreover, they also consider electroneutrality of the electrolyte, in an additional equation (e.g.[5], [6], [7]). A further step is taken when those species are no longer considered inert – they leave or enter the pore solution by chemical reactions or physical adsorption. In the work of Peelen et al. [8], for example, the calcium hydroxide equilibrium was considered in a cathodic protection system. In models describing chloride movement, binding can be included (e.g. [3], [5]).

In this chapter, a multi-ion model for lithium transport in mortar discs during a two-chamber lithium migration experiment is proposed. This type of model was considered because the presence of other ions in the pore solution might influence lithium transport. First, a summary on the theory behind species transport in solution and in concrete is presented. Then, the modeled system is presented. The model is validated with experimental results presented in previous the chapter.

4.2. MATHEMATICAL MODEL

4.2.1. TRANSPORT IN SOLUTION

IN order to describe the mass transfer process in a solution, it is necessary to describe the movement of ions, mass balances, current flow and electroneutrality [9].

Considering a control volume as the one in Figure 4.1, the variation of concentration

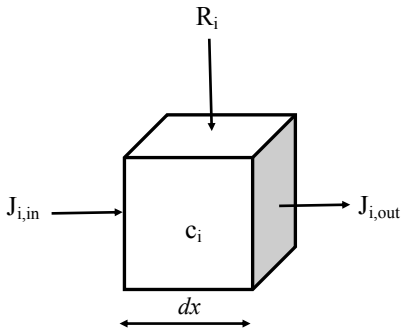

Figure 4.1: The variation of the concentration of a species i in an infinitesimally small cube due to the difference between the fluxes j_i, in and j_i, out, with the addition of the reaction term R_i.

of a species i over time is given by the general conservation of mass equation:

$$\frac{\partial c_i}{\partial t} = -\nabla J_i + R_i \tag{4.1}$$

where c_i is the concentration of species i, in mol/m^3, J_i is the flux, in mol/m^2.s, and R_i is the reaction term, in mol/m^3.s. The flux indicates the direction in which the species are moving and the amount of moles passing through a plane with time. Under an electric field, the flux can be described as a combination of three different transport mechanisms - diffusion, ionic migration and advection:

$$J_i = J_{i,diff} + J_{i,m} + J_{i,a} \tag{4.2}$$

where $J_{i,diff}$ is the flux due to diffusion, in mol/m^2.s, $J_{i,m}$ is the flux due to migration, in mol/m^2.s, and $J_{i,a}$ is the flux due to advection, also in mol/m^2.s. The flux contribution due to diffusion, that is, due to a concentration gradient, is given by Fick's first law:

$$J_{i,diff} = -D_i \nabla c_i \tag{4.3}$$

where D_i is the diffusion coefficient, in m^2/s of the species i. The flux due to ionic migration is proportional to the ionic concentration, the gradient of potential (ϕ, in V) and the ionic mobility ($u_{m,i}$, in m^2/s.V), as expressed in:

$$J_{i,m} = -u_{m,i} c_i \nabla \phi \tag{4.4}$$

Ionic mobility is a property related to the size of the ion, including its adherent water molecules, and it is defined as the velocity of the ion in an electric field of unit strength. Ionic mobility values of some ions can be found in Table 4.1.

The diffusion coefficient of an ion is related to the ionic mobility by the Nernst-Einstein equation [9]:

$$D_i = RT \frac{u_{m,i}}{z_i F} \tag{4.5}$$

where R is the universal gas constant (8314 J/K.mol), T is the absolute temperature, in K; z_i is the valence of ion i and F is the Faraday constant (96485 C/mol). The advective flux is induced by the velocity of the fluid u (in m/s) and it is given by:

Table 4.1: Ionic mobilities in water at 25 °C. [10], [11].

Cation (+)	Ionic mobility (m^2/s. V)	Anion (-)	Ionic mobility (m^2/s.V)
H^+	36.30 x 10^{-8}	OH^-	20.52 x 10^{-8}
K^+	7.62 x 10^{-8}	SO_4^{--}	8.27 x 10^{-8}
Li^+	4.01 x 10^{-8}	Cl^-	7.91 x 10^{-8}
Na^+	5.19 x 10^{-8}	NO_3^-	7.40 x 10^{-8}
Ca^{++}	5.95 x 10^{-8}	HCO_3^-	4.61 x 10^{-8}

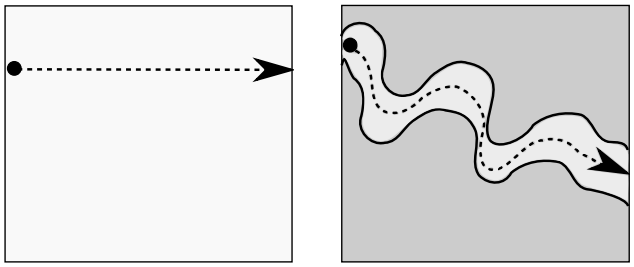

(a) (b)

Figure 4.2: In bulk solution, the ion can move through the shortest path (a), whereas in a porous material, the species has to follow the tortuous path of the water-filled pores (b).

$$J_{i,a} = uc_i \tag{4.6}$$

When rewriting the conservation of mass equation 4.1 with the aforementioned flux terms (equations 4.3, 4.4 and 4.6), the Nernst-Planck equation is obtained:

$$\frac{\partial c_i}{\partial t} = -\nabla(c_i u - D_i \nabla c_i - u_{m,i} c_i \nabla \phi) + R_i \tag{4.7}$$

In the case of charge-carrying species, besides obeying to the principle of conservation of mass, the variation of concentration must be such that the electrolyte remains electrically neutral, that is, the total number of negative and positive charges should be the same. This is the electroneutrality principle, as shown in:

$$\sum_{i=1}^{n} z_i c_i = 0 \tag{4.8}$$

Finally, the current density i_c, in A/m^2, in the electrolyte is due to the movement of the charged particles and it is expressed by:

$$i_c = F \sum_{i=1}^{n} z_i (-D_i \nabla c_i - u_{m,i} c_i \nabla \phi) \tag{4.9}$$

4.2.2. TRANSPORT IN CONCRETE

THE principles described in the previous section are also valid for porous materials, such as concrete or mortar. However, in this case, transport takes place in the water-filled pores. Therefore, species are no longer able to advance along the shortest path, like in bulk solutions, as shown in Figure 4.2. In fact, transport in this type of materials is two to three orders of magnitudes lower than compared to bulk solution [11].

According to Paz-Garcia[12], it is generally accepted that transport is affected by parameters such as porosity, degree of saturation, tortuosity and constrictivity. Tortuosity can be explained as the ratio between the actual length of the pore and the linear distance between the ends of it. Constrictivity, on the other hand, deals with the hindering

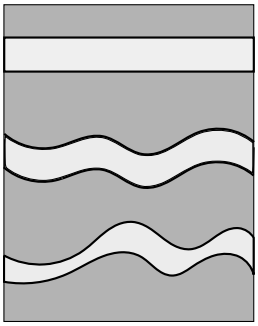

Figure 4.3: Representation of different types of pores. From the top, an idealized cylindrical capillary pore, a tortuous capillary and a pore with high constrictivity (after [12]).

in flow due to variations in the cross-sectional area of the pore (Figure 4.3). The author proposed an effective transport factor (K*) that considers these properties and is given by:

$$K^* = \frac{p\theta}{\tau_c} \tag{4.10}$$

where p is the porosity; θ is the saturation degree and τ_c is the tortuosity-constrictivity factor which is a combination of the effects due to both tortuosity and constrictivity.

The tortuosity-constrictivy factor can be estimated by the ratio between the theoretical (calculated considering the capillary pores as cylindrical tubes) and measured conductivity values (κ_t and κ_{exp}, respectively, both in S/m). The conductivity of the bulk solution can be calculated by [9]:

$$\kappa = F\sum_{i=1}^{n} z_i u_{m,i} c_i \tag{4.11}$$

And, the theoretical conductivity of the specimen can be defined as:

$$\kappa_t = \theta p F\sum_{i=1}^{n} z_i u_{m,i} c_i \tag{4.12}$$

Therefore, tortuosity-constrictivity factor is obtained by:

$$\tau_c = \frac{\kappa_{exp}}{\kappa_t} \tag{4.13}$$

Thus, in a porous material, ionic transport can be described by the modified Nernst-Planck equation:

$$\frac{\partial(p\theta)c_i}{\partial t} = -\nabla(K^* c_i u - K^* D_i \nabla c_i - K^* u_{m,i} c_i \nabla\phi) + (p\theta)R_i \tag{4.14}$$

The advective term can be considered as a combination of transport due to gradients of degree of saturation and electroosmosis and the velocity of the fluid, u, can be described as [12]:

$$u = -D_\theta \nabla\theta - K_{e.o.}\nabla\phi \tag{4.15}$$

where D_θ is the water diffusivity coefficient, in m^2/s and $K_{e.o.}$ is the electroosmotic permeability, in $m^2 s^{-1} V^{-1}$.

Finally, the ionic transport in a porous material can be described by:

$$\frac{\partial(p\theta)c_i}{\partial t} = -\nabla(K^* c_i D_\theta \nabla\theta - K^* D_i \nabla c_i - K^*(u_{m,i} + K_{e.o.})c_i \nabla\phi) + (p\theta)R_i \tag{4.16}$$

4.3. NUMERICAL IMPLEMENTATION

THE modeled experiment was the one-week lithium migration into a mortar disc shown in Chapter 3, specifically, the experiments with LiOH 4.9 M solution as anolyte. Figure 4.4 shows a scheme representing the transport through the pore solution during testing. A mortar disc, here represented having only one large cylindrical pore, was placed between two electrolyte chambers. Initially, on the left, the anolyte chamber contained lithium hydroxide (LiOH) solution with 4.9 M of concentration whereas on the right, the catholyte was a saturated calcium hydroxide ($Ca(OH)_2$) solution, with concentration of 0.023 M. The considered species forming the initial pore solution were potassium, sodium and hydroxyl ions, with their concentrations in Table 4.2. The initial pore solution composition was estimated by adjusting values found in [11] and [5] according to the cement composition used in the experiments and the concentrations experimentally observed in the catholyte solutions.

When the experiment begins, 40 V is applied between electrodes and ionic transport takes place. As illustrated, lithium ions move into and through the specimen, towards the cathode, while sodium and potassium ions move mostly in the same direction. A part of these ions, however, diffuse to the anolyte (not shown in the scheme). Finally, hydroxyl ions move towards the anode. At the electrodes, hydroxyl ions are either consumed (at the anode) or produced (at the cathode). In addition, a part of the lithium ions is (chemically and/or physically) bound to the solid phases at the pore walls.

Table 4.2: Estimated initial pore solution chemical composition.

Ion	Concentration (mol/l)
K^+	0.25
Na^+	0.20
OH^-	0.45

A 1-D model was implemented using the Nernst-Planck mode in COMSOL Multiphysics ®software. Three domains were considered: anolyte, specimen and catholyte, as shown in Figure 4.4. In the solution domains, Equation 4.7 was applied for each species but the hydroxyl ions. In the specimen domain, on the other hand, Equation 4.16 was used for each ion, except for hydroxyl ions. In the case of the hydroxyl ions, the transport equations were not used. Instead, their concentrations were calculated from the electroneutrality equation (Equation 4.8). This method is known as the Equation Elimination Method (EEM)[13]. In each domain, when considering the Equations 4.7 or 4.16

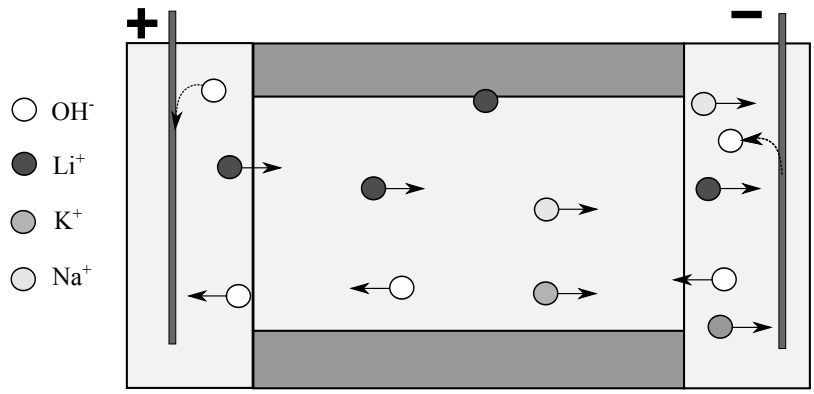

Figure 4.4: Schematic drawing representing the modeled experiment. Initially, the chamber on the left contains the anolyte solution (LiOH 4.9 M), while the chamber on the right contains the catholyte (saturated $Ca(OH)_2$ solution). The specimen is between both chambers and only one large capillary pore is represented. Once the power is switched on, cations (sodium, potassium and lithium) are attracted by the cathode while hydroxyl ions, which are negative, are attracted by the anode. The movement of those ions, due to the electric field, is represented by horizontal arrows. The scheme also represents hydroxyl ions being consumed at the anode and being produced at the cathode. Finally, lithium binding is represented by the ion at the wall of the pore. Ionic movement due to diffusion is not represented for better clarity.

for all species and the electroneutrality equation (Equation 4.8), there are $N+1$ equations for N species. Therefore, a conservation equation of a species can be eliminated and its concentration can be calculated from the electroneutrality equation, as long as no explicit boundary condition is applied to the referred species [13].

Transport by advection is not likely to happen under the present conditions [2]. Therefore, the velocity of the solvent was considered to be zero in all domains. The specimen was considered to be fully saturated (saturation degree of one). The porosity of the specimen was considered to be 20%, based on the findings of [14], where a similar mortar was studied.

Finally, the tortuosity-constrivicty factor was calculated by Equation 4.13. As input, the concentrations in Table 4.2 and experimental resistivity values from Chapter 3 were used. Instead of using the initial specimen resistivity, in order to take into account the effect of the rise in temperature, an average value of resistivity during the experiment (39 Ω.m)
was considered in the calculation. The obtained tortuosity-constrivicty factor was 78, which agrees with values found in literature (e.g. [5], [15]).

In a 1-D model, every domain must have the same cross-sectional area, which is not the case in the actual experiment. In order to take that into account, the modeled anolyte and catholyte compartments were five times longer than their actual size, as shown in Figure 4.5. That way, the concentrations in the electrolyte domains and in the specimen are compatible. The specimen length was maintained the same (50.0 mm) and the electrodes were placed at 2.0 mm from both ends of the specimen domain.

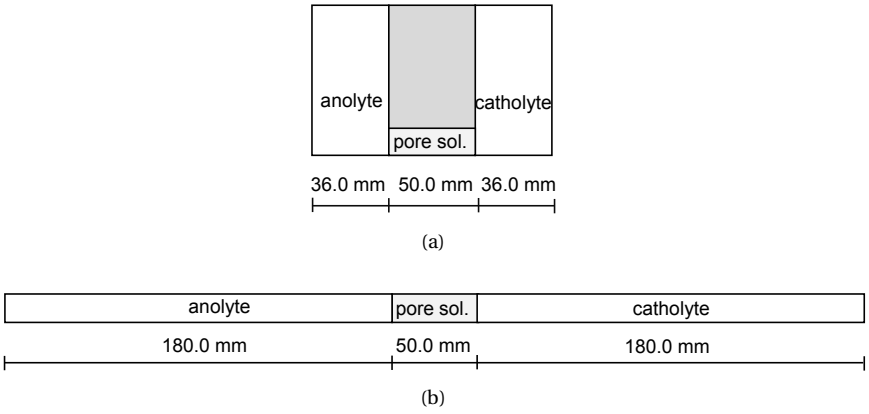

Figure 4.5: Schematic representation of the experimental set-up (a) and of the modeled system (b).

According to electrode reactions in Equations 3.3 and 3.4 (in Chapter 3) hydroxyl ions are consumed in the anolyte and produced in the catholyte, that is, there is a hydroxyl sink in the anolyte and a hydroxyl source in the catholyte. The reaction rates of hydroxyl ions (R_{OH^-}, in mol/m^3.s) in the electrolytes were calculated by:

$$R_{OH^-,anolyte} = -\frac{i_c}{d.F} \tag{4.17}$$

$$R_{OH^-,catholyte} = \frac{i_c}{d.F} \tag{4.18}$$

where d (in m) is the length of the region where the reaction took place. In this case, the adopted value was 1 mm. As mentioned, in the specimen, lithium binding to the pore structure was considered. Indeed, when chemical species penetrate into concrete, they may interact chemically and/or physically with the cement matrix and the aggregate (if the latter is porous or ASR reactive), leaving the pore solution. This process depends not only on the nature of the species and its concentration, but also on factors such as temperature and concrete (mortar) composition [11]. As there is no information on lithium binding in literature, in this thesis it was assumed that binding was linearly proportional to lithium concentration in the pore solution. Therefore, in the specimen domain, the reaction term was

$$R_{Li^+,spec} = -k_{lin} c_{Li^+} \tag{4.19}$$

where k_{lin} is a binding coefficient, in s^{-1}. In this work, three binding coefficients were evaluated: 0 (no binding), 1.0 x 10^{-7} s^{-1} and 2.0 x 10^{-7} s^{-1}. The concentration of bound lithium, Li_b, in mol/kg of solid, was calculated by:

$$(1-p)\rho \frac{\partial Li_b}{\partial t} = k_{lin} c_{Li^+} \tag{4.20}$$

where ρ is the density, in kg/m^3. In this work, mortar density was considered to be 2160 kg/m^3, based on the findings of [14], where a similar mortar was investigated.

4.4. RESULTS AND DISCUSSION

IN this section, results obtained from the model calculation are shown and compared to the experimental ones, presented in Chapter 3.

Figure 4.6 shows the modeled and experimental concentrations of lithium in the anolyte. In the model results, lithium concentrations decreased with time, as the ions left the anolyte and migrated into the specimen. Lithium binding did not affect much those concentrations - they practically coincide. When comparing to the experimental results, nevertheless, a clear difference can be noted. Indeed, as previously mentioned in Chapter 3, the increase in lithium concentration experimentally observed was not expected and it was likely due to water evaporation from the solution. The reduction of the anolyte volume led to the concentration increase. In contrast, in the model, the volume of the solution was considered constant.

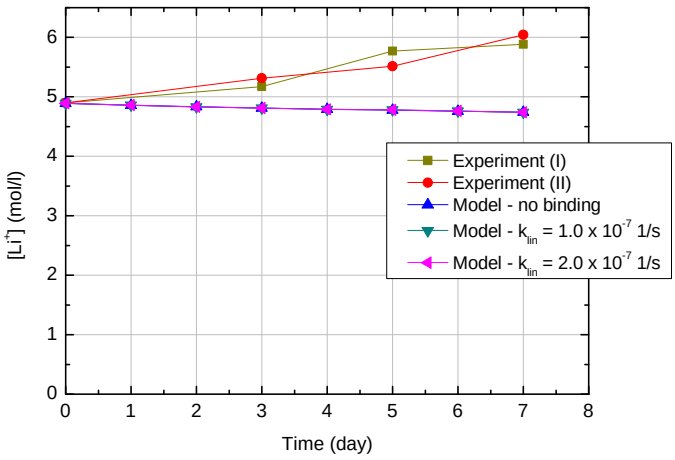

Figure 4.6: Lithium concentrations in anolyte - comparison between experimental results and model calculations. The plots of the model results with different binding coefficients are overlapping.

Sodium and potassium concentrations from the model are much lower than the ones observed during the experiments, as seen in Figure 4.7. A possible explanation for the difference could be that highly concentrated alkali hydroxide solutions are known for attacking concrete, dissolving hydrated phases [16],[17]. As the anolyte was a very concentrated LiOH solution, it is possible that the attack took place during the experiment. However, the attack reaction was not considered in the model, leading to the underestimation of the concentration of those ions. In addition, it is interesting to note that, like in the case of anolyte lithium concentration, lithium binding had a limited role in the transport of those ions into the anolyte as the concentrations calculated by the model practically coincide.

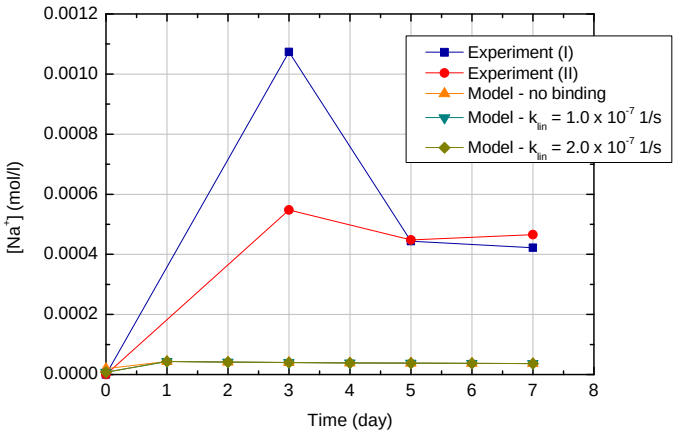

(a)

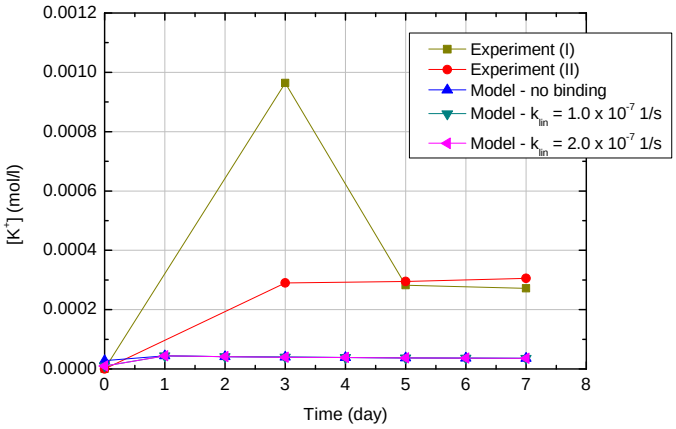

(b)

Figure 4.7: Sodium (a) and potassium (b) concentrations in anolyte - comparison between experimental results and model calculations. The plots from the model results with different binding coefficients are overlapping.

Figure 4.8 shows the sodium and potassium concentrations in the catholyte. As expected, the model results show the accumulation of those ions in the catholyte over time. Potassium ions left the specimen and the concentration increases until the fifth day, when it became constant. Sodium ions, on the other hand, left the pore solution at a lower rate (due to lower concentration and mobility) and reached constant concentration on the sixth day. It is worth noting that, once again, lithium binding had little influence on the removal of those ions from the specimen - the concentrations obtained by the model with different binding coefficients are practically the same. The model results are similar to what was experimentally observed, especially in Experiment (I). In this case, the sodium plots are close for the whole experiment while the potassium plots are close until day three. Nevertheless, the final model and experimental concentrations differ by less than 10%, in the case of Experiment (I).

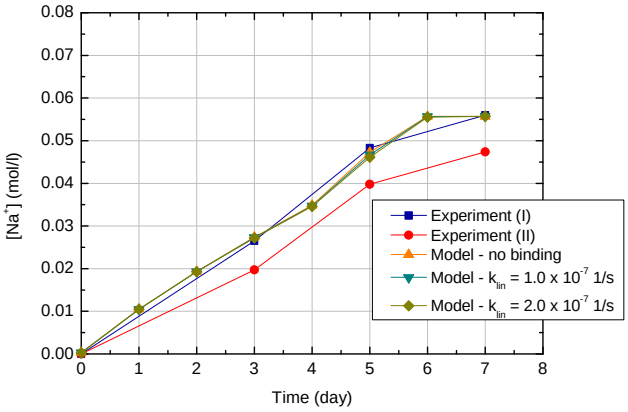

(a)

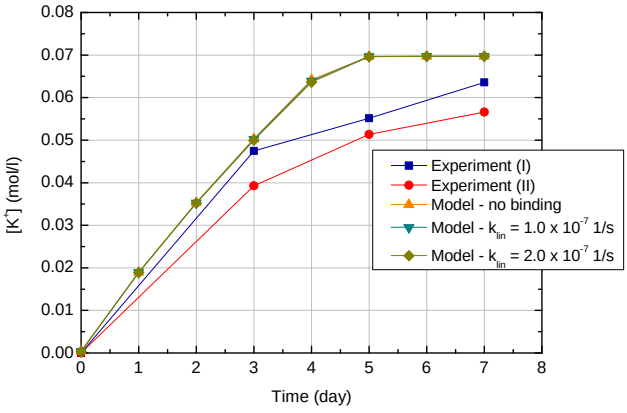

(b)

Figure 4.8: Sodium (a) and potassium (b) concentrations in catholyte - comparison between experimental results and model calculations. The plots from the model results with different binding coefficients are overlapping.

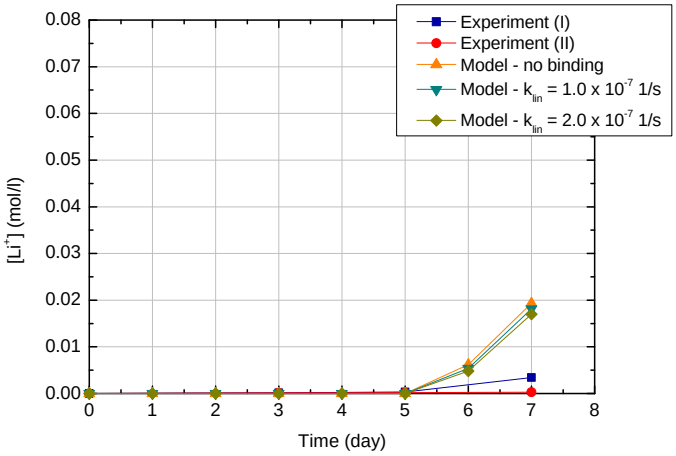

Figure 4.9: Lithium concentrations in catholyte - experimental results and model calculations. The plots overlap until day 5.

In contrast, the effect of lithium binding can clearly be observed in the concentrations of lithium in the catholyte (Figure 4.9). As expected, the higher is the binding coefficient, the less ions leave the specimen into the catholyte solution. This can be noted especially by the end of the experiment. Interestingly, for all model cases, it took six days for lithium to arrive in the catholyte – behavior quite close to what was experimentally observed. However, all final concentrations (with or without binding) are much higher than the experimental one. This could be related to the shape of the lithium profile in the specimen, as will be discussed further.

Concentration profiles of sodium, potassium, lithium and hydroxyl ions in the pore solution, calculated by the model, are shown in the graphs of Figures 4.10, 4.11, 4.12 and 4.15, respectively. As expected, sodium and potassium were attracted by the cathode and progressively left the specimen. All sodium left the pore solution before day six, while all potassium was depleted by day five - like observed in the catholyte concentrations. As previously mentioned, potassium left the pore solution faster than sodium because of its higher mobility and concentration. As potassium moved faster towards the cathode, there was an area without potassium but with sodium. In that region, the sodium profile makes a hump, with higher concentration than initially. This probably happened due to the different mobilities of lithium, sodium and potassium. Lithium moves more slowly than sodium - therefore, there is an area were sodium is the only ion found. In that region, half current must be carried by sodium ion (and the other half by hydroxyl ions). Therefore, there is an accumulation of sodium ions so that there are enough species to carry current in that area. Lithium binding had limited role on sodium and potassium profiles. With higher binding levels, the shape of the profiles was slightly modified, especially from day three on. As lithium left the pore solution (due to being bound to the pore structure), in order to maintain electroneutrality, sodium and potassium had their transport slightly slowed down.

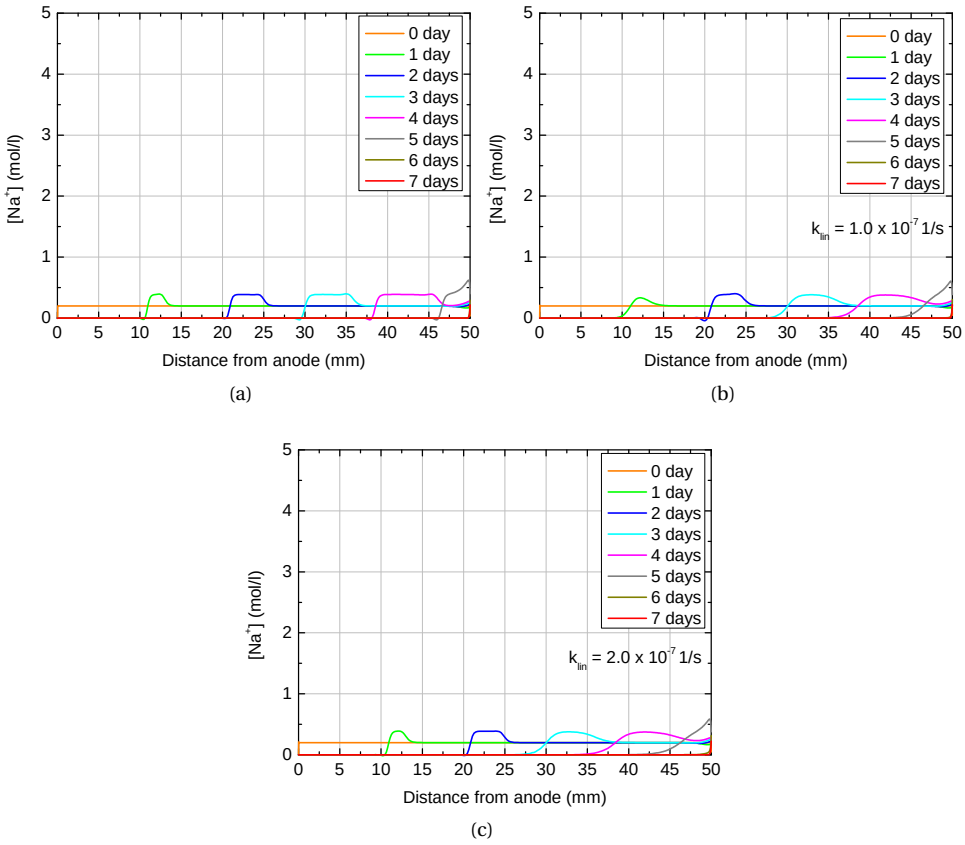

Figure 4.10: Model results for sodium concentration profiles in pore solution for three levels of lithium binding: (a) no binding, (b) k_{lin} = 1.0 x 10^{-7} s^{-1} and (c) k_{lin} = 2.0 x 10^{-7} s^{-1}.

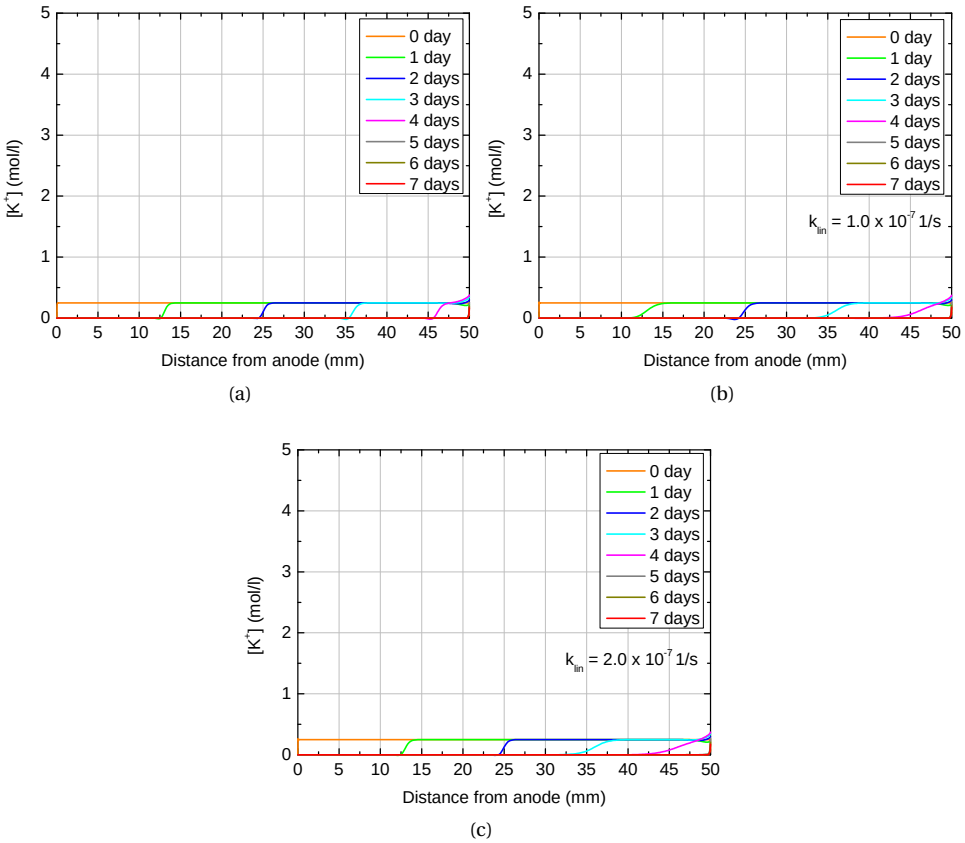

Figure 4.11: Model results for potassium concentration profiles in pore solution for three levels of lithium binding: (a) no binding, (b) $k_{lin} = 1.0 \times 10^{-7}$ s $^{-1}$ and (c) $k_{lin} = 2.0 \times 10^{-7}$ s $^{-1}$.

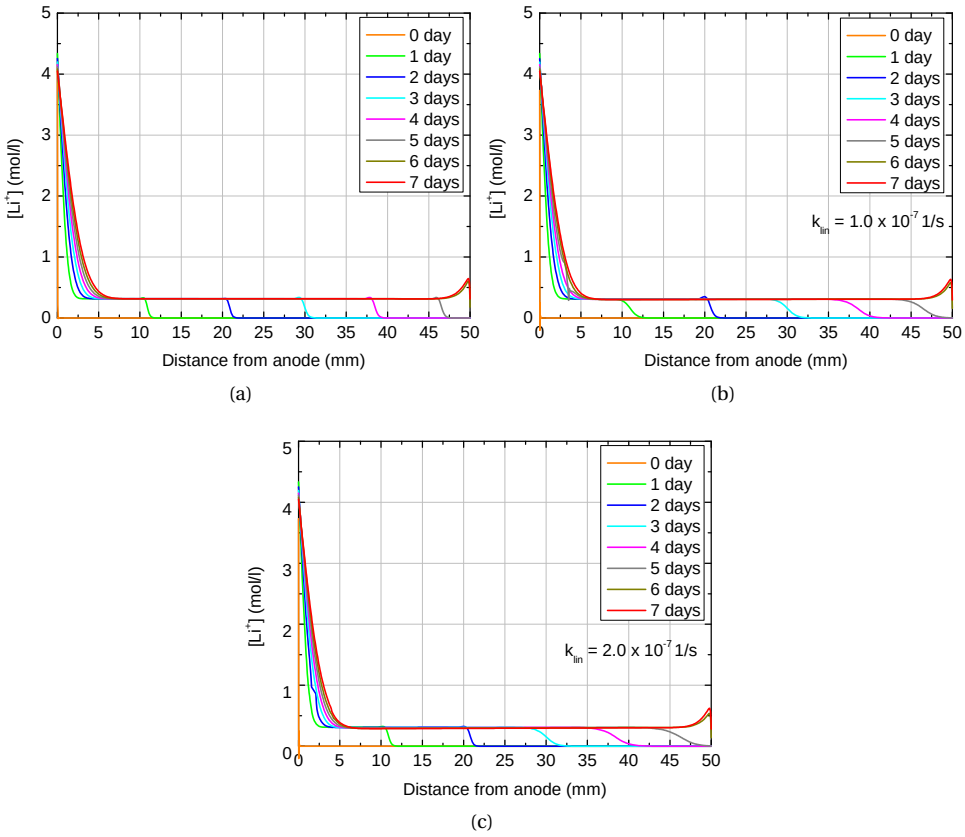

Figure 4.12: Model results for lithium concentration profiles in pore solution for three levels of lithium binding: (a) no binding, (b) k_{lin} = 1.0 x 10^{-7} s^{-1} and (c) k_{lin} = 2.0 x 10^{-7} s^{-1}.

Lithium ions are attracted by the cathode and migrate into and through the specimen, as shown in Figure 4.12. The concentration profiles have, initially, three different regions: a steep drop, followed by a region of constant lithium levels and finally the concentration decreases again. With time, the whole profile advances towards the cathode. In fact, the end of lithium profiles coincides with the beginning of areas with sodium. This is confirmed by the fact that lithium arrives in the catholyte before day six - the same time when all sodium has been removed from the pore solution. Therefore, according to the model, in order for lithium ions to advance in the specimen, it is necessary that sodium and potassium are first removed from its pore solution. As expected, binding modifies the concentrations of lithium - the higher the binding coefficient, the lower levels of lithium were observed in the pore solution. Figure 4.13 shows the plots of bound lithium in the considered cases.

The final total lithium (that is, the combination of ions in the pore solution and bound ions) concentration profile can be seen in Figure 4.14. The profiles obtained by

the model have different shape from what was experimentally observed. Although the model estimates well the average total amount of lithium that migrated into the specimen, especially in the case where k_{lin} is 2.0 x 10^{-7} s $^{-1}$ (Table 4.3), it underestimates the concentration in the region between 5 and 25 mm from the anode and overestimates it in the rest of the specimen. As the calculated concentration is overestimated in the region closer to the catholyte, it is likely that lithium concentration in the catholyte is also higher than the expected level, as seen in Figure4.9.

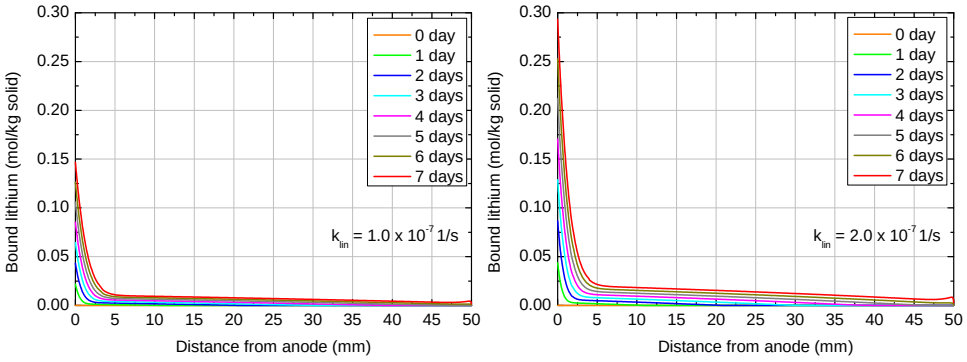

Figure 4.13: Model results for bound lithium in specimen for different levels of binding: (a) k_{lin} = 1.0 x 10^{-7} s $^{-1}$ and (b) k_{lin} = 2.0 x 10^{-7} s $^{-1}$.

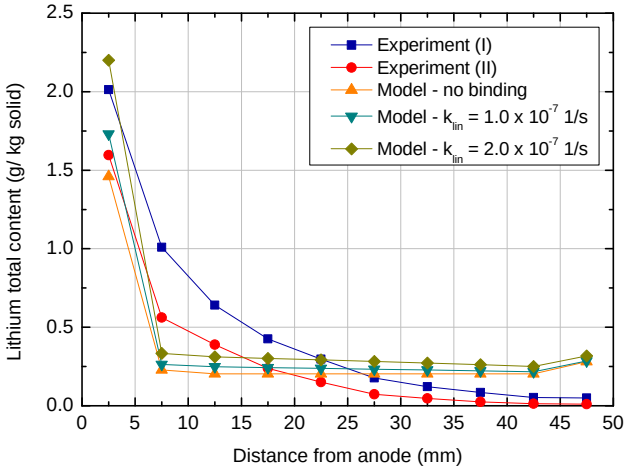

Figure 4.14: Final total lithium content in specimen.

Table 4.3: Average total lithium content in specimen after migration - comparison between experimental and model results.

	Average total lithium (g/kg solid)
No binding	0.340
k_{lin} = 1.0 x 10^{-7} s^{-1}	0.391
k_{lin} = 2.0 x 10^{-7} s^{-1}	0.482
Experimental (I)	0.487
Experimental (II)	0.310

Interestingly, other authors have used similar multi-ionic transport models to predict chloride migration in concrete and have obtained solutions with similar shape, regardless of considering binding (e.g. [5] and [18]) or not (e.g.[6] and [7]). Krabbenhøft and Krabbenhøft [6] attributed this shape to electroneutrality - the limited supply of cations would limit the transport of the anions, such as chlorides, in the system. Spiez [3], on the other hand, credits the differences between model and experimental profiles to wrong assumptions regarding binding and equilibrium between free and bound ions (chlorides, in the case of his work). Indeed, as previously mentioned, due to lack of information on lithium binding, considering it to be linearly proportional to the concentration can be considered as a first approach. Therefore, further investigation is needed in order to obtain models that predict better lithium concentration profiles.

Regarding the hydroxyl concentration profiles, shown in Figure 4.15, they are combinations of the profiles from the positive ions (sodium, potassium and lithium), because hydroxyl concentrations were calculated using the electroneutrality principle. It is important noting that, even though hydroxyl has the highest mobility in the system, its transport (both in concentration and speed) was limited by the transport of the cations in the system. This is a direct consequence of a multi-ion model [6].

Finally, current density plots can be seen in Figure 4.16. The overall trend of the model results is similar to what was observed experimentally. In the model, the specimen was considered to be fully saturated from the start, which led to the highest current as soon as the test began. In the experiment, however, as the specimen was not initially fully saturated, it took a couple of hours before the peak value could be reached. Nevertheless, in both model and experiments, after the point of highest value, the current density slowly decreased and then became nearly constant. Interestingly, the current density values predicted by the model are close to the values observed during Experiment (II).

The suggested model can also be used to estimate lithium migration during other experiments. The model (without binding) was used to estimate lithium transport during the experiment LiOH 0.2 M, also presented in Chapter 3. The experiment was similar to the one discussed previously in this chapter (40 V applied during seven days), but the anolyte was a LiOH 0.2 M solution, instead of LiOH 4.9 M. A summary with the main model results is shown in Table 4.4. It is interesting to notice that the behavior of sodium and potassium ions described by the model is very close for both LiOH 0.2 M and 4.9 M cases, as it was experimentally observed. This could indicate that the alkali removal does

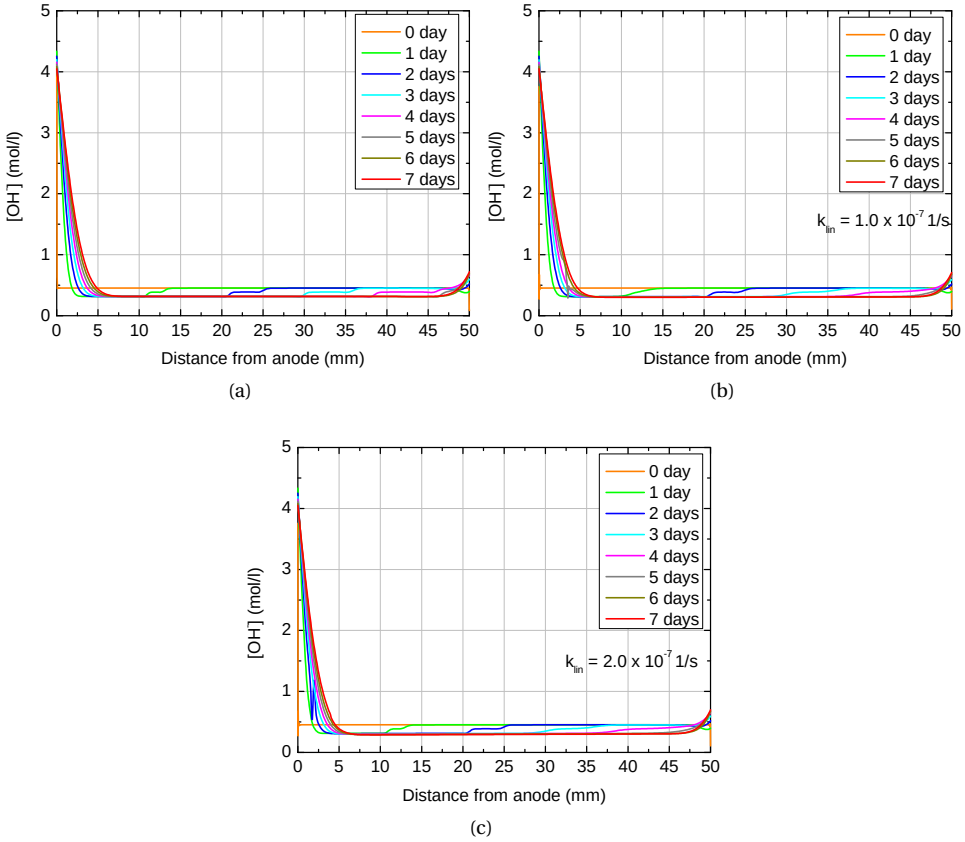

Figure 4.15: Model results for hydroxyl concentration profiles in pore solution.

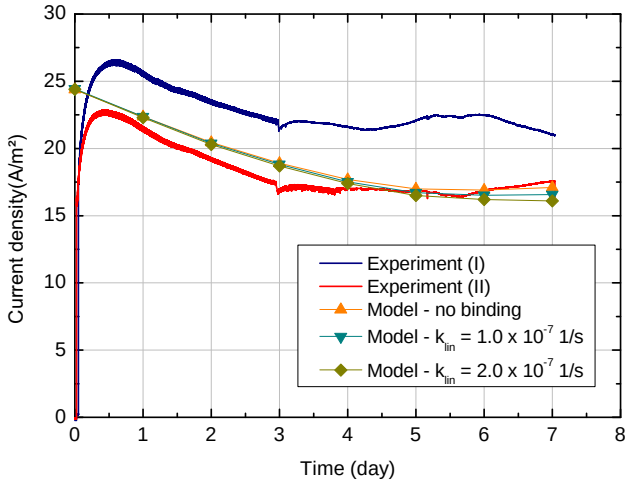

Figure 4.16: Current density passing through the specimen - comparison amongst model and experimental results.

not greatly depend on the concentration of the anolyte solution.

Table 4.4: Summary of the main model and experimental results for the experiment with LiOH 0.2 M as anolyte.

	Model	Experiment
Average lithium content in specimen(g/kg solid)	0.19	0.22
Current density (A/m^2)	16.6	19.9
Final potassium concentration in catholyte (mol/l)	0.07	0.06
Final sodium concentration in catholyte (mol/l)	0.06	0.05
Final lithium concentration in catholyte (mol/l)	0.007	0.006

4.5. CONCLUSIONS

In this chapter, a multi-ion numerical model for lithium transport under an electrical potential gradient was proposed. Lithium binding was assumed to be linearly proportional to lithium concentration at the studied rates as a first approach, due to lack of information on this topic in current literature.

The conclusions are as follows:

- Regarding the concentrations in the anolyte solutions, divergences among model and experimental results highlighted the water evaporation that took place during testing and was not considered in the model. It also brought attention to the possibility of alkali attack occurring during the experiments, as the reaction was not considered in the model.
- Sodium and potassium concentration variations in the catholyte were well predicted by the model results. Lithium concentrations, on the other hand, were overestimated, probably due to the shape of the concentration profile in the specimen.

- Observing the concentration profiles obtained by the model, it is necessary that all sodium and potassium is removed from the pore solution before lithium ions can reach the catholyte. This could be a limiting factor to be considered during treatment design, if the rebar is used as cathode and sodium and potassium are not removed from the pore solution (as pointed out in Chapter 3).
- Even though the model predicted well the average total amount of lithium in the specimen, it did not predict well how those ions are distributed throughout the specimen. This could be due to model assumptions, such as linear lithium binding or no binding at all. Further investigation is needed in order to obtain concentration profiles closer to the experimental ones.
- The current density behavior is reasonably estimated by the model. Differences between model and experimental results can be due to the estimation of the initial chemical composition of the pore solution.
- The suggested model can be used to estimate lithium transport in other experiments. When calculating for the case when LiOH 0.2 M solution was used as anolyte. Modeled and experimental results match well. Lithium migration was greatly influenced by the lower concentration of the anolyte, while the transport of potassium and sodium was similar to the case with LiOH 4.9 M.

REFERENCES

[1] L. M. S. Souza, R. B. Polder, and O. Çopuroğlu, *Study on lithium migration for electrochemical treatment of concrete affected by alkali-silica reaction,* in *Proceedings of concrete solutions, 5th international conference on concrete* (CRC Press, 2014) pp. 237–243.

[2] C. Andrade, J. M. Diez, A. Alaman, and C. Alonso, *Mathematical modelling of electrochemical chloride extraction from concrete,* Cement and concrete research **25**, 727 (1995).

[3] P. Spiesz, M. Ballari, and H. Brouwers, *RCM: a new model accounting for the nonlinear chloride binding isotherm and the non-equilibrium conditions between the free-and bound-chloride concentrations,* Construction and building materials **27**, 293 (2012).

[4] B. Šavija, *Experimental and numerical investigation of chloride ingress in cracked concrete*, Ph.D. thesis, TU Delft, Delft University of Technology (2014).

[5] M. Aguayo, P. Yang, K. Vance, G. Sant, and N. Neithalath, *Electrically driven chloride ion transport in blended binder concretes: Insights from experiments and numerical simulations,* Cement and Concrete Research **66**, 1 (2014).

[6] K. Krabbenhøft and J. Krabbenhøft, *Application of the Poisson–Nernst–Planck equations to the migration test,* Cement and Concrete Research **38**, 77 (2008).

[7] E. Samson, J. Marchand, and K. Snyder, *Calculation of ionic diffusion coefficients on the basis of migration test results,* Materials and Structures **36**, 156 (2003).

[8] W. Peelen, R. Polder, E. Redaelli, and L. Bertolini, *Qualitative model of concrete acidification due to cathodic protection,* Materials and corrosion **59**, 81 (2008).

[9] J. Newman and K. E. Thomas-Alyea, *Electrochemical systems* (John Wiley & Sons, 2012).

[10] W. J. Moore, *Physical chemistry* (Englewood Cliffs, New Jersey: Prentice-Hall, Inc., 1962).

[11] L. Bertolini, B. Elsener, P. Pedeferri, E. Redaelli, and R. B. Polder, *Corrosion of steel in concrete: prevention, diagnosis, repair*, 2nd ed. (John Wiley & Sons, 2013).

[12] J. M. Paz-Garcia, A. Riberio, J. M. Rodriguez-Maroto, B. Johannesson, and L. M. Ottosen, *Physicochemical and numerical modeling of electrokinetics in inhomogenous matrices*, Ph.D. thesis, Technical University of Denmark, Danmarks Tekniske Universitet (2012).

[13] F. Gagnon, D. Ziegler, and M. Fafard, *Electrochemical modelling using electroneutrality equation as a constraint,* Journal of Applied Electrochemistry **44**, 361 (2014).

[14] L. M. S. Souza, *Development of sugar cane bagasse ash as admixture in durable concretes with low CO_2 emission and energy consumption (in Portuguese)*, Bachelor's thesis, Universidade Federal do Rio de Janeiro (2008).

[15] S. Ahmad, A. K. Azad, and K. F. Loughlin, *Effect of the key mixture parameters on tortuosity and permeability of concrete,* Journal of Advanced Concrete Technology **10**, 86 (2012).

[16] H. F. Taylor, *Cement chemistry* (Thomas Telford, 1997).

[17] P. Hewlett, *Lea's chemistry of cement and concrete* (Butterworth-Heinemann, 2003).

[18] O. Truc, J.-P. Ollivier, and L.-O. Nilsson, *Numerical simulation of multi-species transport through saturated concrete during a migration test—MsDiff code,* Cement and Concrete Research **30**, 1581 (2000).

5

EFFECT OF LITHIUM MIGRATION ON ASR INDUCED EXPANSION

5.1. INTRODUCTION

THE effect of lithium migration on ASR expansion has been studied by various authors, with different conclusions. With laboratory size specimens, some works (e.g. [1], [2], [3]) treated ASR affected concrete in two-chamber set-ups – not only lithium was transported into the specimens, but sodium and potassium ions were also removed. The combination of both effects led to the reduction of post-treatment expansion rate in those studies. Interestingly, the result was positive even in the cases in which most lithium concentrated in the region closer to the anolyte, indicating that the removal of alkalis may have played an important role.

Other studies treated ASR affected concrete using a reinforcement bar in laboratory-size specimens (e.g. [4], [5], [6], [7], [8], [9]). Even though, in those studies, the use of an embedded cathode led to the accumulation of potassium and sodium in the region around it, in some cases (especially when the temperature of the anolyte was increased), reduction of expansion rate was observed. On the other hand, when large-scale specimens or real structures were treated, the results were different. The treatment of large-scale reinforced cylindrical concrete columns using the reinforcement as cathode did not mitigate nor reduce ASR expansion [10]. Similar results were found after the treatment of bridge columns affected by ASR. In fact, cracks were found in columns five years after treatment [10]. The divergent conclusions indicate that further research is still needed. In this chapter, an experimental study into the effect of lithium migration on ASR induced expansion will be presented.

5.2. EXPERIMENTAL PROCEDURE

5.2.1. MATERIALS AND SPECIMEN PREPARATION

CONCRETE specimens were prepared with water to cement ratio (w/c) of 0.4 and Ordinary Portland cement type CEM I 42.5 N, commercially available in the Netherlands, with chemical composition shown in Table 3.1. As for the aggregate, the fine portion was non-reactive siliceous sand while the coarse aggregate was an Icelandic gravel, provided by Mannvit, which has shown to be ASR reactive elsewhere [11], [12]. The gravel was analyzed by polarized light microscopy and it is composed by volcanic rock with glass groundmass (Figure 5.1). Volcanic glass is known to be ASR reactive in some cases [13], [14]. A more detailed analysis of the aggregate can be found in Appendix A.

NaOH was added to the mixture so that the Na_2O_{eq} (sodium oxide equivalent) by mass of cement was 1.25 wt.%. The total Na_2O_{eq} of the concrete was 5.9 kg/m^3. The proportions of the materials used are shown in Table 5.1. The mixing procedure was carried out following the recommendations on RILEM Recommended Test Method: AAR-4.1 - Detection of Potential Alkali-Reactivity - 60°C [15]. Properties of the fresh mixture, namely slump (NEN-EN 12350-2) and air content (NEN-EN 12350-7), are shown in Table 5.1.

Cylindrical specimens, with diameter of 98 and 50 mm of height, were cast in order to evaluate the effects of ASR induced expansion on lithium migration. In order to evaluate the effects of lithium migration on expansion, concrete prisms (280 x 75 x 75 mm) were cast with stainless steel studs at the ends of each prism. The diagram of Figure 5.2 shows the positions of the studs in the specimen. After curing for a day, the specimens were

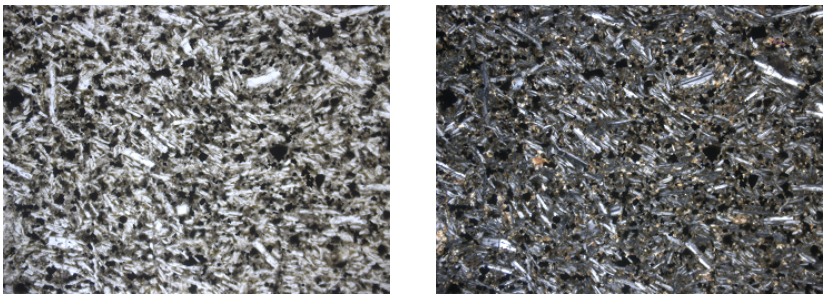

(a) (b)

Figure 5.1: Optical micrographs of an aggregate particle. It has a volcanic texture, with the presence of plagioclase. The darker areas are volcanic glass groundmass. (a)Plane polarized light and (b)Crossed polarized light. Field of view: 1.5mm

Table 5.1: Material proportions and properties of fresh concrete mixture.

Material	
Cement CEM I 42.5 N (kg/m^3)	488
Water, w/c = 0.4 (kg/m^3)	195
Fine aggregate < 4 mm (kg/m^3)[a]	471
Coarse aggregate 4 to 16 mm (kg/m^3)[b]	1114
NaOH (kg/m^3)	4.0
Slump (mm)	180
Air content (%)	0.8

[a] Non-reactive siliceous (river) sand .
[b] Reactive Icelandic gravel (rounded and used as received).

demolded. The prismatic specimens were placed in stainless steel containers while the cylindrical ones were placed in plastic boxes, as shown in Figure 5.3. The boxes and containers were closed and placed in an ASR reactor, at 60 °C and R.H. of 100%. Therefore, the specimens were placed in the reactor at one day of age.

5.2.2. METHODS

THE expansive behavior of the concrete without any treatment was evaluated following the recommendations from RILEM in AAR-4.1 [15]. For this, as previously mentioned, concrete prisms were cast and placed in an ASR reactor (60 °C and R.H. of 100%). Three replicates were used. The lengths of the specimens were measured in a vertical length comparator (with accuracy of 0.0005 mm) every 5 weeks, during 20 weeks. These specimens did not go through any other procedure besides ASR acceleration.

The migration experiments were conducted in two-chamber migration cells. In the case of the cylindrical specimens, the set-up was the same used in Chapter 3 (Figure 3.1). The anolyte was a 4.9 M LiOH solution while the catholyte was a saturated $Ca(OH)_2$ solution. LiOH 4.9 M solution was chosen because of its high lithium concentration

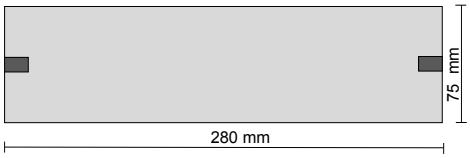

Figure 5.2: Diagram of a prismatic specimen with the stainless steel studs (in dark gray) at each end.

(a) (b)

Figure 5.3: Cylindrical specimens in plastic box (a) and prismatic specimens in metallic container (b). Both box and container had a grid on the bottom with a water film under it.

and high pH, which prevents the acidification of the solution and deterioration of the concrete (Chapter 3). The applied voltage was of 26.7 V (0.53 V/mm) and the test lasted four weeks. Two different levels of pre-treatment expansion were tested. For that, two specimens were cured in the ASR reactor for 3 weeks prior to the migration tests while the other two specimens were cured for 10 weeks prior to testing.

For the prismatic specimens, prismatic acrylic cells were used, as shown in Figure 5.4. Rectangular titanium meshes were used as electrodes. LiOH 4.9 M or saturated $Ca(OH)_2$ solution was used as anolyte solutions. Each electrolyte chamber contained 710 ml of solution. The use of $Ca(OH)_2$ was intended for the evaluation of the isolated effect of the removal of alkali ions on the expansion. Saturated $Ca(OH)_2$ solution was used as catholyte in all tests. The applied voltage was 40 V (0.53 V/mm) and the migration tests lasted four weeks. Although the applied voltage is different from the one applied in the experiments with the cylindrical specimens, the magnitude of the electric fields is the same in both cases. Therefore, the migration results should be comparable. Besides migration tests, diffusion experiments (without current) were also conducted with the same solutions for four weeks. Table 5.8 presents a summary of the experimental conditions for the prismatic specimens. Each experimental condition was tested with three replicates. Migration and diffusion tests were carried out in specimens exposed to ASR accelerating conditions (60 °C and R.H. of 100%) for 3 or 10 weeks, as pre-treatment. One day after finishing the migration experiments, the specimens were placed in the reactor again. Expansion was measured every 5 weeks (when possible) and before and after treatment, following the procedures described in RILEM recommendations AAR

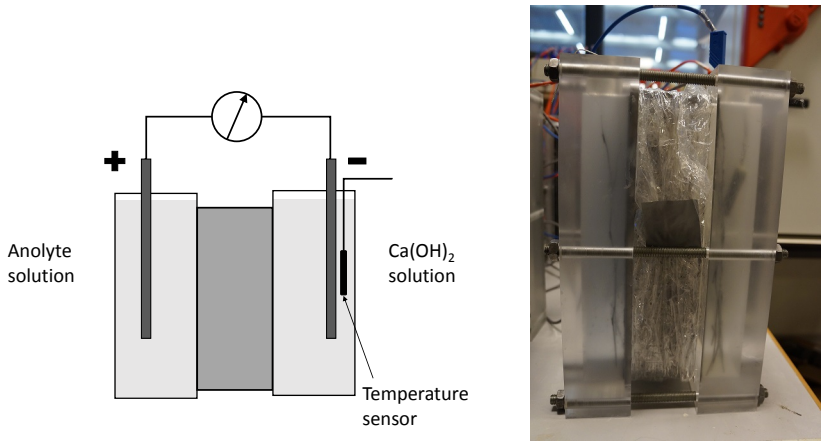

(a) (b)

Figure 5.4: Schematic diagram of prismatic acrylic cell with specimen (a) and the experimental set-up (b). Each electrolyte chamber contained 710 ml of solution.

4.1 [15]. During the migration experiments of the 3-week specimens, the reference studs corroded, causing cracking and leakage of the electrolyte solutions. Therefore, the reference studs of all migration specimens were removed. The remaining hole was filled with a repair mortar commercially available in the Netherlands. After one day of curing the mortar, new stainless steel studs were placed on the repair with a two-component glue (Plex 7742 and Pleximon 801).

All migration and diffusion experiments were carried out in a climate controlled laboratory, at 20.0 ± 2.0 °C and R.H. of 50± 5 %. Passing current and catholyte temperature were continuously monitored and recorded by a data logger (with accuracy of 1 x 10^{-6} mA and 1 x 10^{-6} °C, respectively). The electrical resistance of the specimens and the pH of the electrolytes were measured once a week, in the case of the migration tests. In the case of the diffusion experiments, those measurements were made less often.

Like in the experiments of Chapter 3, the electrical resistance was measured with a LCR meter, at 120 Hz in resistance mode, with accuracy of 0.1 Ω. Specimen resistivity was calculated from the resistance values using Equation 3.1. The pH values of the electrolytes were measured with pH test strips (with accuracy of 0.5 or 1, depending on the pH level).

Samples of the electrolyte solutions were collected once a week, in the case of the migration tests, or at the beginning and at the end of the diffusion experiments. They were analyzed by inductively coupled plasma optical emission spectroscopy (ICP-OES), to obtain the concentration of sodium, potassium, lithium and calcium ions (the latter only in anolyte solutions), like in Chapter 3. The detection limits were 0.02 mg/l for potassium and 0.05 mg/l for lithium, sodium and calcium. Standard solutions were used for control. Most ICP-OES concentration measurements had variations below 3% and the error bars were omitted from the graphs. In order to avoid variations in concentration due to the evaporation of water, the electrolytes were filled up with deionized water prior

Table 5.2: Summary of the experimental conditions applied to prismatic specimens.

Time in ASR reactor * prior testing	Applied voltage	Anolyte	Catholyte
3 weeks	40 V	LiOH 4.9 M	$Ca(OH)_2$ saturated
	40 V	$Ca(OH)_2$ saturated	
	0 V	LiOH 4.9 M	
	0 V	$Ca(OH)_2$ saturated	
10 weeks	40 V	LiOH 4.9 M	$Ca(OH)_2$ saturated
	40 V	$Ca(OH)_2$ saturated	
	0 V	LiOH 4.9 M	
	0 V	$Ca(OH)_2$ saturated	

* At 60 °C and 100% R.H.

to sampling. Ionic concentration profiles after migration were obtained from the cylindrical specimens. They were cut in slices of approximately 5 mm. Each slice was ground in a micro ball mill and the obtained powder was dissolved in 3.0 M HNO_3, following the same procedure described in Chapter 3. The obtained filtered solutions were analyzed by ICP-OES for lithium, sodium and potassium concentrations.

The effects of migration treatment were also evaluated by means of microanalysis. For that, polished sections were prepared from cylindrical specimens before and after migration testing. Ethanol was used as coolant liquid during cutting and polishing. A Philips XL30 environmental electron microscope with energy-dispersive spectrometer (EDS) under hi-vac condition was used. During the EDS analysis the accelerating voltage was 15 kV. The beam current was regularly measured by the use of a picoammeter and a Faraday cap and it was about 1 nA. The beam current was included into the ZAF quantification. For each specimen, 10 areas were analyzed. Twenty spot microanalysis were carried out on each area.

5.3. RESULTS AND DISCUSSIONS

5.3.1. EXPANSIVE BEHAVIOR OF CONCRETE WITHOUT ANY TREATMENT

THE expansive behavior of the concrete specimens that did not receive any treatment is shown in Figure 5.5. The quite high scattering levels observed in the expansion (up to 17% of variation in relation to the average) can probably be explained by the heterogeneous nature of the aggregate. By the fifteenth week, this concrete had expansion above the limit of 0.03% and can be classified as ASR reactive, according to [15].

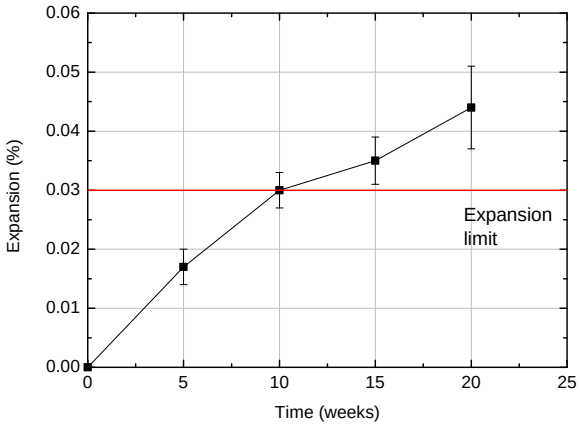

Figure 5.5: Expansion behavior of the concrete without any treatment. The expansion limit for a concrete to be considered non-reactive is 0.03% at 15 weeks [15].

5.3.2. INFLUENCE OF ASR EXPANSION ON MIGRATION

CURRENT DENSITY, TEMPERATURE AND RESISTIVITY

THE influence of ASR induced expansion on lithium migration was investigated with cylindrical specimens. Figure 5.6 (a) shows the current density that passed through the specimens during the migration tests. All specimens had current densities below 5 A/m^2 - therefore, below the limit applied in electrochemical treatments in order to avoid undesirable side effects [16], as mentioned in Chapter 3.

Differently from what was observed in Chapter 3, the specimens did not present a rapid increase in current in the first couple of hours. This might indicate that they were fully (or close to fully) saturated at the beginning of the experiment. The specimens that were under ASR accelerating conditions for 3 weeks prior to testing exhibited the highest current densities due to their initial resistivity (5.7). The currents slowly decreased until about day 15, when they started increasing until the end of the test. The specimens LiOH 4.9 M 10 w., on the other hand, had decreasing currents from the beginning until the end of the experiments.

The charges that passed through the specimens during the experiments (Equation 3.2) are shown in Table 5.3. The 3-week specimens had higher charges than the 10-week specimens. This was expected as the 3-week specimens had higher currents throughout the experiments. The average charge for the 3-week specimens was 69 ± 2 kC while for

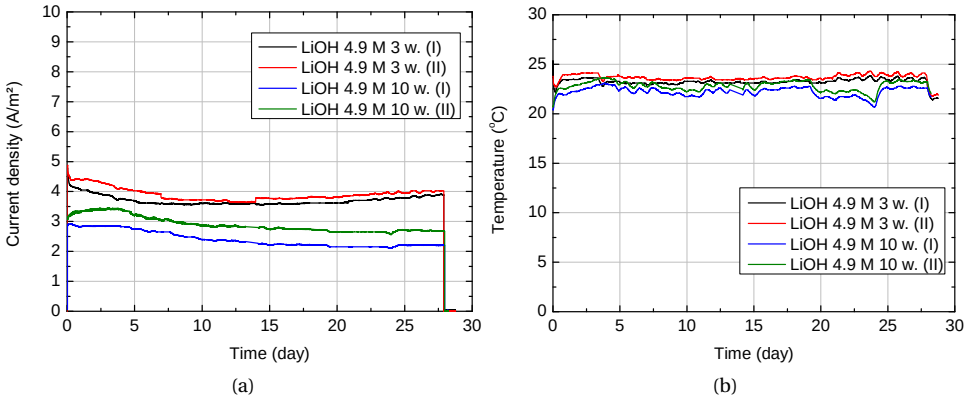

Figure 5.6: Current density (a) and catholyte temperatures during testing of the cylindrical specimens exposed to ASR accelerating conditions for 3 and 10 weeks prior to testing.

5

Table 5.3: Total charge that passed through the cylindrical specimens exposed to ASR accelerating conditions during 3 and 10 weeks prior to testing.

Specimen	Charge (kC)
LiOH 4.9 M 3 w. (I)	67
LiOH 4.9 M 3 w. (II)	71
LiOH 4.9 M 10 w. (I)	44
LiOH 4.9 M 10 w. (II)	53

the 10-week specimens it was 48 ± 5 kC.

Figure 5.6 (b) shows the temperature behavior of the catholyte solutions. They were all rather constant, around 23 °C. Local variations were observed in replicates and are most likely due to variations in room temperature. Nevertheless, it is possible to correlate the passing current density with temperature – the specimens with the highest temperature are the ones that had the highest current densities.

The resistivity behavior of the specimens during the experiments is shown in Figure 5.7. The average initial resistivity of the specimens exposed to ASR accelerating conditions for 3 weeks was 95 ± 2 Ω.m while for the specimens in ASR reactor for 10 weeks was 145 ± 8 Ω.m. The difference in initial resistivity may be explained by different factors or by a combination of them. The different ages of the specimens at the beginning of the migration experiments could have influenced the initial resistivity values. The 3-week specimens may have had higher porosity due to a lower degree of hydration than the 10-week specimens. In that case, the temperature of 60 °C may not have been enough to accelerate most of the hydration reactions in 3 weeks. However, other authors have reported different behavior regarding the influence of high curing temperatures on the hydration of cement pastes [17], [18]. In the work of Gallucci et al. [17], cement pastes cured at 60 °C had over 80% of degree of hydration by 14 days of age. From 14 days until 90 days, the increase was less than 5%. Similar findings were reported by Neville [18].

Therefore, although it is possible, it is unlikely that the difference in age significantly contributed for the different initial resistivity values.

An alternative explanation is that there might have been differences in the pore solution composition at the beginning of the migration experiments. Kim et al. [19] investigated the evolution of sodium and potassium concentrations in the pore solution during ASR development. Their results show that those concentrations decreased as the reaction progressed. Thus, it is possible that the 10-week specimens had lower concentrations of alkalis in their pore solution at the beginning of the experiments, which would have led to higher resistivity. Interestingly, the expansion level had limited influence on the resistivity at the beginning of the migration experiments. It was expected that cracking due to ASR development would lead to a decrease of resistivity. However, in the present study, cracking formation was not enough to overcome the effect from the factors previously mentioned. It is worth noting that no visible cracks were observed on the specimens, before or after treatment.

During the migration experiment, all specimens presented resistivity values higher than the initial ones. As can be observed in Figure 5.6 (b), the temperature of the cells did not change significantly during the experiment. Therefore, the effect of temperature is limited. Indeed, after 24 hours without power and at room temperature, the resistivity values of all cells were higher than the initial ones. This indicates that irreversible changes in pore structure and/or pore solution composition are likely to have happened.

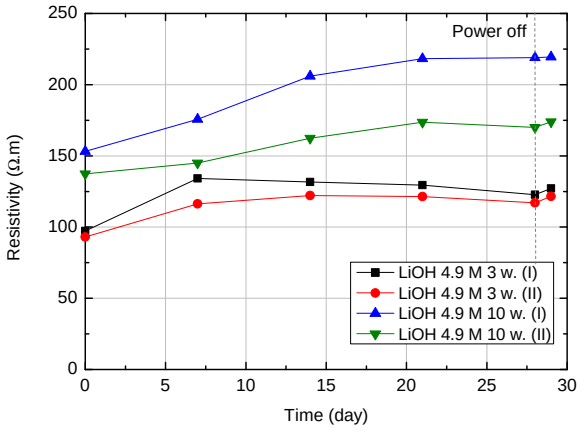

Figure 5.7: Resistivity of cylindrical specimens exposed to ASR accelerating conditions during 3 and 10 weeks prior to testing.

CHEMICAL COMPOSITION AND PH OF ELECTROLYTE SOLUTIONS

THE pH of the anolyte and catholyte solutions are shown in Figure 5.8. The anolyte pH was 14 throughout the experiment. On the other hand, the catholyte pH of all cells increased to 13 after a week of testing and remained at that level until the end of testing. The slight increase in pH might be explained by the fact that not all of the hydroxyl ions produced at the cathode (Equation 3.3) were transported into the specimen, in the

direction of the anode. In fact, some hydroxyl ions remained in the catholyte to balance the positive charge from sodium and potassium ions that were transported to the catholyte solution. As both electrolytes remained basic, the deterioration of the surface of the specimens by acid attack was avoided.

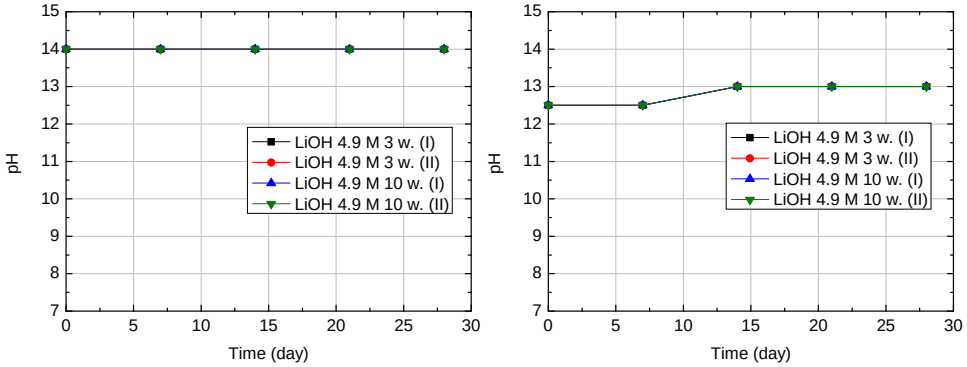

Figure 5.8: Anolyte (a) and catholyte (b) pH variations during experiments with cylindrical specimens exposed to ASR accelerating conditions for 3 and 10 weeks before testing. In each graph, the plots from different tests are overlapping, as the solutions had the same pH measured.

The sodium, potassium, calcium and lithium concentrations in the anolyte solutions are shown in Figures 5.9. Limited amounts of sodium, potassium and calcium ions leached from the specimens due to diffusion and possibly due to alkali attack, as previously mentioned in Chapters 3 and 4. Those ions left the specimen during the first week and their concentration in the anolyte solutions remained almost constant throughout the experiments. Sodium concentrations are higher due to its higher concentration in the pore solution caused by the addition of NaOH in the concrete mixture. Lithium ions left the anolyte solutions and were transported into the specimens. The cells with the highest passing charges had the lower final lithium concentrations in their anolyte solutions.

Sodium, potassium and lithium concentrations in the catholyte solutions are shown in Figure 5.10. Sodium and potassium ions, attracted by the cathode, left the specimens. Their concentration built up in the catholyte solutions during the migration experiment. Unlike what was observed in Chapter 3 the concentrations did not reach a constant value, indicating that not all free sodium and potassium left the specimen during testing. This was confirmed by the sodium and potassium concentration profiles in the specimens (Figures 5.11 and 5.12). Sodium concentrations were higher than potassium concentrations due to the extra NaOH added to the concrete mixture. Limited lithium arrived to the catholyte after day 21. The higher specimen resistivity combined with the lower applied voltage resulted in much slower lithium migration than the ones observed in Chapter 3. The specimens that had the highest passing charge had the highest sodium and potassium concentrations in the catholyte. However, the same cannot be said regarding lithium concentration, as no clear relation can be observed

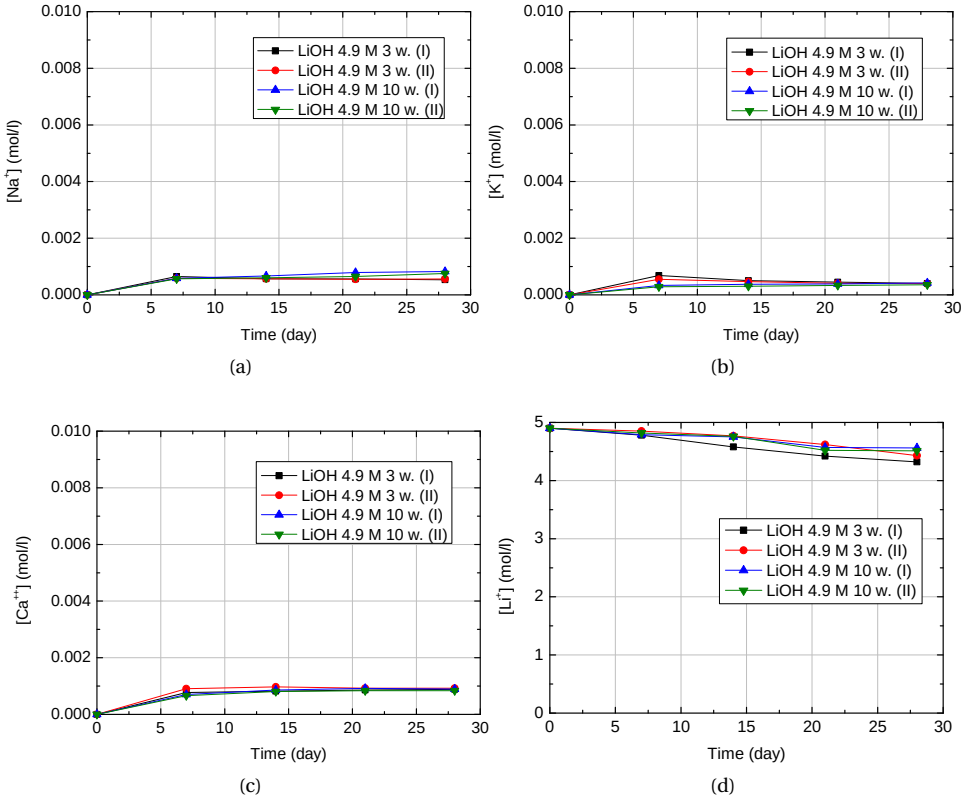

Figure 5.9: Concentrations of sodium (a), potassium (b) calcium (c) and lithium in the anolyte solutions of the experiments with cylindrical specimens exposed to ASR accelerating conditions during 3 and 10 weeks prior to testing. In (a), (b) and (d), the plots from LiOH 4.9 M 10. (I) and (II)are overlapping. In (c) the plots from LiOH 4.9 M 10. (I) and (II) and 3 w. (I) are also overlapping.

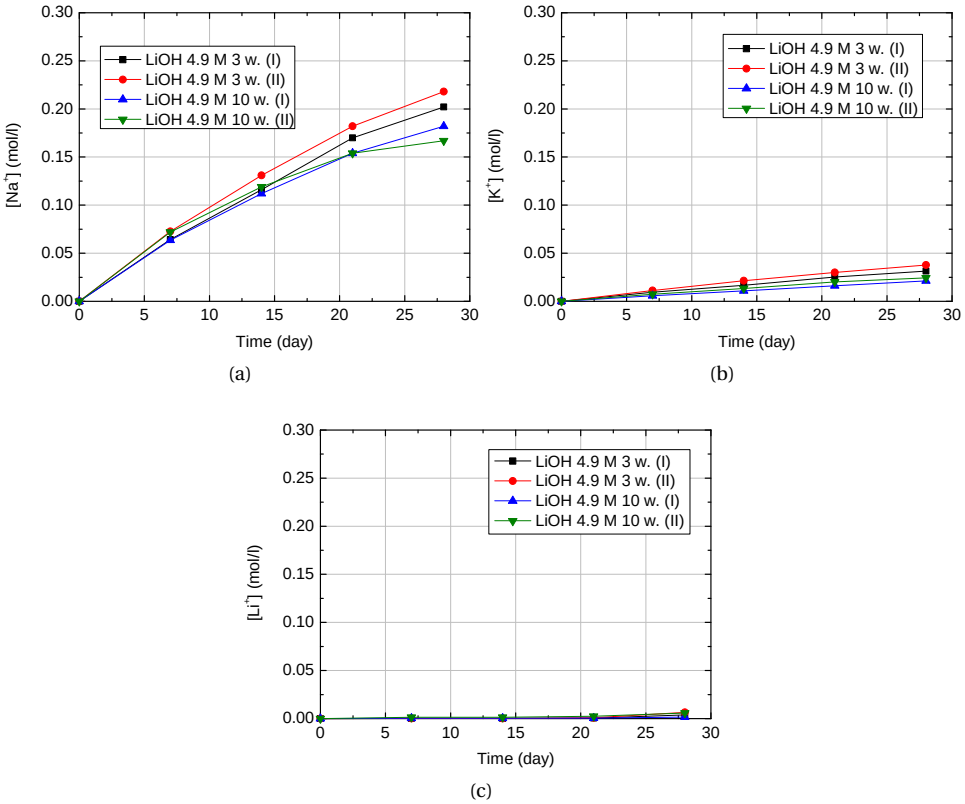

Figure 5.10: Concentrations of sodium (a), potassium (b) and lithium (c) in the catholyte solutions of the experiments with cylindrical specimens exposed to ASR accelerating conditions during 3 and 10 weeks prior to testing.

CONCENTRATION PROFILES IN THE SPECIMENS

SODIUM and potassium total concentration profiles of specimens after migration testing are shown in Figures 5.11 and 5.12, respectively. The control lines show the total concentration before the migration experiments. The profiles of both ions show fronts moving towards the cathode. This indicates that not all free sodium and potassium were removed from the specimens during testing, as previously mentioned. Nevertheless, the 3-week specimens presented less of those ions, as expected, considering they also presented the highest passing charges.

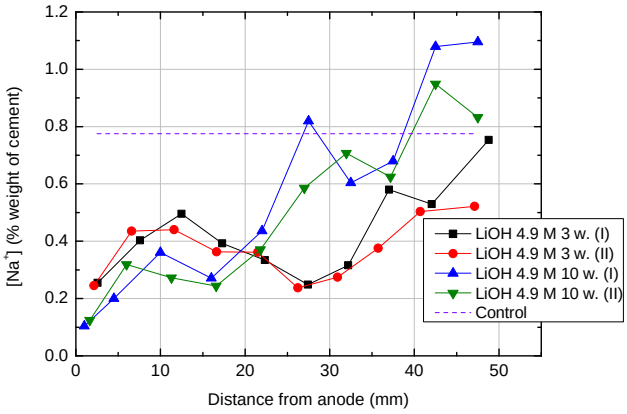

Figure 5.11: Sodium total concentration profiles in the cylindrical specimens exposed to ASR accelerating conditions during 3 and 10 weeks prior to testing.

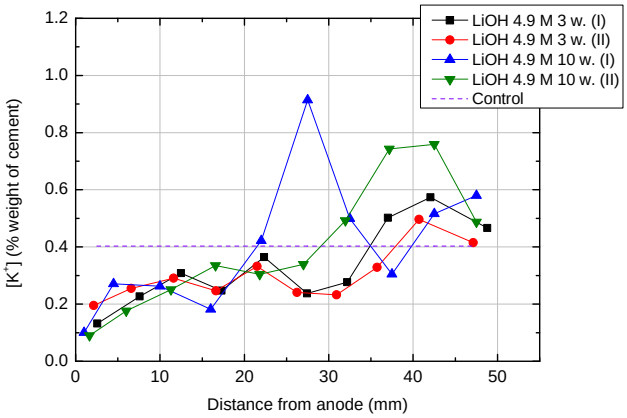

Figure 5.12: Potassium total concentration profiles in the cylindrical specimens exposed to ASR accelerating conditions during 3 and 10 weeks prior to testing.

Figure 5.13 shows total lithium concentration profiles in the specimens after testing. The profiles are very close, with the exception of the specimen LiOH 4.9 M 10 w. (I). Like in previous experiments, the basic shape remained the same – the concentrations are

higher closer to the anolyte and they decrease towards the catholyte. As previously mentioned, although a sharp concentration profile would be expected from a migration experiment through a porous medium [20], the obtained shapes are similar to the findings of other authors (e.g. [20], [21], [22]). Table 5.4 shows the average lithium concentration of all specimens. The specimen LiOH 4.9 M 10w. (I) had much lower lithium content than the other specimens. This is probably due to the resistivity build up this specimen went through, which led to lower passing charge and resulted in lower lithium concentration. Surprisingly, the specimen LiOH 4.9 M 10w. (II) presented average lithium content around 13% higher than the levels found in both specimens LiOH 4.9 M 3 w., even though they had higher passing charge (Table 5.3).

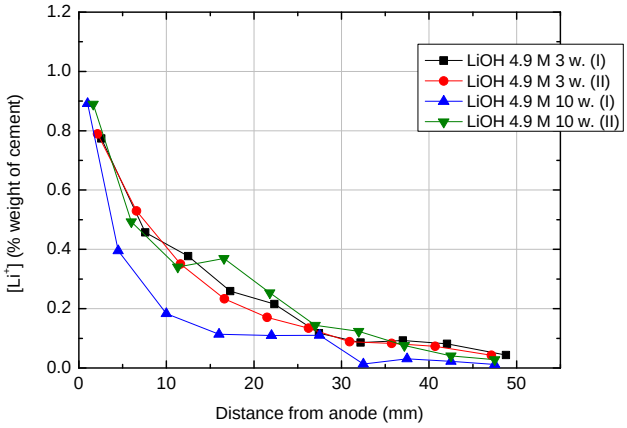

Figure 5.13: Lithium total concentration profiles in the cylindrical specimens exposed to ASR accelerating conditions during 3 and 10 weeks prior to testing.

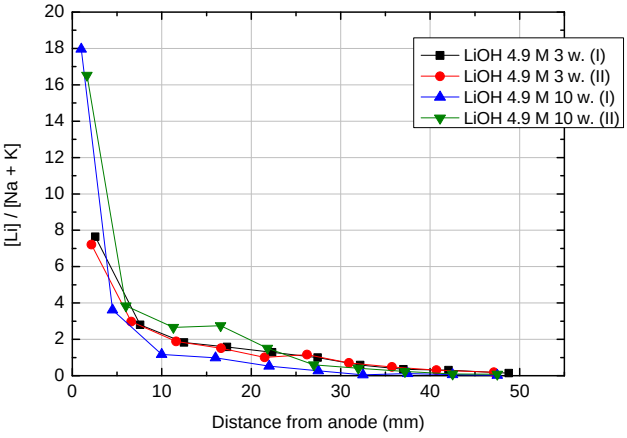

Figure 5.14: Lithium to sodium plus potassium molar ratio profiles in the cylindrical specimens exposed to ASR accelerating conditions during 3 and 10 weeks prior to testing.

Table 5.4: Average lithium concentration in the cylindrical specimens.

Specimen	Average lithium concentration (% weight of cement)
LiOH 4.9 M 3w. (I)	0.24
LiOH 4.9 M 3w. (II)	0.23
LiOH 4.9 M 10w. (I)	0.14
LiOH 4.9 M 10w. (II)	0.26

Table 5.5: Average Ca/ (Na+K)and Ca/Si atomic ratios of C-S-H gel areas closer to the anode and areas to the cathode. The ratios were obtained from the EDS analyses

	Closer to anode		Closer to cathode	
	Untreated	Treated	Untreated	Treated
Ca/(Na+K)	26 ± 41	149 ± 102	31 ± 41	99 ± 59
Ca/Si	2.1 ± 0.7	2.2 ± 0.5	2.2 ± 0.7	2.0 ± 0.5

The lithium to sodium plus potassium molar ratio profiles in the specimens after testing are shown in Figure 5.14. As previously mentioned (Chapter 3), for lithium used as admixture, the minimum lithium to alkali ratio to prevent deleterious ASR expansion varies from 0.65 to 1.00, depending on the type of lithium compound and/or aggregate [23]. Considering the ratio of 1.0, none of the specimens were fully treated. In fact, most specimens would have only the first 25-30 mm treated. For LiOH 4.9 M 10w. (I), only the first 15 mm would have enough lithium to suppress the reaction. However, it is possible that the mechanism to suppress ASR expansion in existing structures is not the same as when lithium is used as an addition to a fresh mixture. In that case, a different ratio could be needed.

Figure 5.15 shows the results from the EDS analyses performed on the specimen LiOH 4.9 M 10w. (II). Two regions were analyzed – Figure (a) shows the results from the region closer to the anode while Figure (b) shows the results from the region closer to the cathode. Calcium silicate hydrate (C-S-H) areas were analyzed. Lithium cannot be detected by EDS, as its characteristic X-ray energy is too low to be detected. Therefore, the effect of the treatment was evaluated by plotting the Ca/Si versus Ca/(Na+K) atomic ratios. Table 5.5 presents the average values of the atomic ratios in each analyzed region. In both graphs of Figure 5.15, two groups can be clearly observed. The untreated specimen had lower Ca/(Na+K) atomic ratios than the treated ones, regardless of the position (anode or cathode side). During the treatment, alkali ions that were initially in the pore solution were transported to the catholyte. In addition, it is possible that lithium ions replaced alkali ions in the ASR gel, releasing the latter to the pore solution [24]. The released alkali ions would then be removed from the pore solution by the migration treatment. Thus, the removal of sodium and potassium from the specimen resulted in higher Ca/(Na+K) ratios. It is interesting to notice that, in the treated specimen, the areas closer to the anode had the average Ca/(Na+K) ratio higher than the regions closer to the cathode, which agrees with the concentration profiles from Figures 5.11 and 5.12. In contrast, the Ca/Si ratios were not affected by the migration treatment (Table 5.5).

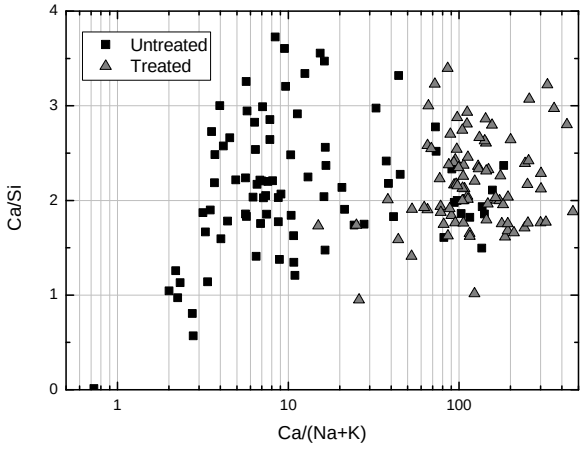

(a)

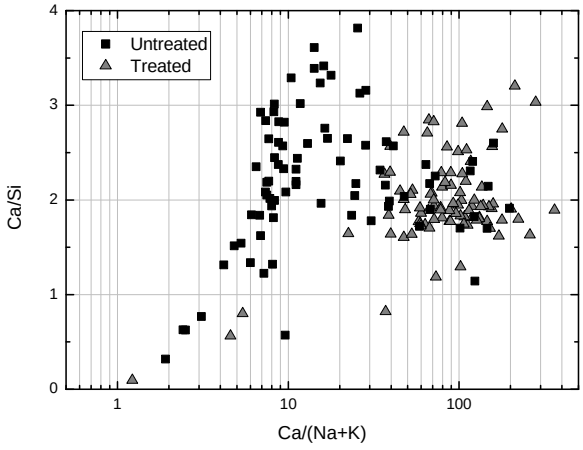

(b)

Figure 5.15: Comparison of Ca/ (Na+K)and Ca/Si atomic ratios of C-S-H gel regions closer to the anode (a) and areas closer to the cathode (b). The ratios were obtained from the EDS analyses.

5.3.3. INFLUENCE OF LITHIUM MIGRATION ON ASR EXPANSION

CONCRETE prisms were exposed to ASR accelerating conditions for 3 or 10 weeks prior to the beginning of the treatment. Nevertheless, the 3-week specimens that went under applied voltage presented corrosion of the stainless steel reference studs, used for the length measurements. The corroded studs caused cracking of the specimens and leakage of the electrolyte solutions. Therefore, the experiments had to be interrupted so that the studs could be removed and replaced by external studs. In order to avoid possible corrosion, the studs of the 10-week specimens were also removed and replaced by week 5. Treatment results will be discussed in the following section.

MIGRATION AND DIFFUSION TREATMENTS

FIGURE 5.16 shows the current density behavior of the specimens cured for 3 weeks before migration. During the first two days, due to an experimental error, the applied voltage was 25 V and, therefore, lower currents were observed for all specimens. The cells that had LiOH solution as anolyte presented higher current densities than the ones with $Ca(OH)_2$ solution as anolyte, probably due to the difference in concentrations. Nevertheless, all currents were below 10 A/m^2.

On the third day, a copper wire that made the connection between the titanium mesh and the plug of the cell LiOH 4.9 M 3w. (III) corroded. The solution was changed by a new one and the power source cable was directly connected to the titanium mesh by the use of an alligator plug, eliminating the use of a copper wire. The connection of the other migrations cells was also modified, to avoid possible future corrosion problems.

After 11 days, the cells LiOH 4.9 M 3w. (I, II and III) and $Ca(OH)_2$ sat 3w. (I) were leaking. The leakage was temporarily stopped by the use of silicon glue. However, after a couple of days, all cells under current suffered from heavy leakage. By day 17, it was possible to notice that the stainless steel reference studs (used for length measurements) corroded and there were cracks in the region around them. The corrosion was caused by stray current – as the metallic studs were in the specimens, the current passed through them, as they offered less resistance than the concrete. Figure 5.17 shows one of the studs that corroded.

The higher the current of the cell was, the more corroded were the studs. The power was then switched off and the cells were disassembled. The corroded studs were removed and the holes were filled with a commercial repair mortar (Figure 5.18 (a)), which was left to cure overnight. On the following day, new studs were glued on the repair mortar using a two-component glue (Figure 5.18 (b)). On day 22, the experiments were restarted, with new solutions.

The temperature behavior of the 3-week specimens followed the current trends – the higher the passing current, the higher was the temperature (Figure 5.19). Nevertheless, all catholytes had temperatures lower than 30 °C.

As previously mentioned, in order to avoid corrosion of the studs, the 10-week specimens had their studs replaced in the fifth week. One of the specimens that were supposed to be treated under current with LiOH was, instead, treated with $Ca(OH)_2$ without current. That way, a specimen with replaced studs could act as control. However, problems with the replaced studs did not allow expansion measurements of that specimen.

Figure 5.20 shows the current density that passed through the 10-week specimens.

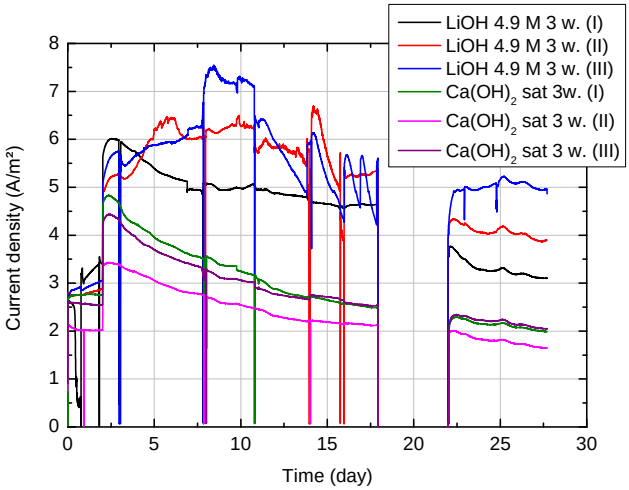

Figure 5.16: Current density that passed through prismatic specimens exposed to ASR accelerating conditions for 3 weeks prior to treatment.For the gap between days 16 and 23, see text (section 5.3.3).

Figure 5.17: Two of the stainless steel studs that corroded during migration experiments of the 3-week specimens.

(a) (b)

Figure 5.18: After the corroded studs were removed, the holes were filled with repair mortar (a) and new studs were glued on the repair (b).

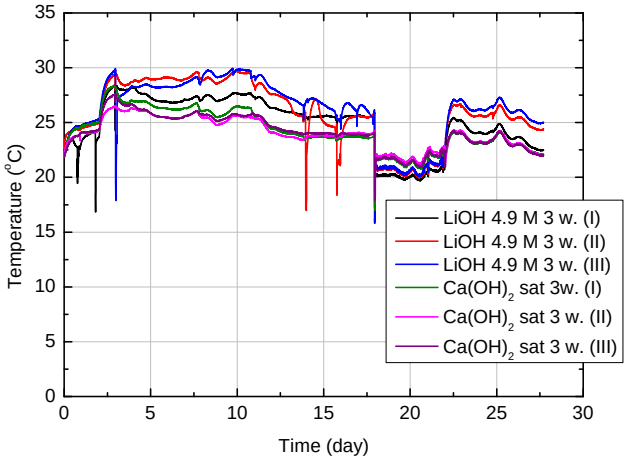

Figure 5.19: Temperature behavior during the migration treatment of prismatic specimens exposed to ASR accelerating conditions for 3 weeks.

All 10-week specimens had current density below 5 A/m^2 - therefore, undesirable side effects due to the application of higher current are unlikely to have happened. The current density of the specimens treated with LiOH are similar to the ones observed in the migration test of cylindrical specimens. The prisms treated with LiOH had increasing current in the initial stages, followed by a decrease until around day 15, when they assumed somewhat constant values until the end of the experiments. The specimens treated with $Ca(OH)_2$, on the other hand, had decreasing currents during tests. The catholyte temperature variations of those cells are shown in Figure 5.21. All 10-week cells had limited temperature increase, with temperatures below 28 °C, due to the limited current densities.

Table 5.6 shows the charges that passed through the prismatic specimens during migration treatment. The specimens treated with LiOH had higher passing charge than the ones treated with $Ca(OH)_2$, regardless of the time in the ASR reactor prior to the treatment.

The average initial resistivity of the 3-week specimens was 105 ± 10 Ω.m, while for the 10-week specimens, it was 146 ± 7 Ω.m . Similar resistivity values observed for the cylindrical specimens. The resistivity behavior of the specimens during the migration experiments is shown in Figure 5.22. Two distinct trends can be observed, depending on the anolyte solution. The specimens that had $Ca(OH)_2$ as anolyte had increasing resistivity until the end of the test. On the other hand, the specimens treated with LiOH had an initial decrease followed by an increase. Nevertheless, the specimens treated with $Ca(OH)_2$ had higher resistivity values by the end of the experiments than the specimens treated with LiOH. Interestingly, similar trends could be observed for both 3 and 10-week specimens. However, the resistivity results from the 3-week specimens need to be interpreted with caution, as cracks were formed due to the corrosion of the studs. The formation of the cracks depended on the current density levels - the specimens with the highest currents had more visible cracking. It is possible that cracking affected the

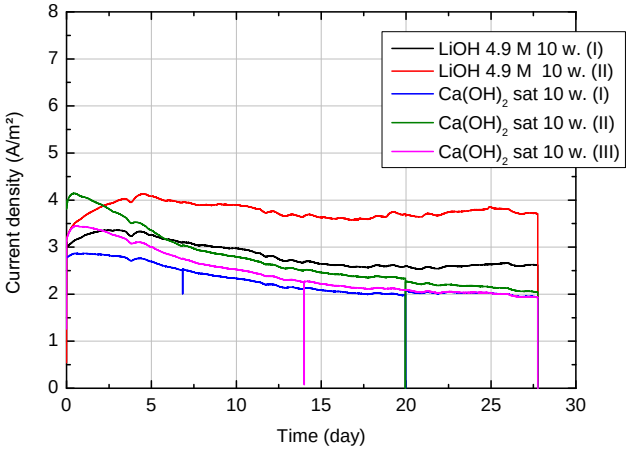

Figure 5.20: Current density that passed through the prismatic specimens exposed to ASR accelerating conditions for 10 weeks prior to treatment.

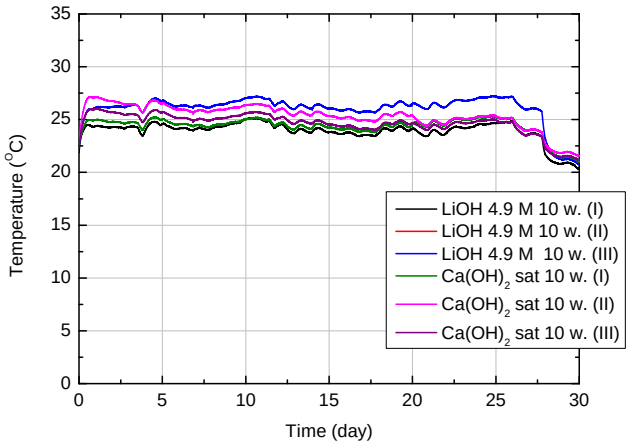

Figure 5.21: Catholyte temperature during the migration treatment of the 10-week prismatic specimens.

Table 5.6: Passing charges during the migration experiments with prismatic specimens.

Time in ASR reactor prior to treatment	Specimens	Charge (kC)	Average kC
3 weeks	LiOH 4.9 M 3 w. (I)	189	213 ± 18
	LiOH 4.9 M 3 w. (II)	218	
	LiOH 4.9 M 3 w. (III)	231	
	$Ca(OH)_2$ sat. 3 w. (I)	127	117 ±12
	$Ca(OH)_2$ sat. 3 w. (II)	100	
	$Ca(OH)_2$ sat. 3 w. (III)	122	
10 weeks	LiOH 4.9 M 10 w. (I)	142	165 ± 24
	LiOH 4.9 M 10 w. (II)	189	
	$Ca(OH)_2$ sat. 10 w. (I)	114	124 ±9
	$Ca(OH)_2$ sat. 10 w. (II)	136	
	$Ca(OH)_2$ sat. 10 w. (III)	123	

resistivity.

At the end of the migration experiments of the 10-week specimens, the power was switched off and resistances were measured again, at room temperature. The same was not possible for the 3-week specimens, due to the experimental issues previously mentioned. All 10-week specimens treated with $Ca(OH)_2$ had higher resistivity than the initial ones. These results suggest that irreversible changes in pore solution and/or pore structure took place in those specimens. In the case of the specimens treated with LiOH, the specimen LiOH 4.9 M 10w. (I) had higher resistivity than the initial one, while the resistivity of specimen LiOH 4.9 M 10 w. (II) returned to a value close to the initial one. Comparing to the results observed during the experiments with cylindrical specimens, specimen resistivity was expected to increase at the end of the experiment. As migration is not the only process taking place, it could be that the behavior of LiOH 4.9 M 10w. (II) was also influenced by ASR development. Even though the specimen was not under ASR accelerating conditions, it is likely that the reaction was still taking place - at a lower rate, though. Therefore, it is possible that ASR induced microcracks were formed during the treatment, which would lead to a drop in resistivity. Nevertheless, it is important to note that no visible cracks were observed on the surface of the specimen, after treatment.

The resistivity behavior of the prismatic specimens during the diffusion treatments is shown in Figure 5.23. In comparison to the migration specimens, the diffusion specimens had lower variations. All specimens had an initial drop in resistivity, probably caused by the saturation of their pore structures. After that point, the 3-week specimens treated with $Ca(OH)_2$ had a slight increase while the ones treated with LiOH had almost constant resistivity (except for LiOH 4.9 M 3 w. (III)). As for the 10-week specimens, after the initial drop, they all has almost constant resistivity values until the end of the tests.

Due to the leakage and change of solutions, pH and concentrations of the electrolytes of the 3-week specimens were not measured.

The pH variations of the anolyte and catholyte solutions during the migration treatment of the 10-week specimens are shown in Figure 5.24. The LiOH anolyte solutions

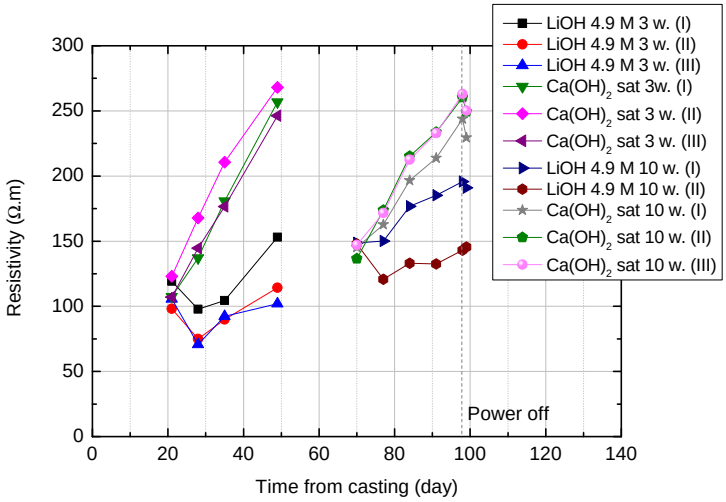

Figure 5.22: Resistivity variations during migration treatment of prismatic specimens.

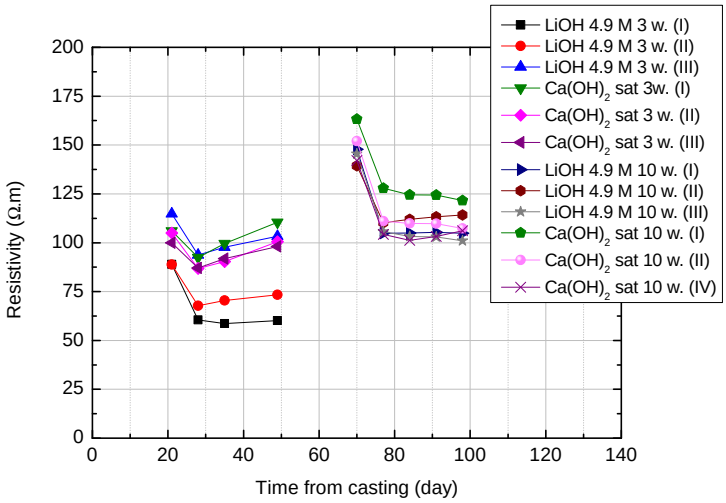

Figure 5.23: Resistivity variations during diffusion treatment of prismatic specimens.

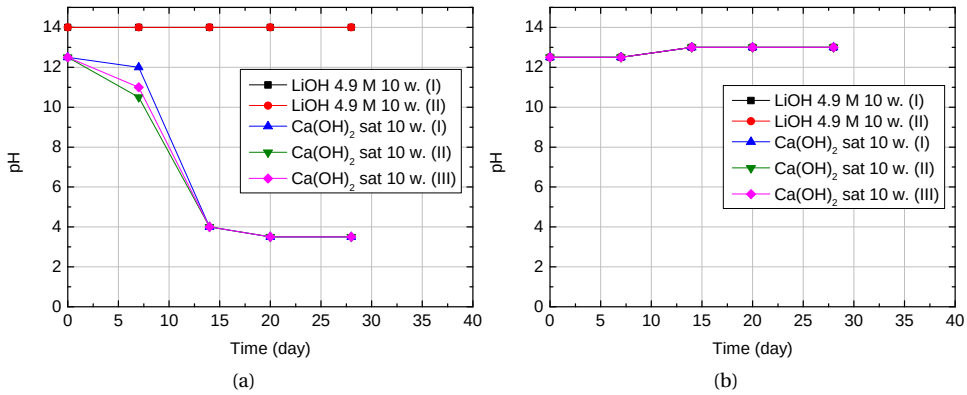

Figure 5.24: Anolyte (a) and catholyte (b) pH during the migration treatment of 10-week prismatic specimens. In (a) the plots from tests with LiOH are overlapping while in (b) plots from all tests are overlapping.

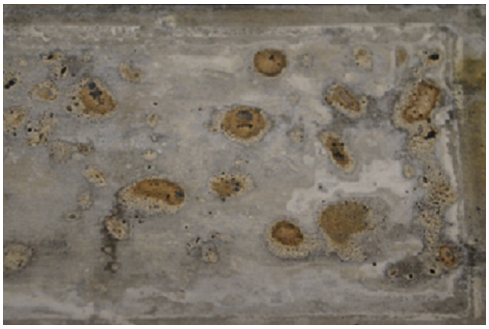

Figure 5.25: Detail of the surface deterioration due to acid attack of a prismatic specimen treated with $Ca(OH)_2$ under current.

were initially very alkaline and the pH remained very high until the end of the experiment. That was not the case with the $Ca(OH)_2$ anolyte solutions. As their initial pH was around 12.5, the anodic reaction (Equation 3.4) caused the pH to drop and become acidic. The acidification of those anolyte solutions caused the deterioration of the anodic surface of those specimens due to acid attack (like observed in the experiments on Chapter 3). Figure5.25 shows the deterioration of the surface of one of those specimens. On the other hand, all catholyte solutions showed an increase in pH, as seen in previous experiments. Regarding the diffusion experiments, the pH of all solutions remained unaltered (14 for LiOH solution and 12.5 for $Ca(OH)_2$ solution) during the tests, regardless of the experimental conditions.

Sodium, potassium, calcium and lithium concentrations in the anolyte solutions during the migration treatments of the 10-week specimens are presented in Figure 5.26. As observed in previous tests, some sodium and potassium leached from the specimens due to diffusion and possibly due to chemical attack, either alkali or acid, depending on whether LiOH or $Ca(OH)_2$ were used, respectively. Regarding calcium concentra-

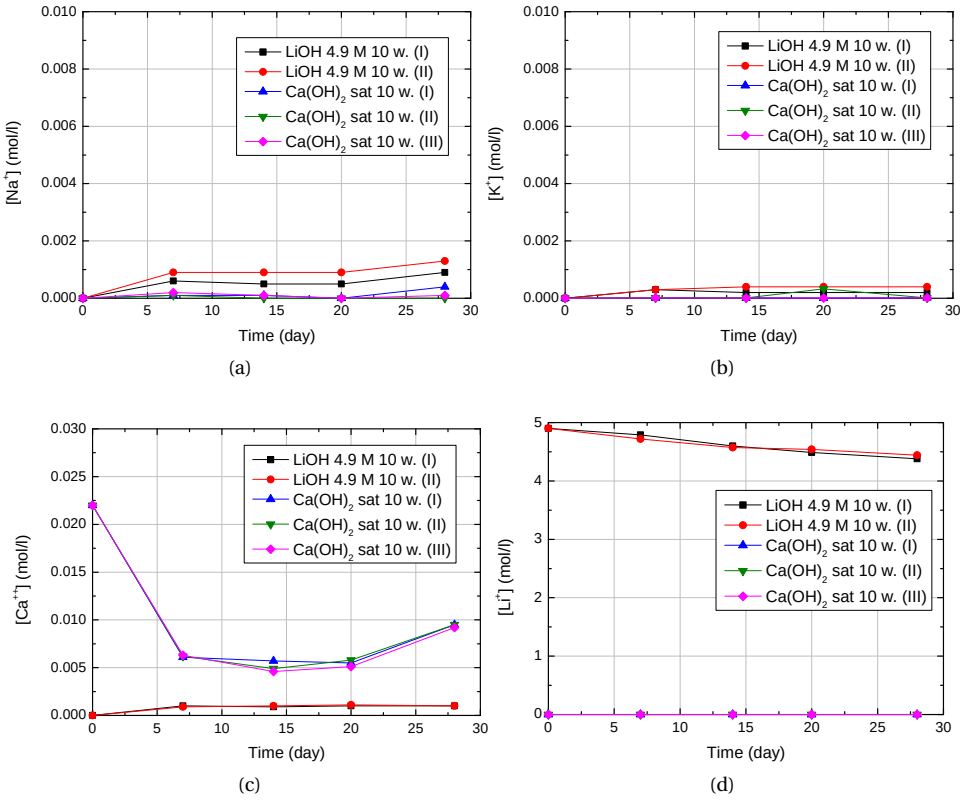

Figure 5.26: Sodium (a), potassium (b), calcium (c) and lithium (d) anolyte concentration variations during migration treatment of the 10-week prismatic specimens. In (b), the plots from the tests $Ca(OH)_2$ (I) and (III) are overlapping and well ans the plots from tests with LiOH in (c). In (d), the lithium concentration was zero for the tests with $Ca(OH)_2$.

tions, the specimens treated with LiOH had limited leaching to the anolyte. In the case of $Ca(OH)_2$ anolytes, some of the initial calcium was transported into the specimen in the first week. The calcium level remained constant until around day 20. The increase observed after that moment is possibly due to acid attack. As for the lithium contents, the LiOH anolytes had decreasing concentrations, as lithium ions left the anolyte and were transported into the specimen. Interestingly, even though cell LiOH 4.9 M 10 w. (II) had higher charge than LiOH 4.9 M 10 w. (I), their anolyte concentrations are similar.

Sodium, potassium and lithium concentrations in the catholyte solutions during migration experiments of the 10-week specimens presented in Figure 5.27. Like observed in the experiments with cylindrical specimens, sodium and potassium were attracted by the cathode and left the specimen, building up their concentrations in the catholytes. By the end of the experiment, the concentrations had not reached constant values, which indicates that probably not all free sodium and potassium left the specimens. Once again, sodium concentrations were higher due the addition of NaOH to the fresh con-

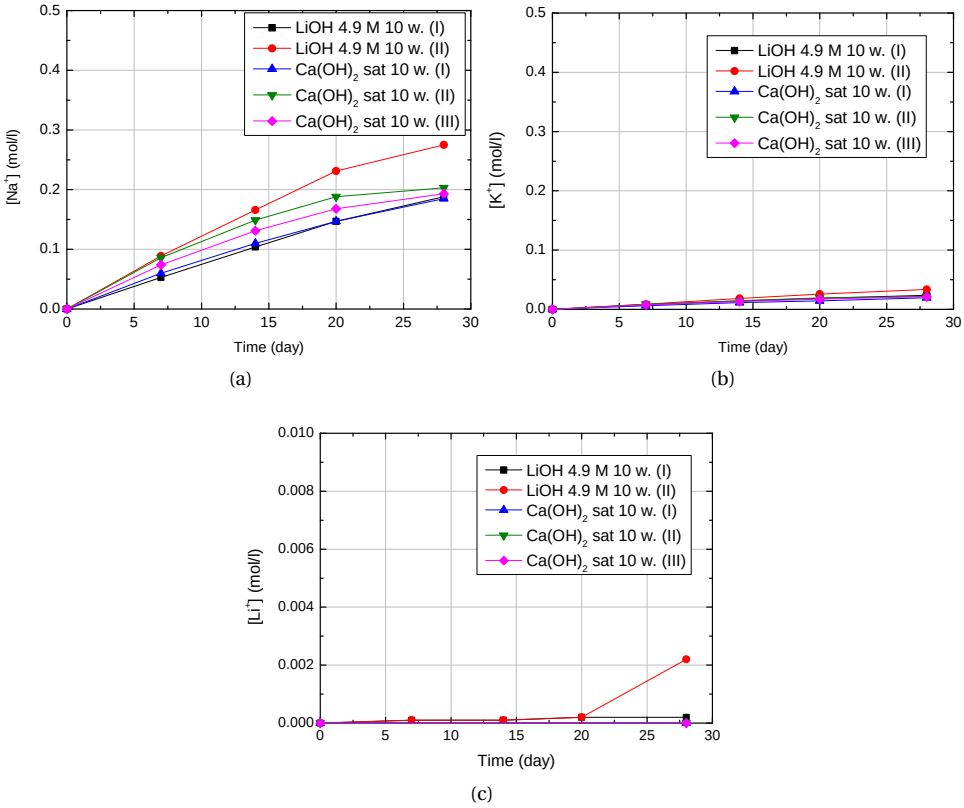

Figure 5.27: Sodium (a), potassium (b) and lithium (c) catholyte concentrations variations during migration treatment of the 10-week prismatic specimens. In (b), the plots from the tests with $Ca(OH)_2$ and LiOH 10 w. (I) are overlapping. In (c), lithium concentrations in the tests with $Ca(OH)_2$ are zero.

crete mixture. Sodium and potassium concentrations correlate with passing charge, especially in the cases where LiOH was the anolyte – the higher the charge, the higher are the concentrations. Very limited lithium arrived to the catholyte solutions of the specimens treated with LiOH after 21 days and the specimen with the highest concentration was LiOH 4.9 M 10 w. (II), as expected due to its highest charge.

Figure 5.28 shows the sodium, potassium, calcium and lithium concentrations in the anolyte [1] solutions during the diffusion tests. Sodium and potassium ions diffused from the specimen into the solution. The concentrations of those ions are higher than the ones from the migration experiments, as there was no electric field to transport them in the opposite direction. Calcium ions diffused from the $Ca(OH)_2$ solutions into the specimens and from the specimen to the LiOH solutions, as expected. Lithium ions diffused from the LiOH solutions into the specimen. As expected, these concentrations

[1] The terms "anolyte" and "catholyte" are normally used to describe the solutions in an electrochemical cell. Here, they will be used to describe the also solutions in the diffusion experiments, following the Table 5.8.

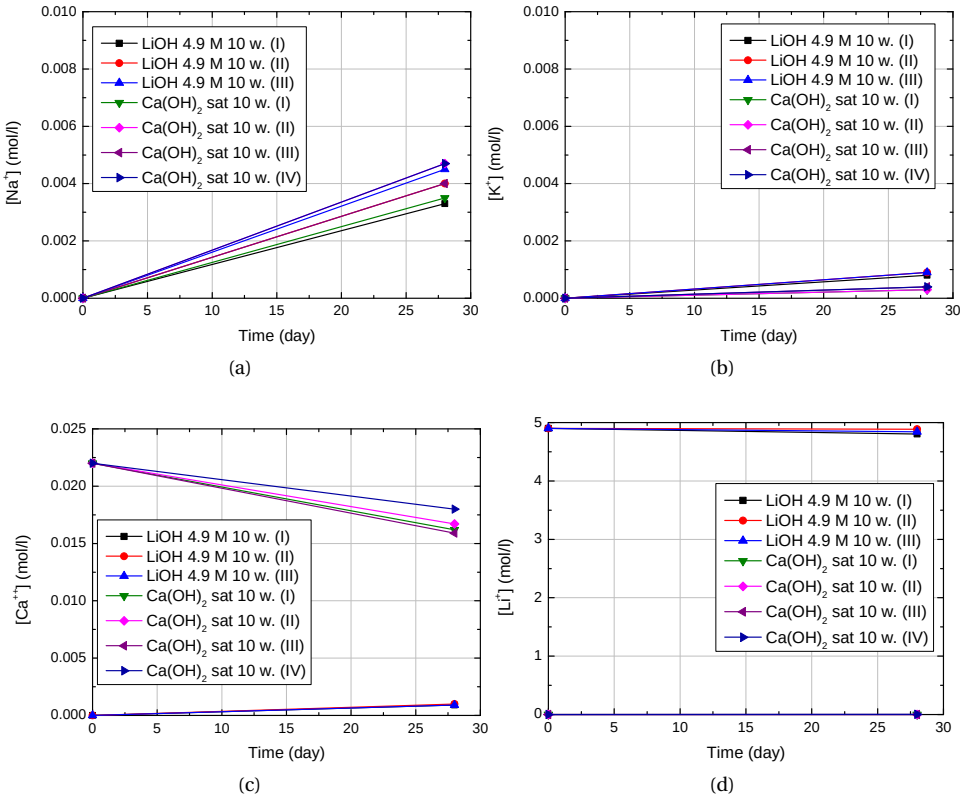

Figure 5.28: Sodium (a), potassium (b), calcium (c) and lithium (d) anolyte concentrations variations during diffusion treatment of the 10-week prismatic specimens. In (a), the plots from the tests with $Ca(OH)_2$ sat. 10 w. (II) and (IV) are overlapping and so are the plots LiOH 4.9M 10 w. (II) and $Ca(OH)_2$ sat. 10 w. (III). In (b), the plots from the tests with LiOH are overlapping and so are the ones from the tests with $Ca(OH)_2$. In (c) the plots from the tests $Ca(OH)_2$ (I), (II) and (III) are overlapping, and so are the plots from the tests with LiOH. In (d), the concentration of lithium in the cells of tests with $Ca(OH)_2$ is zero.

remain higher than the ones observed during the migration experiments, meaning that less lithium ions were transported from the anolyte into the specimen during the diffusion tests.

Sodium and potassium concentrations in the catholyte solutions are shown in Figure 5.29. Some sodium and potassium ions leached from the specimens to the catholyte solutions at similar levels to the ones observed in the anolyte solutions. In fact, when $Ca(OH)_2$ was used as both solutions, sodium and potassium concentrations were practically the same. When LiOH was the anolyte solution, potassium had slightly higher concentration in the anolyte than in the catholyte while sodium had practically the same concentration in both solutions. It is noteworthy that no detectable lithium reached the catholyte solutions by diffusion.

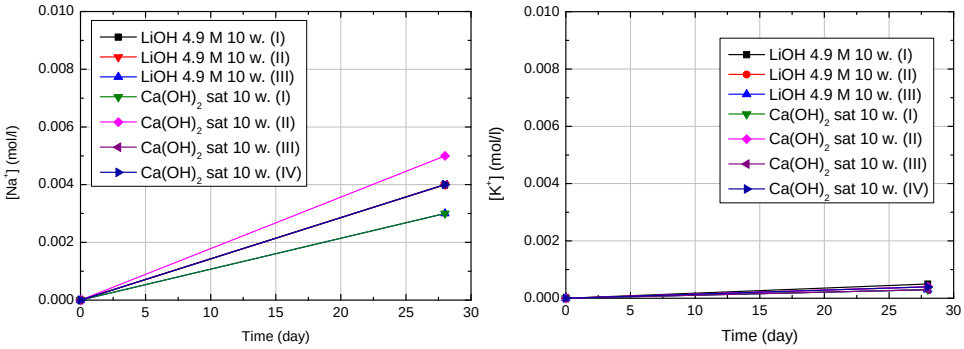

Figure 5.29: Sodium (a) and potassium (b) catholyte concentrations variations during diffusion treatment of the 10-week prismatic specimens. In (a), the plots from the tests LiOH 4.9 M (III) and $Ca(OH)_2$ (I) are overlapping, as well as the plots from the tests LiOH 4.9 M(I) and (II) and $Ca(OH)_2$ (III) and (IV). In (b), the plots from the tests LiOH 4.9 M (II) and $Ca(OH)_2$ (II) and (IV) are overlapping, as well the plots from the tests LiOH 4.9 (III), $Ca(OH)_2$ I and (III).

5

EXPANSIVE BEHAVIOR

As mentioned in the previous sections, during the migration treatment of the 3-week specimens, the reference studs were corroded. This corrosion led to the cracking of the area around the studs and also to expansion of the specimens, as it will be further discussed. As a consequence of the formation of cracks, heavy electrolyte leakage was observed in some of the cells. At that moment, the experiment was interrupted for the replacement of the studs. The corroded studs were removed, the remaining holes were filled with a repair mortar and new studs were attached onto the repair, with the use of a two-component glue. In order to avoid such corrosion problems during the migration experiments of the 10-week specimens, their studs were replaced five weeks before the beginning of the treatment, following the procedure already described. As it will be further detailed, the corrosion issue during the treatment of the 3-week and the curing of the glue affected the measured expansion values of the 3-week specimens. In the case of the 10-week specimens, only the glue influenced the expansion values.

The measured expansive behavior of the specimens exposed to ASR accelerating conditions for 10 weeks prior to treatment is shown in Figure 5.30. The term "measured expansion" in this thesis refers to the combination of expansion due to ASR and artifacts caused by corrosion of the studs (in the case of the 3-week specimens) and by curing of the glue. Interestingly, from week 5 until week 10, the specimens that had their studs replaced (i.e. the migration specimens) exhibited higher measured expansion than the ones that had their original studs (i.e. the diffusion specimens). As those measurements were taken before any treatment occurred, the extra expansion is likely to be an artifact caused by the replacement of the reference studs, more specifically, due to the expansion of the glue during that period. During the period of treatment, between weeks 10 and 14, the measured expansion rate of the migration specimens decreased. In fact, they were close to the rate of expansion of the specimens treated with $Ca(OH)_2$ and no cur-

rent. This suggests that the expansion of the glue probably took place in the first couple of days (or weeks) after the replacement and subsequently stabilized.

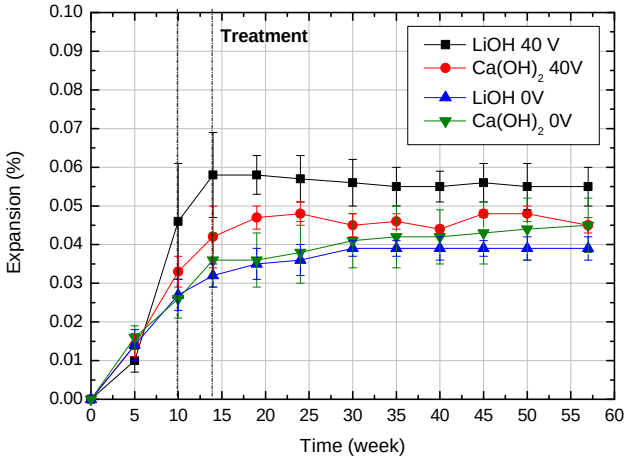

Figure 5.30: Measured expansive behavior of the specimens exposed to ASR accelerating conditions for 10 weeks prior to treatment.

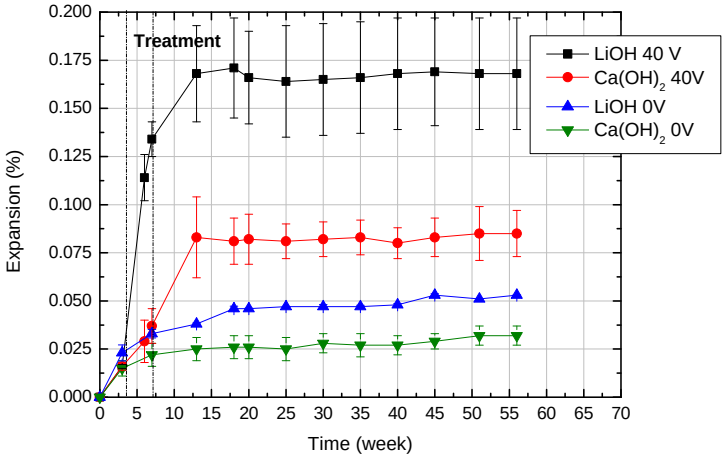

Figure 5.31: Measured expansive behavior of the specimens exposed to ASR accelerating conditions for 3 weeks prior to treatment.

Figure 5.31 shows the measured expansions of the prism that were exposed to ASR conditions for 3 weeks prior to treatment. The migration specimens had an extra measuring point at week six – that was the moment when the studs were replaced. The measured expansion of the specimens treated by migration with LiOH from the beginning of the treatment until week 7 is higher than the expansion of the diffusion specimens. That behavior was probably caused by the corrosion of the studs. When the studs were re-

moved, there was, indeed, accumulation of corrosion products at the bottom of some of them, which probably resulted in higher measured expansion. It is interesting to notice that the specimens treated with LiOH had much higher expansion during that period and, as seen in Figure 5.16, those specimens also had highest currents. The higher the current, the more corrosion occurred and the more corrosion products were formed. In addition, those were the specimens that had the most cracks. After the replacement of the studs, the expansion rate decreased, until the end of the treatment.

The post-treatment behavior of the concrete prisms exposed to ASR curing conditions for 10 weeks is shown in Figure 5.32. As previously mentioned, it is expected that the post-treatment behavior is free from the artifacts caused by the replacement of the studs. The specimens treated by migration with LiOH had some shrinkage after the treatment and assumed a somewhat constant negative expansion level. The specimens treated by migration with $Ca(OH)_2$ had varying expansion levels that seem to oscillate in a constant range. The standard deviations of these specimens are high and, even though their average post-treatment expansion is lower than the average expansions observed in diffusion specimens, they are statistically similar. On the other hand, the specimens treated by diffusion with LiOH had initially increasing expansion and, surprisingly, reached almost constant levels after week 15. The control specimens treated by diffusion with $Ca(OH)_2$ had increasing post-treatment expansion until the end of the experiment, with higher expansion than the specimens treated by migration with LiOH. Interestingly, the specimens treated by diffusion with both LiOH and $Ca(OH)_2$ had similar expansion levels after week 25. It is worth noting that the expansion values of specimens treated by migration had higher variability than the values observed for diffusion specimens. The higher variability is probably caused by the differences in passing charge between replicates during treatment. Different passing charges result in different levels of transport of lithium, sodium and potassium, which, consequently, may affect expansion values.

In the case of the 3-week specimens, as their studs were replaced during the treatment, expansion values measured after the end of the treatment are likely to be affected by the artifacts caused by the stud replacement. Therefore, in this case, the post-treatment expansion refers to the expansion observed after week 13 (i.e. seven weeks after the replacement of the studs) and it is shown in Figure 5.33. The specimens treated by migration with LiOH had expansion values that oscillated around the initial value (i.e. the value observed at week 13) and stabilized towards the end of the experiment at that level. The specimens treated by migration with $Ca(OH)_2$ had initially a decrease in expansion followed by an increase and finally stabilizing at levels close to what was initially observed (at week 13). The diffusion specimens, on the other hand, showed increasing expansion until the end of the experiment. The specimens treated by diffusion and LiOH had the highest post treatment expansion values. This is probably due to the fact that the LiOH solution was very alkaline and it is likely to have increased the pH of the pore solution as hydroxyl ions diffused into the specimen. At the same time, lithium ions also diffused into the specimen, but at lower rate, as lithium ions have lower mobility than hydroxyl ions. The increase in alkalinity of the pore solution is likely to have increased the dissolution of the reactive silica and accelerated the reaction. Interestingly, the 10-week specimens treated by diffusion with LiOH had different behavior. On the other hand, both 3 and 10-week prisms treated by diffusion with $Ca(OH)_2$ had similar

post-treatment expansion.

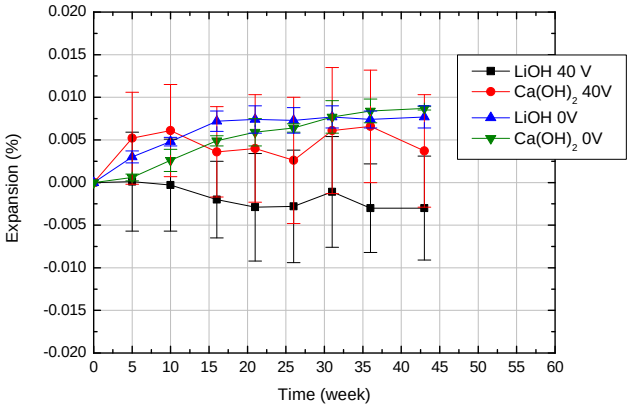

Figure 5.32: Post-treatment expansive behavior of the specimens exposed to ASR accelerating conditions for 10 weeks prior to treatment.

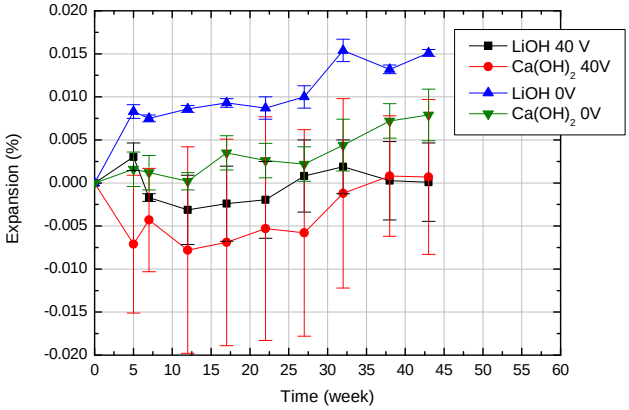

Figure 5.33: Post-treatment expansive behavior of the specimens exposed to ASR accelerating conditions for 3 weeks prior to treatment.

Overall, the migration treatment with LiOH led to lower post-treatment expansions than the ones observed for the control cases (i.e. diffusion with $Ca(OH)_2$). Diffusion treatment with LiOH resulted in expansive behavior similar (in the case of 10-week specimens) or worse (for the 3-week specimens) than what was observed in the control cases. The migration treatment with $Ca(OH)_2$ led to average post-treatment expansions lower than the control, probably due to the removal of sodium and potassium ions from the pore solution. However, due to the high variability amongst replicates, the results from the migration treatment with $Ca(OH)_2$ are inconclusive.

The results show that lithium migration successfully reduced post-treatment ASR expansion, when compared to the control cases. Nevertheless, these results need to be

considered with caution. The mechanism by which lithium reduces ASR expansion in hardened concrete is still unknown. However, in the case of the addition of lithium-cased admixtures to fresh concrete mixtures, the type of reactive aggregate determines the dosage necessary to prevent ASR expansion. Therefore, it is possible that concretes with different types of reactive aggregate react differently to the migration treatment.

5.4. MAIN FINDINGS

TABLES 5.7 and 5.8 present the main electrical results obtained from the experiments with cylindrical and prismatic specimens, respectively. Table 5.9 shows the final post-treatment expansion values of prismatic specimens.

Table 5.7: Summary of the main results from migration experiments with cylindrical specimens.

	Average mean current density (A/m^2)	Average charge (kC)	
LiOH 4.9 M 3 w.	3.7 ± 0.1	69 ± 2	
LiOH 4.9 M 10 w.	2.6± 0.2	48 ± 5	
	Initial resistivity (Ω.m)	Final resistivity (Ω.m)	Resistivity after 24 h (Ω.m)
LiOH 4.9 M 3 w.	95 ± 2	120 ± 3	124 ± 3
LiOH 4.9 M 10 w.	145 ± 8	195 ± 25	197 ± 23
	Final anolyte lithium concentration (mol/l)	Average specimen lithium content (% wt. of cement)	
LiOH 4.9 M 3 w.	4.375 ± 0.055	0.235 ± 0.004	
LiOH 4.9 M 10 w.	4.535 ± 0.025	0.199 ± 0.056	
	Final catholyte lithium concentration (mol/l)	Final catholyte sodium concentration (mol/l)	Final catholyte potassium concentration (mol/l)
LiOH 4.9 M 3 w.	0.005 ± 0.001	0.210 ± 0.008	0.035 ± 0.003
LiOH 4.9 M 10 w.	0.004 ± 0.002	0.175 ± 0.007	0.023 ± 0.002

Table 5.8: Summary of the main results from migration and diffusion experiments with prismatic specimens.

	Average mean current density (A/m^2)		Average charge (kC)
LiOH 4.9 M 3 w.	5.0 ± 0.4	LiOH 4.9 M 3 w.	212 ± 18
$Ca(OH)_2$ sat. 3w.	2.7 ± 0.3	$Ca(OH)_2$ sat. 3w.	116 ± 12
LiOH 4.9 M 10 w.	3.3 ± 0.5	LiOH 4.9 M 10 w.	166 ± 24
$Ca(OH)_2$ sat. 10 w.	2.5 ± 0.2	$Ca(OH)_2$,sat. 10 w.	124 ± 9
	Initial resistivity (Ω.m)		Final resistivity (Ω.m)
LiOH 4.9 M/ $Ca(OH)_2$ 3 w.	105 ± 10	LiOH 4.9 M 40V 3 w.	123 ± 22
LiOH 4.9 M/ $Ca(OH)_2$ 10 w.	146 ± 7	$Ca(OH)_2$ sat. 40 V 3 w.	257 ± 9
		LiOH 4.9 M 40V 10 w.	169 ± 26
	Resistivity after 24 h (Ω.m)	$Ca(OH)_2$ sat 40V 10 w.	255 ± 9
LiOH 4.9 M 40V 10 w.	168 ± 23	LiOH 4.9 M 0V 3 w.	79 ± 18
$Ca(OH)_2$ sat. 40V 10 w.	243 ± 10	$Ca(OH)_2$ sat. 0V 3w.	103 ± 5
		LiOH 4.9 M 0V 10 w.	107 ± 6
		$Ca(OH)_2$ sat. 0V 10 w.	111 ± 6
	Final anolyte lithium concentration (mol/l)		Final catholyte lithium concentration (mol/l)
LiOH 4.9 M 40V 10 w.	4.411 ± 0.031	LiOH 4.9 M 40V 10 w.	0.0012 ± 0.0010
LiOH 4.9 M 0V 10 w.	4.845 ± 0.034	LiOH 4.9 M 0V 10 w.	no Li detected
	Final catholyte sodium concentration (mol/l)		Final catholyte potassium concentration (mol/l)
LiOH 4.9 M 40V 10 w.	0.2315 ± 0.0435	LiOH 4.9 M 40V 10 w.	0.0287 ± 0.0050
$Ca(OH)_2$ sat. 40V 10 w.	0.1937 ± 0.0074	$Ca(OH)_2$ sat. 40V 10 w.	0.0210 ± 0.0011
LiOH 4.9 M 0V 10 w.	0.0037 ± 0.0005	LiOH 4.9 M 0V 10 w.	0.0004 ± 0.0001
$Ca(OH)_2$ sat. 0V 10 w.	0.0040 ± 0.0007	$Ca(OH)_2$ sat. 0V 10 w.	0.0004 ± 0.0001

Table 5.9: Final post-treatment expansion of prismatic specimens.

Time in ASR reactor prior to treatment	Specimen	Post-treatment expansion (%)
3 weeks	LiOH 40 V	0.000± 0.005
	$Ca(OH)_2$ 40V	0.001 ± 0.009
	LiOH 0V	0.015 ± 0.008
	$Ca(OH)_2$ 0V	0.008 ± 0.003
10 weeks	LiOH 40 V	-0.003± 0.006
	$Ca(OH)_2$ 40V	0.004 ± 0.007
	LiOH 0V	0.008 ± 0.001
	$Ca(OH)_2$ 0V	0.009 ± 0.000

5.5. CONCLUSIONS

IN this chapter, lithium migration into ASR affected concrete specimens was evaluated. The effect of the expansion level on ionic transport was investigated. ASR reactive concrete prisms were cast, placed under ASR accelerating conditions for 3 and 10 weeks, and treated by migration with LiOH as anolyte. The use of $Ca(OH)_2$ solution as anolyte was also studied, in order to evaluate the effect of alkali removal on expansion. Extra sets of specimens were treated by diffusion (no current), with the same solutions as used during migration.

The conclusions are as follows:

- The initial (i.e. at the beginning of migration tests) resistivity values of the specimens exposed to ASR accelerating conditions for 3 weeks were lower than ones from the specimens exposed for 10 weeks, contrary to what was expected. This could be related to different hydration degrees or, more likely, to changes of the pore solution composition with time. Usually, ASR expansion leads to the formation of cracks. As expansion progresses, more and wider cracks are formed and, thus, more paths for ionic transport become available [25],[26]. Ionic migration takes place in aqueous solutions - therefore, the more saturated the crack is, more ions can be transported [16]. Even though cracks formed by ASR might not be initially fully saturated, they are likely to become so during treatment, when in contact with the electrolyte solutions. In this way, those cracks become extra paths for ionic migration.

  Nevertheless, in this work, the specimens did not present visible cracking before treatment, regardless of the expansion level. Even though microcracking may have taken place, it was not enough to increase ionic transport (i.e. decrease resistivity). The difference in resistivity values influenced the lithium migration levels. The 10-week specimens presented lower levels of lithium. Therefore, the expansion level did not positively influence lithium migration as, in the conditions studied, it had not caused the formation of significant cracks.

- The prismatic specimens treated by migration with LiOH as anolyte had higher current densities (and, consequently, higher passing charges) than the ones treated with $Ca(OH)_2$. This can be due to the fact that LiOH 4.9 M solution is more concentrated than the saturated $Ca(OH)_2$. In addition, the migration specimens treated with $Ca(OH)_2$ had higher increase in resistivity measured after 24 h without current than the specimens treated with LiOH. It is likely that non-reversible changes in pore structure and/or pore solution took place and affected more the specimens treated with $Ca(OH)_2$.

- The 10-week specimens treated by migration with LiOH had more sodium and potassium removed from their pore solutions than the specimens treated with $Ca(OH)_2$, as expected. However, it is unlikely that all sodium and potassium ions were removed, regardless the type of anolyte used. Limited amounts of lithium arrived in the catholyte after 21 days of treatment.

- Regarding the treatment by diffusion of prismatic specimens, low levels of sodium and potassium were removed from the pore solution of the 10-week specimens,

as expected. Some lithium ions left the LiOH solutions into the specimens but did not reach the opposite chamber. As expected, the use of an electrical field provided much higher rate of ionic transport.

- Specimens treated by migration with LiOH had lower post-treatment expansions than the control specimens (treated by diffusion with $Ca(OH)_2$), regardless of the time in the ASR reactor before treatment. The diffusion treatment with LiOH resulted in expansions statistically similar (for 10-week specimens) or higher (for 3-week specimens) than the ones observed for the control specimens. Finally, the migration treatment with $Ca(OH)_2$ led to inconclusive results, due to the high variability of the post-treatment expansion between replicates. This indicates that alkali removal alone is not responsible for controlling ASR expansion. Based on these results, lithium migration (with alkali removal as a side effect) was effective in reducing post-treatment ASR expansion, when comparing to the control cases. However, these results need to be considered with caution. The mechanisms by which lithium reduces ASR expansion in hardened concrete are still not understood and the effect of the treatment may vary according to the type of reactive aggregate in the concrete.

REFERENCES

[1] C. Lee, C. Liu, and W. Wang, *Effect of the distance between electrodes on the performance of using electrochemical technique to repair the concrete damaged by AAR,* in *Proceedings of the 13th International Conference on Alkali-Aggregate Reaction in Concrete* (2008) pp. 234–2459.

[2] W. Wang, C. Lee, C. Liu, and C. Lee, *Effect of the electrolyte on the performance in electrochemical repairing technique for the concrete affected by ASR,* in *Proceeding of the 14th International Conference on Alkali-Aggregate Reaction* (2012).

[3] J. Lizarazo-Marriaga, J. Lozano, J. Silva, L. Fonseca, G. Hermida, and P. Claisse, *A novel assessment of the electrochemical lithium impregnation treatment used to mitigate alkali-silica reaction in concrete,* Concrete Solutions 2014 , 205 (2014).

[4] T. Ueda, Y. Yoshida, K. Yamaguchi, and M. Ashida, *Effect of electrochemical penetration of lithium ions on ASR expansion of concrete,* in *Proceedings of the third international conference on engineering materials* (2005).

[5] T. Ueda, Y. Yoshida, K. Yamaguchi, and M. Ashida, *Electrochemical migration of lithium ions into hardened concrete and ASR expansion after treatment,* Proceedings of structural faults & repair-2006 (2006).

[6] T. Ueda, T. Kameda, T. Maeda, and A. Nanasawa, *Suppression of ASR expansion due to electrochemical penetration of lithium supplied by DFRCC anode system,* in *Proceedings of the 6th International Conference on Concrete under Severe Conditions* (2010) pp. 1229–1236.

[7] T. Ueda, Y. Baba, and A. Nanasawa, *Effect of electrochemical penetration of lithium ions on concrete expansion due to ASR,* Journal of Advanced Concrete Technology **9**, 31 (2011).

[8] T. Ueda, J. Kushida, M. Tsukagoshi, and A. Nanasawa, *Influence of temperature on electrochemical remedial measures and complex deterioration due to chloride attack and ASR,* Construction and Building Materials **67**, 81 (2014).

[9] T. Ueda, A. Nanasawa, and M. Tsukagoshi, *Influence of electrochemical lithium penetration from various kinds of lithium solution on ASR expansion of concrete,* in *Proceedings of the 4th International Conference on Concrete Repair, Rehabilitation and Retrofitting* (CRC Press, 2015).

[10] A. Bentivegna, E. Giannini, and K. Folliard, *Use of electrochemical migration to mitigate alkali-silica reaction in large scale concrete structures,* Concrete Solutions (2011).

[11] B. Wigum, *Assessment and development of performance tests for alkali aggregate reaction in Iceland,* in *Proceedings of the 14th International Conference on Alkali-Aggregate Reaction in Concrete* (2012).

[12] B. J. Wigum and G. J. Einarsson, *Alkali Aggregate Reactions – Performance Testing,* Tech. Rep. Project nr. 7.009.290 (Mannvit, 2012).

[13] O. Çopuroğlu, Ö. Andiç-Çakir, M. A. Broekmans, and R. Kühnel, *Mineralogy, geochemistry and expansion testing of an alkali-reactive basalt from western Anatolia, Turkey,* Materials Characterization **60**, 756 (2009).

[14] A. Poole, *Introduction to alkali-aggregate reaction in concrete,* (Blackie, London, 1992) pp. 1–29.

[15] P. J. Nixon and I. Sims, *RILEM Recommendations for the Prevention of Damage by Alkali-Aggregate Reactions in New Concrete Structures: State-of-the-Art Report of the RILEM Technical Committee 219-ACS*, Vol. 17 (Springer, 2015).

[16] L. Bertolini, B. Elsener, P. Pedeferri, E. Redaelli, and R. B. Polder, *Corrosion of steel in concrete: prevention, diagnosis, repair*, 2nd ed. (John Wiley & Sons, 2013).

[17] E. Gallucci, X. Zhang, and K. Scrivener, *Effect of temperature on the microstructure of calcium silicate hydrate (csh),* Cement and Concrete Research **53**, 185 (2013).

[18] A. M. Neville, *Properties of concrete*, 5th ed. (Pearson, 2011).

[19] T. Kim, J. Olek, and H. Jeong, *Alkali–silica reaction: Kinetics of chemistry of pore solution and calcium hydroxide content in cementitious system,* Cement and Concrete Research **71**, 36 (2015).

[20] J. Pacheco and R. B. Polder, *Preliminary study of electrochemical lithium migration into cementitious mortar,* in *2nd International Symposium on Service Life Design for Infrastructures* (RILEM Publications SARL, 2010) pp. 1093–1100.

[21] T. Ueda, Y. Baba, and A. Nanasawa, *Penetration of lithium into ASR affected concrete due to electro-osmosis of lithium carbonate solution,* Construction and Building Materials **39**, 113 (2013).

[22] C.-C. Liu, W.-C. Wang, and C. Lee, *Behavior of cations in mortar under accelerated lithium migration technique controlled by a constant voltage,* Journal of Marine Science and Technology **19**, 26 (2011).

[23] X. Feng, M. Thomas, T. Bremner, B. Balcom, and K. Folliard, *Studies on lithium salts to mitigate ASR-induced expansion in new concrete: a critical review,* Cement and Concrete Research **35**, 1789 (2005).

[24] J. F. Schneider, N. P. Hasparyk, D. A. Silva, and P. J. Monteiro, *Effect of lithium nitrate on the alkali-silica reaction gel,* Journal of the American Ceramic Society **91**, 3370 (2008).

[25] D. Whitmore and S. Abbott, *Use of an applied electric field to drive lithium ions into alkali-silica reactive structures,* in *Proceedings, 11th International Conference on Alkali-Aggregate Reaction* (2000) pp. 1089–1098.

[26] M. Thomas and D. Stokes, *Lithium impregnation of ASR-affected concrete: preliminary studies,* in *Proceedings of the 12th International Conference on Alkali-Aggregate Reaction in Concrete* (2004) pp. 659–667.

6

CONCLUDING REMARKS

6.1. GENERAL CONCLUSIONS

IN this section, the main findings of the present work are summarized.

- *The concentration of the lithium solution used as anolyte, rather than the type of lithium salt in it, played a role on lithium content in the specimen after migration.*

  In Chapter 3, migration experiments in two-chamber set-ups (with external electrodes) were conducted with anolyte solutions from different lithium salts at various concentrations. During those tests, it was possible to observe that the concentration of the lithium solution used as anolyte affected the passing charge and lithium content in the specimens, regardless of the lithium salt in it. More concentrated solutions led to higher levels of lithium ions in the specimens. Therefore, the use of highly soluble lithium compounds resulted in more effective transport.

- *Longer periods of lithium migration did not result in much higher final lithium content in the specimens.*

  In Chapter 3, longer migration tests were performed in two-chamber set-ups, with external electrodes. Results showed that a twofold increase in the duration of lithium migration tests had little influence on the final lithium content in the specimens, under the tested conditions. This indicates that the efficiency of lithium migration decreased with time, probably due to the decreasing lithium content in the anolyte solutions during testing.

- *When using embedded cathode during lithium migration, sodium and potassium ions accumulated in the region close to the cathode and very few lithium ions reached that region.*

  Chapter 3 also described migration experiments in which the cathode was an embedded titanium mesh in each specimen. In this case, only one chamber received the anolyte solution (and an external anode) while the catholyte was the specimens' pore solution. Results show that alkali ions accumulated in the region close to the cathode. In addition, very few lithium ions were detected in that region. This is a potentially dangerous side effect, regarding the treatment of ASR affected concrete. The accumulation of alkalis leads to the accumulation of hydroxyls ions (due to electroneutrality), which may accelerate silica dissolution and progression of the reaction, especially if not enough lithium ions reach the area. These effects are not observed when the cathode is placed externally to the specimen, as the external cathode allows the removal of alkali ions.

- *Numerical modeling of multi-ionic transport in concrete (mortar) provided further understanding of mechanisms that occur during lithium migration experiments.*

  In Chapter 4, a mathematical model was presented for multi-ionic transport in concrete (mortar) and it was implemented for experiments presented in Chapter 3. Differences between model and experimental results highlighted mechanisms that may have occurred during testing and were not considered in the model, such as the possible alkali attack that might have taken place on the surface of

the specimens. In addition, the model predicted well sodium and potassium concentrations in the catholyte solutions, as well the total average lithium content in the specimen. Finally, the model predicted that it is necessary for all sodium and potassium to be removed from the pore solution before lithium ions arrive in the catholyte.

- *Longer exposure time to ASR accelerating conditions prior to migration treatment led to lower levels of lithium transport into the specimen.*

  In Chapter 5, contrary to what was expected from the literature, the resistivity values of specimens exposed to ASR accelerating conditions for three weeks were lower than the resisitvities of specimens exposed for ten weeks. This was likely caused by changes in the pore solution during ASR development. Even though microcracking might have occurred, the specimens did not present visible cracking, regardless of the expansion level. The possibly formed cracks were not enough to decrease the resistivity and boost lithium transport into the specimens. As a result, the specimens exposed to ASR accelerating conditions for ten weeks had lower lithium content than the ones exposed for three weeks.

- *Lithium migration successfully reduced post-treatment expansion due to ASR*

  In Chapter 5, it was observed that specimens treated by migration with LiOH as anolyte had lower post-treatment expansion levels than specimens treated by diffusion with $Ca(OH)_2$ solution. This was observed in specimens exposed to ASR accelerating conditions for both three and ten weeks. On the other hand, the diffusion treatment with LiOH led to expansions similar or higher than the ones observed for the specimens treated by diffusion with $Ca(OH)_2$, depending on the pre-treatment time in an ASR reactor. Finally, the results from the migration treatments with $Ca(OH)_2$ are inconclusive, due to the variability of the post-treatment expansion between replicates. Nevertheless, this indicates that alkali removal alone is not effectively responsible for controlling ASR expansion.

6.2. RECOMMENDATIONS FOR FURTHER RESEARCH

THIS thesis aimed to investigate the use of lithium migration to mitigate deleterious ASR expansion in existing concrete structures. However, due to limited time, some aspects were not studied. This section presents suggestion for future research.

- Treating by lithium migration large-scale specimens with removable cathodes.

  In the literature, during the treatment of existing structures or large-scale specimens, the rebar was used as cathode. The distance between electrodes and the accumulation of alkali ions around the reinforcement are likely to limit lithium migration. Therefore, the installation of removable external electrodes would allow the treatment of smaller areas between electrodes and the removal of sodium and potassium ions.

- Investigating the mechanisms by which lithium mitigates (or reduces) deleterious ASR expansion in hardened concrete.

  Much effort has been placed on driving lithium ions into existing ASR affected concrete. However, the mechanism by which lithium mitigates ASR expansion in already existing concrete structures is still unknown. It is still necessary to fully understand the effects of lithium on already formed gel and to evaluate how much lithium is necessary to stop or reduce further expansion.

- Further work on modeling of lithium transport due to an electric field in concrete and lithium binding.

  The mathematical model presented in Chapter 4 estimated the average amount of lithium in the specimen well. However, the shape of the concentration profile predicted by the model is different from what was experimentally observed. This could have been due to assumptions made in the modeling, such as linear lithium binding. Further research on modeling lithium transport in concrete due to an electric field and on lithium binding is necessary.

- Testing the effects of lithium migration on ASR expansion of existing concrete composed by different types of reactive aggregates.

  When using lithium compounds as admixtures to prevent ASR expansion in fresh mixtures, different aggregates require different dosages and even different lithium compounds to effectively prevent expansion. This could be true in the case of treatment of existing concrete by lithium migration. Therefore, the effect of lithium migration on the expansion of concretes with different types of reactive aggregate should be investigated.

A

Appendix A

A

THE coarse aggregate used in this thesis was an Icelandic gravel constituted by volcanic rock with alkali reactive components. Some aggregate particles were analyzed with polarized light microscopy in order to identify the minerals present in them. Two thin sections were analyzed, each with seven and six particles. Optical photomicrographs from different particles are presented below.

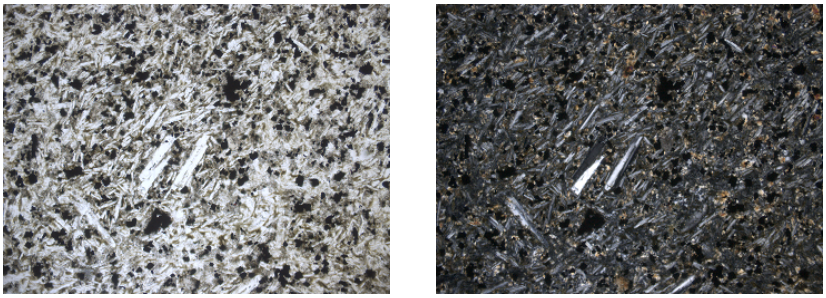

(a) (b)

Figure A.1: Thin section 1 - Particle A. Available phases: Plagioclasse, montmorillonite and olivine microliths; maybe some glass in the matrix. (a) Plane polarized light and (b) cross polarized light photomicrographs. Field of view: 1.50mm

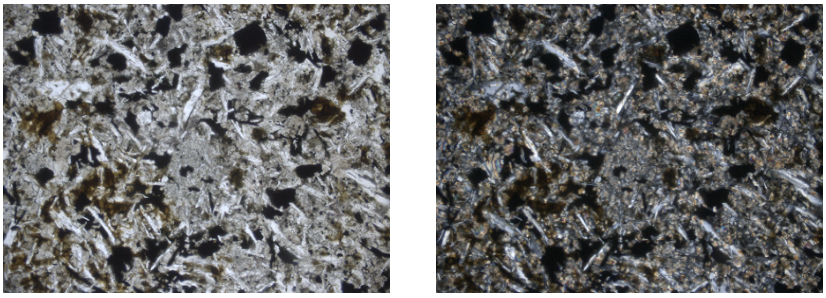

(a) (b)

Figure A.2: Thin section 1 - Particle B. Available phases: rare plagioclase phenocrysts; plagioclase and opaque phases (most probaby Fe and/or Fe-Ti oxides) as microliths and glass present in the matrix and as large inclusions. Resorption of plagioclase to glass. (a) Plane polarized light and (b) cross polarized light photomicrographs. Field of view: 1.50mm

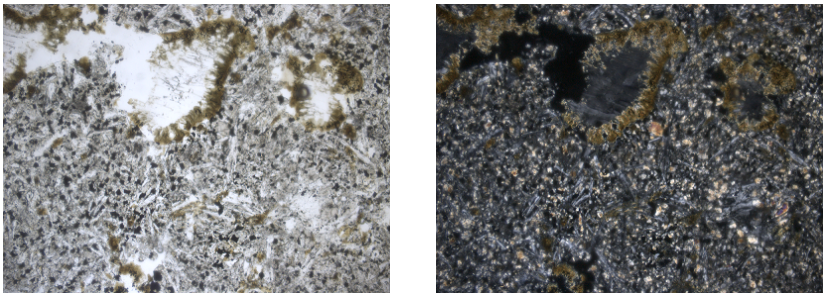

(a) (b)

Figure A.3: Thin section 1 - Particle C. Available phases: plagioclase, opaque phases (most probaby Fe and/or Fe-Ti oxides) and olivine microliths; veins and ocelli with chalcedony, quartz, white mica and some unidentified minerals. (a) Plane polarized light and (b) cross polarized light photomicrographs. Field of view: 1.50mm

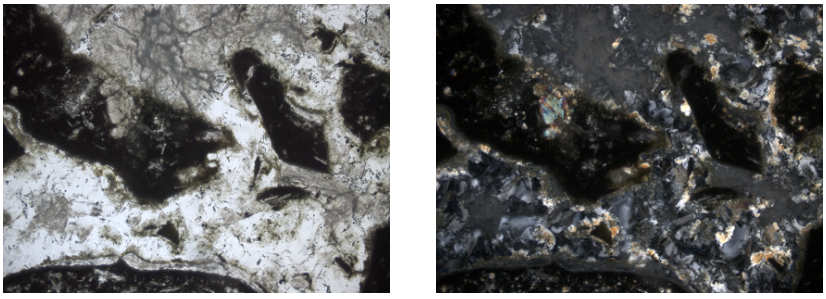

(a) (b)

Figure A.4: Thin section 1 - Particle D. Available phases: plagioclase and olivine phenocrysts; glass present in the matrix and as inclusions.(a) Plane polarized light and (b) cross polarized light photomicrographs. Field of view: 1.50mm

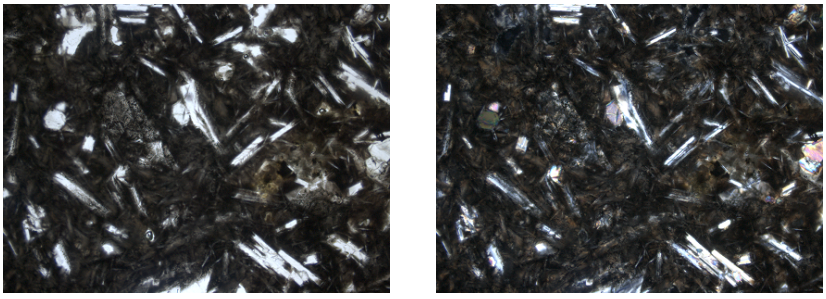

(a) (b)

Figure A.5: Thin section 1 - Particle E. Available phases: plagioclase phenocrysts; plagioclase, olivine and abundant opaque phases microliths; very fine grained matrix; quartz present in ocelli. (a) Plane polarized light and (b) cross polarized light photomicrographs. Field of view: 1.50mm

A

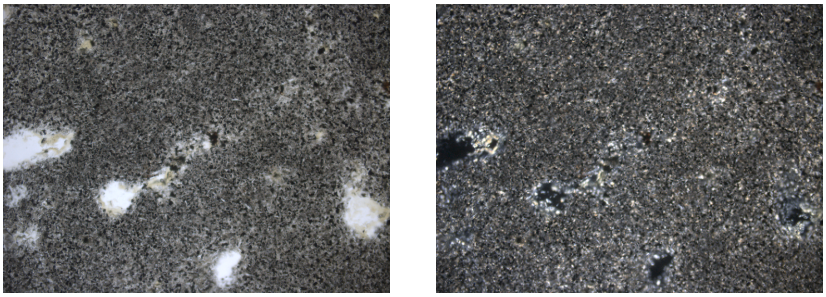

(a) (b)

Figure A.6: Thin section 1 - Particle F. Available phases: plagioclase and olivine microliths. (a) Plane polarized light and (b) cross polarized light photomicrographs. Field of view: 1.50mm

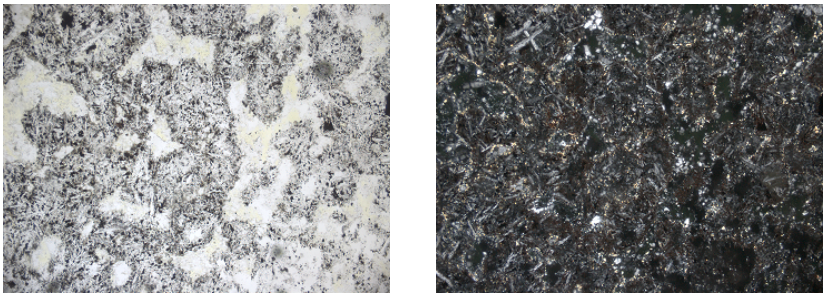

(a) (b)

Figure A.7: Thin section 1 - Particle G. Available phases: some plagioclase phenocrysts; plagioclase, olivine and opaque phases microliths. (a) Plane polarized light and (b) cross polarized light photomicrographs. Field of view: 1.50mm

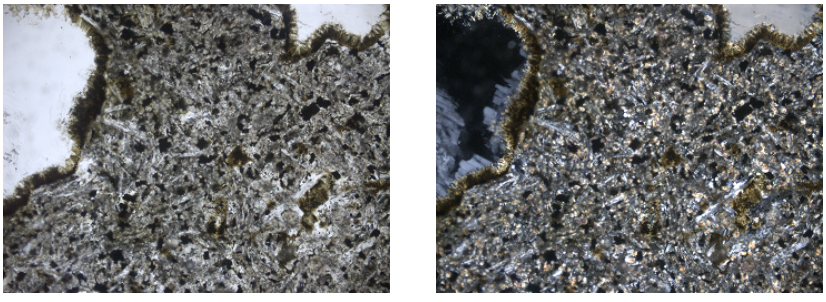

(a) (b)

Figure A.8: Thin section 2 - Particle A. Available phases: plagioclase phenocrysts; plagioclase, olivine and opaque phases microliths; glass as inclusions. Resorption of plagioclase to glass. (a) Plane polarized light and (b) cross polarized light photomicrographs. Field of view: 1.50mm

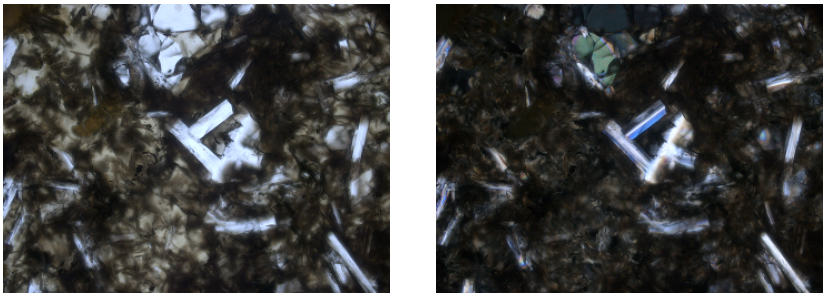

(a) (b)

Figure A.9: Thin section 2 - Particle B. Available phases: plagioclase and olivine phenocrysts; glass present in the matrix and as inclusions. (a) Plane polarized light and (b) cross polarized light photomicrographs. Field of view: 1.50mm

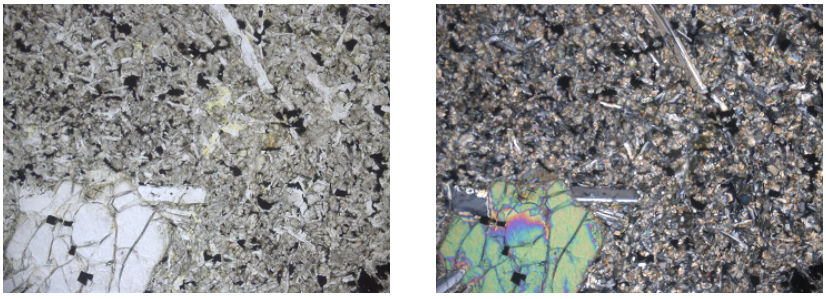

(a) (b)

Figure A.10: Thin section 2 - Particle C. Available phases: plagioclase and olivine phenocrysts; olivine, plagioclase and opaque phases microliths. (a) Plane polarized light and (b) cross polarized light photomicrographs. Field of view: 1.50mm

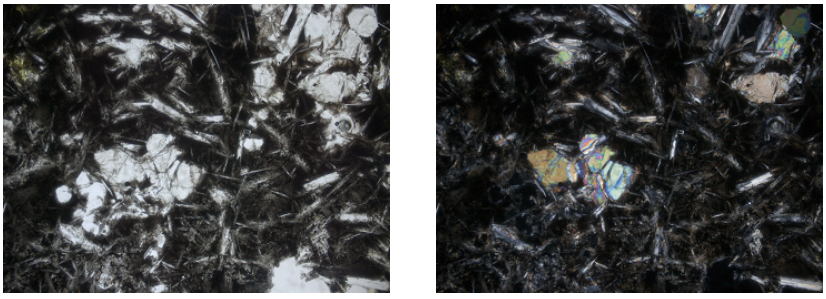

(a) (b)

Figure A.11: Thin section 2 - Particle D. Available phases: olivine phenocrysts; olivine and opaque phases as microliths; maybe glass present in the matrix.(a) Plane polarized light and (b) cross polarized light photomicrographs. Field of view: 1.50mm

A

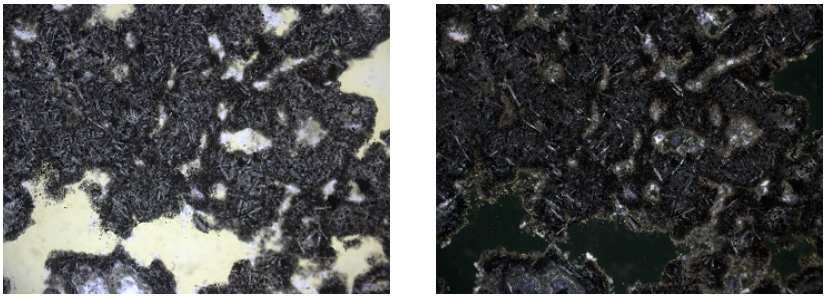

(a) (b)

Figure A.12: Thin section 2 - Particle E. Available phases: plagioclase and altered olivine phenocrysts; plagioclase, opaque phases and olinive microliths.(a) Plane polarized light and (b) cross polarized light photomicrographs. Field of view: 1.50mm

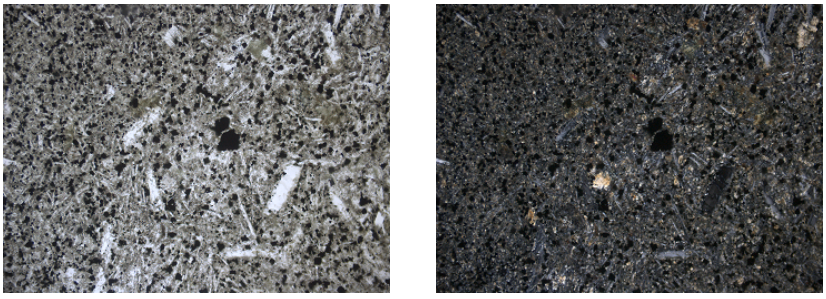

(a) (b)

Figure A.13: Thin section 2 - Particle F. Available phases: opaque phases and plagioclase as phenocrysts and microliths; quartz in ocelli. (a) Plane polarized light and (b) cross polarized light photomicrographs. Field of view: 1.50mm

B

Appendix B

TABLES B.1 and B.2 present the measured expansion and post-treatment expansion values for the specimens placed in ASR reactor for 10 weeks before treatment. Tables, B.3 and B.4 show the measured expansion and post-treatment expansion values for the 3-week specimens.

Table B.1: Measured expansion of the specimens exposed to ASR accelerating conditions 10 weeks prior to treatment.

	LiOH 40 V		$Ca(OH)_2$ 40V		LiOH 0V		$Ca(OH)_2$ 0V	
Time (weeks)	Av. Exp. (%)	Std dev. (%)	Av. Exp. (%)	Std dev. (%)	Av. Exp. (%)	Std dev. (%)	Av. Exp. (%)	Std dev. (%)
0	0.000	0.000	0.000	0.000	0.000	0.000	0.000	0.000
5	0.010	0.003	0.014	0.003	0.014	0.004	0.016	0.003
10	0.046	0.015	0.033	0.004	0.027	0.004	0.026	0.005
14	0.058	0.011	0.042	0.008	0.032	0.003	0.036	0.007
19	0.058	0.005	0.047	0.003	0.035	0.004	0.036	0.007
24	0.057	0.006	0.048	0.003	0.036	0.004	0.038	0.008
30	0.056	0.006	0.045	0.003	0.039	0.002	0.041	0.007
35	0.055	0.005	0.046	0.002	0.039	0.002	0.042	0.008
40	0.055	0.004	0.044	0.001	0.039	0.003	0.042	0.007
45	0.056	0.005	0.048	0.001	0.039	0.002	0.043	0.008
50	0.055	0.006	0.048	0.002	0.039	0.003	0.044	0.008
57	0.055	0.005	0.045	0.002	0.039	0.003	0.045	0.007

Table B.2: Post-treatment expansion of specimens exposed to ASR accelerating conditions for 10 weeks before treatment.

	LiOH 40 V		$Ca(OH)_2$ 40V		LiOH 0V		$Ca(OH)_2$ 0V	
Time (weeks)	Av. Exp. (%)	Std dev. (%)	Av. Exp. (%)	Std dev. (%)	Av. Exp. (%)	Std dev. (%)	Av. Exp. (%)	Std dev. (%)
0	0.000	0.000	0.000	0.000	0.000	0.000	0.000	0.000
5	0.000	0.006	0.005	0.005	0.003	0.001	0.001	0.000
10	0.000	0.005	0.006	0.005	0.005	0.001	0.003	0.001
16	-0.002	0.005	0.004	0.005	0.007	0.001	0.005	0.001
21	-0.003	0.006	0.004	0.006	0.007	0.002	0.006	0.002
26	-0.003	0.007	0.003	0.007	0.007	0.002	0.006	0.001
31	-0.001	0.007	0.006	0.007	0.008	0.001	0.008	0.002
36	-0.003	0.005	0.007	0.007	0.007	0.001	0.008	0.001
43	-0.003	0.006	0.004	0.007	0.008	0.001	0.009	0.000

Table B.3: Measured expansion of the specimens exposed to ASR accelerating conditions 3 weeks prior to treatment.

	LiOH 40 V		$Ca(OH)_2$ 40V		LiOH 0V		$Ca(OH)_2$ 0V	
Time (weeks)	Av. Exp. (%)	Std dev. (%)	Av. Exp. (%)	Std dev. (%)	Av. Exp. (%)	Std dev. (%)	Av. Exp. (%)	Std dev. (%)
0	0.000	0.000	0.000	0.000	0.000	0.000	0.000	0.000
3	0.016	0.001	0.016	0.002	0.023	0.004	0.015	0.004
6	0.114	0.012	0.029	0.011	–	–	–	–
7	0.134	0.009	0.037	0.009	0.033	0.002	0.022	0.006
13	0.168	0.025	0.083	0.021	0.038	0.001	0.025	0.006
18	0.171	0.026	0.081	0.012	0.046	0.001	0.026	0.006
20	0.166	0.024	0.082	0.013	0.046	0.000	0.026	0.006
25	0.164	0.029	0.081	0.009	0.047	0.000	0.025	0.006
30	0.165	0.029	0.082	0.009	0.047	0.001	0.028	0.005
35	0.166	0.029	0.083	0.009	0.047	0.001	0.027	0.006
40	0.168	0.029	0.080	0.008	0.048	0.001	0.027	0.005
45	0.169	0.028	0.083	0.010	0.053	0.001	0.029	0.004
51	0.168	0.029	0.085	0.014	0.051	0.000	0.032	0.005
56	0.168	0.029	0.085	0.012	0.053	0.000	0.032	0.005

Table B.4: Post-treatment expansion of specimens exposed to ASR accelerating conditions for 3 weeks before treatment.

	LiOH 40 V		$Ca(OH)_2$ 40V		LiOH 0V		$Ca(OH)_2$ 0V	
Time (weeks)	Av. Exp. (%)	Std dev. (%)	Av. Exp. (%)	Std dev. (%)	Av. Exp. (%)	Std dev. (%)	Av. Exp. (%)	Std dev. (%)
0	0.000	0.000	0.000	0.000	0.000	0.000	0.000	0.000
5	0.003	0.002	-0.007	0.008	0.008	0.001	0.002	0.002
7	-0.002	0.000	-0.004	0.006	0.008	0.000	0.001	0.002
12	-0.003	0.004	-0.008	0.012	0.009	0.000	0.000	0.001
17	-0.002	0.004	-0.007	0.012	0.009	0.001	0.004	0.002
22	-0.002	0.004	-0.005	0.013	0.009	0.001	0.003	0.002
27	0.001	0.004	-0.006	0.012	0.010	0.001	0.002	0.002
32	0.002	0.003	-0.001	0.011	0.015	0.001	0.004	0.003
38	0.000	0.005	0.001	0.007	0.013	0.001	0.007	0.002
43	0.000	0.005	0.001	0.009	0.015	0.000	0.008	0.003

ACKNOWLEDGEMENTS

"Tt takes a whole village to raise a child." In many ways I consider my thesis my child (especially when it comes to the sleepless nights) and I had a great "village" to help me "raise" it. This PhD dissertation would not have been accomplished without the contribution of many. I am grateful to everyone who somehow contributed for this work.

I gratefully acknowledge the financial support from STW and the program "Integral Solutions for Sustainable Constructions" (IS2C). I would like to acknowledge Prof. Eddie Koenders, the head of the program and Leo Pel, the leader of our project.

I consider myself to be a lucky person to be surrounded by so many brilliant and inspiring people. I would like to thank my promotor, Prof. Rob Polder. He guided me through this not-always-so-smooth process, inspiring me to be more curious. I am also enormously grateful for the never ending help from my co-promotor Oğuzhan Çopuroğlu. Thank you both so much! You both constantly amazed me with your knowledge and great ideas throughout this process.

I am thankful to the amazing team that helped me during these PhD years. John van der Berg, Ger Nagtegaal, Maiko van Leeuwen and Arjan Thijssen, thank you all so much! I would also like to thank Kees van Beek and everyone at EMSD – CE& G for all the help with the power sources.

I gratefully acknowledge the support I received from TNO - especially the help from Timo Nijland on the optical microscopy analysis of the reactive gravel and from Willem Suitela during many of the acid dissolutions. I would also like to acknowledge CorrPRE Engineering and Care4Concrete for providing the titanium electrodes.

I would like to thank my office mate Renée Mors for the help with all Dutch translations during these years: from discovering where my residence permit had been issued to helping with the samenvatting. Thanks, Renée! Still on the Dutch translation/paper work field, I would like to thank our secretary Nynke Verhulst for her endless support - even during her holidays! Obrigada, amiga! I also would like to thank Prof. Klaas van Breugel for the help with the samenvatting.

I would like to thank my colleagues from Microlab for all time we spent together: all the conversations, scientific or not, jokes and so on. Working in such a multinational environment was a valuable experience. I will certainly miss our coffee talks. Thanks to you all! I would like to especially thank my paranymphs Stefan Figueiredo and Fernando Mendonça. Not only you guys helped me out with experiments, but it was also great to be able to discuss all things Brazilian (especially during this crazy year).

I learned that even after moving to another continent, I could still count on friends back home. I would like to thank my dear friend Camila Abelha for all the discussions we had online. I am very happy that, even though we were no longer office mates, we were still able to discuss our theses, among other topics. Thanks, Camila! I am enormously grateful for the beautiful art-work my dear friend-of-almost-two-decades Cissa Monteiro made for my cover. I have always known you were incredibly talented, and yet,

you still manage to amaze me. Thanks, Cissa! And thanks to Carina Rocha for "supervising" Cissa's work.

I have an amazing family that knows no boundaries to show their support. It has always been like that and not even an ocean between us changed it. I am extremely grateful for all the chats, calls and visits. I would like to thank them – Eloisa Souza, Odeir Souza, Aparecida "Cici" Silva, Pedro Souza and Marcela Angarita. Muito obrigada por tudo! Amo vocês!

At last but not least, I am grateful for all the support I got from my partner in crime Dennis Voets. For all the times when I was too busy, too tired or too stressed out and you always had a smile and a nice gesture. Thank you so much, my love.

SUMMARY

Alkali-silica reaction (ASR) is a deterioration process that affects the durability of concrete structures worldwide. During the reaction, hydroxyl and alkali ions present in the pore solution react with reactive silica from the aggregate, forming a hygroscopic ASR gel. Alternatively, the silica structure is attacked by hydroxyl ions and the degraded structure acts as a hygroscopic silica gel. Either way, the gel (or gel-like structure) swells, which may cause expansion and cracking of the concrete element. It is a slow reaction – it usually takes from 5 to 15 years for its symptoms to be noted. Therefore, even though preventive measures have been known for decades, it is still possible to have newly diagnosed cases.

Methods to prevent ASR development in new structures have been successfully applied for decades. Nevertheless, when ASR is detected in existing structures, the currently available intervention options to stop further ASR expansion are far more limited. Current procedures, such as limiting the access of external water by the application of sealants, have limitations and their effectiveness has shown to be variable. In this framework, the development of effective intervention methods for ASR in existing concrete structures is still necessary and the application of lithium compounds has been proposed as a possible mitigation method.

For decades, the addition of lithium based admixtures has been known to successfully reduce or prevent deleterious ASR expansion in new concrete structures. Numerous works have reported the beneficial influence of various lithium compounds (such as $LiNO_3$, LiOH and others) on the expansive behavior of concretes and mortars composed with different types of reactive aggregates. In new concrete structures, lithium compounds can be incorporated to the fresh mixture. In the case of existing structures, however, such incorporation is no longer possible and lithium ions need to be transported into the concrete.

Research has been done on potential lithium-based treatment methods, such as topical application and vacuum impregnation, and results have shown that, in those cases, the penetration depth was limited. Some experimental studies compared different techniques such as immersion, vacuum impregnation, wet-dry cycles and electrochemical migration, and the latter has shown to be the most suitable to drive lithium ions into concrete, providing deeper penetration and higher concentration.

Electrochemical lithium migration is a technique that uses an electric field to transport lithium into concrete. Under the action of the electric field, positive ions migrate towards the negative electrode (cathode) and negative ions move in the opposite direction. The same principle is applied in treatments such as electrochemical chloride extraction (ECE). The use of electrochemical lithium migration as a treatment against ASR has been investigated by several authors. However, there is no agreement on its effectiveness against ASR expansion.

This thesis aims to contribute with further insights on the feasibility of lithium migration as a treatment against ASR. For that, the basics of lithium migration oriented towards application and its possible effects on ASR affected concrete were investigated.

The influence of different parameters during lithium migration was evaluated with standard mortar specimens in two-chamber migration set-ups (with external electrodes). The influence of the type of lithium compound and concentration used in the anolyte solution was studied. Results pointed out that the concentration of the solution, rather than the type of lithium salt, played a role in the experiments. The anolytes with the highest concentrations provided the highest levels of lithium in the specimens. The effect of the duration of the experiments was also investigated. Interestingly, under the investigated conditions, longer testing periods did not lead to much higher lithium transport.

During electrochemical treatments such as ECE, the reinforcement is often used as cathode. Therefore, the use of an embedded cathode during lithium migration was also evaluated. After testing, it was observed that this type of configuration led to the accumulation of alkalis in the region close to the embedded cathode and not many lithium ions were able to reach that area. If a ASR affected concrete structure would be treated with this configuration, the accumulation could lead to further ASR development (as long as there is still reactive silica, moisture and calcium ions). The alkali accumulation was not observed when the cathode was placed externally to the specimens. In those cases, sodium and potassium were removed from the pore solution.

Numerical models are useful tools which may provide further understanding of the mechanisms during an experiment. In this thesis, a mathematical model for multi-ionic transport in concrete under the effect of an electric field was presented. The model was numerically implemented for some of the migration experiments with mortar specimens. When comparing to the experimental results, the model predicted well sodium and potassium concentrations in the catholyte as well the final average lithium concentration in the specimens. The model indicated that the removal of all sodium and potassium ions from the pore solution was necessary before lithium ions could reach the catholyte chamber.

The influence of different expansion levels (and possibly different cracking levels) on lithium migration was investigated. ASR-reactive specimens were cast and placed under ASR accelerating conditions (60°C and R.H. 100%) for three or ten weeks prior to migration testing. In this work, cracks were not visually observed on the surface of the specimens, regardless of the expansion level. In fact, the resistivity of the specimens increased with the pre-testing time. The increase in resistivity led to a decrease in passing currents. Therefore, in this work, the specimens with the highest initial expansion had the lowest final lithium concentrations.

Finally, the effects of different treatments on ASR expansion were analyzed. For that, ASR-reactive specimens were placed under ASR accelerating conditions prior to testing. In two-chamber set-ups, the specimens were submitted to migration treatments with LiOH or $Ca(OH)_2$ solutions as anolyte, or to diffusion with the same solutions. After treatment, the specimens were placed again in the ASR reactor and their expansions were monitored. Overall, the lithium migration treatment led to lower expansion values than the other treatments.

SAMENVATTING

Alkali-silica reactie (ASR) is een aantastingsproces dat wereldwijd de duurzaamheid van betonconstructies beïnvloedt. Gedurende de reactie reageren hydroxyl en alkali-ionen in het poriewater met reactieve silica uit het toeslagmateriaal. Daaruit ontstaat een hygroscopische ASR gel. Ook kan de silicastructuur worden aangetast door hydroxylionen en fungeert de aangetaste structuur als een hygroscopische silica gel. In beide gevallen zwelt de gel (of gel-achtige structuur), wat kan resulteren in uitzetting en scheuren in betonelementen. Het is een trage reactie – het duurt normaliter 5 tot 15 jaar voor de symptomen worden opgemerkt. Daarom is het nog steeds mogelijk dat er nieuwe gevallen worden gediagnosticeerd, ondanks dat er al decennialang preventieve maatregelen bekend zijn.

Methodes om ASR ontwikkeling in nieuwe constructies te voorkomen, worden al decennialang met succes toegepast. Echter, wanneer ASR wordt gevonden in bestaande constructies dan zijn de momenteel beschikbare interventiemogelijkheden om verdere ASR expansie te stoppen veel beperkter. Huidige procedures, zoals het beperken van het binnendringen van water door het aanbrengen van afdichtingsmiddelen, hebben beperkingen en hun doeltreffendheid blijkt verschillend te zijn. In dit kader is de ontwikkeling van effectieve interventiemethoden voor ASR in bestaande betonconstructies nog steeds noodzakelijk en het aanbrengen van Lithium verbindingen is voorgesteld als een mogelijke methode om ASR tegen te gaan.

Decennialang is het gebruik van op lithium gebaseerde hulpstoffen ter voorkoming of vermindering van schadelijke ASR expansie in nieuwe betonconstructies bekend. Veel onderzoeken vermelden een gunstige invloed van verschillende lithiumverbindingen (zoals $LiNO_3$, LiOH en andere) op de expansie van beton en mortel samengesteld met verschillende reactieve toeslagmaterialen. In nieuwe betonconstructies kan een lithiumverbinding worden toegevoegd aan het verse betonmengsel. In het geval van bestaande constructies is deze toevoeging niet meer mogelijk en dienen de lithiumionen op een andere manier in beton te worden ingebracht.

Er is onderzoek gedaan naar mogelijke lithium-gebaseerde behandelingsmethodes, zoals lokale toepassing en vacuümimpregnatie. De resultaten laten zien dat in die gevallen de indringdiepte beperkt is. Sommige experimentele studies vergeleken verschillende technieken zoals onderdompeling, vacuümimpregnatie, nat-droog cycli en elektrochemische migratie. Hieruit blijkt dat de laatste methode het meest geschikt is om lithium te introduceren in beton; deze geeft grotere indringingsdiepte en een hogere lithiumconcentratie.

Elektrochemische lithiummigratie is een techniek waarbij een elektrisch veld wordt gebruikt om lithium in beton te transporteren. Onder invloed van het elektrische veld migreren positieve ionen naar de negatieve elektrode (kathode) en bewegen negatieve ionen in de omgekeerde richting. Hetzelfde principe wordt toegepast in behandelingen zoals elektrochemische chloride-extractie (ECE). Het gebruik van elektrochemische li-

thiummigratie als maatregel tegen ASR is onderzocht door verschillende auteurs. Er is echter verschil van mening over de effectiviteit ervan tegen ASR expansie.

Dit proefschrift heeft als doel een bijdrage te leveren aan beter inzicht in de mogelijkheid van lithiummigratie als behandeling tegen ASR. Daarom zijn de principes van het toepassen van lithiummigratie en de mogelijke effecten op ASR-aangetast beton onderzocht.

De invloed van verschillende parameters op lithiummigratie werd geanalyseerd met standaard mortelproefstukken in een tweecompartimenten migratie-opstelling (met externe elektroden). De invloed van het type lithiumzout en de gebruikte concentratie van de anolytoplossing zijn bestudeerd. De resultaten laten zien dat vooral de concentratie van de oplossing een rol speelt, veel meer dan het type lithiumzout. De anolytes met de hoogste concentraties gaven de hoogste hoeveelheden van lithium in de proefstukken. Het effect van de duur van de experimenten is ook onderzocht. Interessant is dat, in alle onderzochte omstandigheden, langere test periodes niet leidden tot een veel hoger lithiumtransport.

Gedurende elektrochemische behandelingen, zoals (ECE), wordt de wapening vaak gebruikt als kathode. Daarom is het gebruik van een ingebedde kathode tijdens lithiummigratie ook geëvalueerd. Na het testen werd waargenomen dat een dergelijke configuratie leidt tot de accumulatie van alkaliën in de zone dichtbij de ingebedde kathode, en zijn er weinig lithiumionen die dit gebied kunnen bereiken. Als een door ASR aangetaste betonconstructie wordt behandeld met deze methode, kan de accumulatie leiden tot verdere ASR ontwikkeling (indien er nog steeds reactieve silica, vocht en calciumionen zijn). De alkali-accumulatie werd niet waargenomen bij de proefstukken met een extern geplaatste kathode. In die gevallen waren natrium en kalium verwijderd uit de porie-oplossing.

Numerieke modellen zijn nuttige hulpmiddelen om mechanismen beter te begrijpen. In dit proefschrift wordt een wiskundig model gepresenteerd voor multi-ionen transport in beton onder invloed van een elektrisch veld. Het numerieke model is toegepast voor een aantal van de migratie-experimenten met mortelproefstukken. Bij het vergelijken van de experimentele resultaten, bleek dat het model zowel de natrium en kalium concentraties in de katholyten als de uiteindelijke gemiddelde lithiumconcentratie in de proefstukken goed voorspelde. Het model geeft aan dat verwijdering van natrium en kaliumionen uit de porie-oplossing nodig is alvorens de lithiumionen het katholyt-compartiment kunnen bereiken

De invloed van verschillende expansieniveaus (en eventueel verschillende scheurniveaus) op lithium migratie is onderzocht. Daarvoor werden ASR- reactieve proefstukken onder ASR bevorderende omstandigheden geplaatst (60 °C en R.V. 100%), gedurende drie of tien weken voorafgaand aan de migratiebehandeling. In dit onderzoek werden er visueel geen scheuren geconstateerd aan het oppervlak van de proefstukken, ongeacht het expansieniveau. De stijging in de elektrische weerstand leidde tot een afname van de stroom. Daarom hebben, in deze studie, de proefstukken met de hoogste initiële expansie de laagste uiteindelijke lithiumconcentraties.

Tenslotte werden de effecten van verschillende maatregelen tegen ASR expansie geanalyseerd. Hiervoor werden ASR-reactieve proefstukken onder ASR bevorderende omstandigheden geplaatst voorafgaand aan de proeven. In de tweecompartimenten opstel-

lingen werden de proefstukken onderworpen aan migratiebehandelingen met LiOH of $Ca(OH)_2$ oplossingen als anolyt of diffusies met dezelfde oplossingen. Na de behandeling werden de proefstukken opnieuw geplaatst in de ASR reactor en werd de expansie gemeten. Als algemene conclusie kan worden gezegd dat de lithiummigratie behandeling tot lagere expansiewaarden leidde dan de andere maatregelen.

CURRICULUM VITÆ

Lourdes Maria SILVA DE SOUZA

15-02-1985 Born in Rio de Janeiro, Brazil.

EDUCATION

2003–2008 BSc. Civil Engineering
Universidade Federal do Rio de Janeiro, Rio de Janeiro, Brazil

2009–2011 MSc. Civil Engineering
Universidade Federal do Rio de Janeiro, Rio de Janeiro, Brazil

2011–2016 PhD. Civil Engineering
Delft University of Technology, Delft, The Netherlands

Thesis:	Electrochemical lithium migration to mitigate alkali-silica reaction in existing concrete structures
Promotor:	Prof. dr. R.B. Polder
Co-promotor:	Dr. O. Çopuroğlu

WORK EXPERIENCE

2005–2008 LabEST – COPPE/UFRJ, Undergraduate Researcher
Rio de Janeiro, Brazil

2008–2009 COPPETEC-PEC/ LabEST – COPPE/UFRJ, Undergraduate Researcher
Rio de Janeiro, Brazil

2010–2011 LEOP Engenharia, Real Estate Evaluation Engineer
Rio de Janeiro, Brazil

Sept. 2016 Pontifícia Universidade Católica do Rio de Janeiro, Post-doc Researcher
Rio de Janeiro, Brazil

LIST OF PUBLICATIONS

1. **L.M.S. Souza**, E.M.R. Fairbairn, G.C. Cordeiro, R.D. Toledo (2014). Influence of initial CaO/SiO_2 ratio on the hydration of rice husk ash-$Ca(OH)_2$ and sugar cane bagasse ash-$Ca(OH)_2$ pastes. Quím. Nova, São Paulo, v. 37, n. 10, p. 1600-1605.

2. **L.M.S. Souza**, R.B. Polder, O. Çopuroğlu (2015). Lithium migration in mortar specimens with embedded cathode. Concrete Repair, Rehabilitation and Retrofitting IV: 4^{th} International Conference on Concrete Repair, Rehabilitation and Retrofitting (ICCRRR-4), Leipzig, Germany. CRC Press. p. 39.

3. **L.M.S. Souza**, R.B. Polder, O. Çopuroğlu (2015). Influence of Anolyte on Lithium Migration in Concrete. Andrade, C., Gulikers, J. and Polder, R.B. (Eds.) Durability of Reinforced Concrete from Composition to Protection. Selected papers of the 6th International RILEM PhD Workshop, Delft, The Netherlands. Springer International Publishing. p. 27-34.

4. **L.M.S. Souza**, RB. Polder, O. Çopuroğlu (2014). Investigation on lithium migration for treating alkali-silica reaction affected concrete. Justnes, H. (Eds.) Proceedings of the 1^{st} concrete innovation conference - CIC 2014, Oslo, Norway. NCF. p. 1-9.

5. **L.M.S. Souza**, RB. Polder, O. Çopuroğlu (2014). Study on lithium migration for electrochemical treatment of concrete affected by alkali-silica reaction. Grantham, M., et al. (Eds.) Proceedings of concrete solutions, 5^{th} international conference on concrete repair, Belfast, Northern Ireland. CRC Press. p. 237-243.

6. **L.M.S. Souza**, E.M.R. Fairbairn, G.C. Cordeiro, R.D. Toledo (2012). Hydration study of sugar cane bagasse ash and calcium hydroxide pastes of various initial c/s ratios. Guang, Y. et al.(Eds.) RILEM Proceedings pro083: Microstructural-related durability of cementitious composites, second international conference on microstructural-related durability of cementitious composites, Amsterdam, The Netherlands. RILEM. p. 181-188.

7. **L.M.S. Souza**, R.B. Polder (2012). Studies on electrochemical lithium migration for remediation of Alkali-Silica Reaction at macro level in concrete structures. Ferreira, R.M., Gulikers, J., Andrade, C. (Eds.) Fifth International PhD student workshop on durability of reinforced concrete; From composition to service life design. Espoo, Finland. VTT Technical Research Center. p. 50-62.